EARLY TO MIDDLE PALEOZOIC VOLCANISM OF WESTERN PENINSULAR MALAYSIA

QUEK LONG XIANG

FACULTY OF SCIENCE
UNIVERSITY OF MALAYA
KUALA LUMPUR

2018

EARLY TO MIDDLE PALEOZOIC VOLCANISM OF WESTERN PENINSULAR MALAYSIA

QUEK LONG XIANG

THESIS SUBMITTED IN FULFILMENT OF THE REQUIREMENTS FOR THE DEGREE OF DOCTOR OF PHILOSOPHY

DEPARTMENT OF GEOLOGY
FACULTY OF SCIENCE
UNIVERSITY OF MALAYA
KUALA LUMPUR

2018

UNIVERSITY OF MALAYA

ORIGINAL LITERARY WORK DECLARATION

Name of Candidate: **Quek Long Xiang**

Matric No: **SHC 150035**

Name of Degree: **Doctor of Philosophy (Except mathematics & science philosophy)**

Title of Project Paper/Research Report/Dissertation/Thesis ("this Work"):

Early to Middle Paleozoic Volcanism of Western Peninsular Malaysia

Field of Study: **Geology**

I do solemnly and sincerely declare that:

(1) I am the sole author/writer of this Work;
(2) This Work is original;
(3) Any use of any work in which copyright exists was done by way of fair dealing and for permitted purposes and any excerpt or extract from, or reference to or reproduction of any copyright work has been disclosed expressly and sufficiently and the title of the Work and its authorship have been acknowledged in this Work;
(4) I do not have any actual knowledge nor do I ought reasonably to know that the making of this work constitutes an infringement of any copyright work;
(5) I hereby assign all and every rights in the copyright to this Work to the University of Malaya ("UM"), who henceforth shall be owner of the copyright in this Work and that any reproduction or use in any form or by any means whatsoever is prohibited without the written consent of UM having been first had and obtained;
(6) I am fully aware that if in the course of making this Work I have infringed any copyright whether intentionally or otherwise, I may be subject to legal action or any other action as may be determined by UM.

Candidate's Signature Date:

Subscribed and solemnly declared before,

Witness's Signature Date:
Name: **Prof. Dr. Azman A. Ghani**
Designation:

EARLY TO MIDDLE PALEOZOIC VOLCANISM

OF WESTERN PENINSULAR MALAYSIA

ABSTRACT

This study reports new whole-rock major and trace elements data with zircon U-Pb age and Lu-Hf isotope data from the Early to Middle Paleozoic meta-volcanic rocks in Western Peninsular Malaysia, consisting of Gerik-Dinding meta-volcanic rocks, meta-dolerite intrusions and Rephens meta-volcanic rocks. The Early Paleozoic meta-volcanic rocks are represented by the Gerik-Dinding meta-volcanic rocks, which crystallized in the Early to Middle Ordovician (480-460 Ma). They are comparable to high-K calc-alkaline rhyolite and enriched in Th, U, and light rare-earth elements (LREEs). They are also depleted in Nb, Ta, Ti, and P, which are typically observed in arc-related rocks. Their zircon $\varepsilon Hf_{(T)}$ values vary from +0.85 to −15.7, with T_{DM2} ages from 1.3 to 2.4 Ga. Accordingly, the meta-volcanic rocks are interpreted as resulting from the partial melting of Mid-Mesoproterozoic to Mid-Paleoproterozoic crustal material with minor mantle-derived material. We propose that the Gerik-Dinding meta-volcanic rocks were formed in a lithospheric delamination tectonic setting following the crustal thickening from the final amalgamation of Asian micro-continental fragments (AMF) onto the East Gondwana Proto-Tethys margin. Meta-dolerite intrusions that occur irregularly on Western Peninsular Malaysia are associated with Early Paleozoic meta-sedimentary formations and could be constrained to Late Cambrian until Early Silurian (500-430 Ma). They have weak to absent Nb-Ta negative anomalies on the primitive mantle normalized spidergram, low La/Nb (<2), low Th/Ce and low Th/La, which suggest the absence of subduction signature. Their trace element geochemical data patterns, supported by tectonic discrimination plot, indicate that the magma was likely emplaced in an active continental rift or a within-plate setting. The lithospheric delamination event (475-460

Ma) in East Gondwana following the continental collision with AMF and lithospheric thickening may have caused an extensional regime at the East Gondwana Proto-Tethys margin, which permitted the meta-dolerite magma to intrude into the thinned continental crust. The Middle Paleozoic meta-volcanic rocks are represented by the Rephens meta-volcanic rocks, which crystallized in the Early Carboniferous (~342 Ma and ~354 Ma). Two types of Rephens meta-volcanic rocks have been observed: (1) meta-andesite and (2) meta-lithic tuff. Both meta-volcanic rocks have trace element geochemical features suggesting a subduction-related origin (depletion in Nb, Ti, and P). The meta-andesite zircon $\varepsilon Hf_{(T)}$ values range from +3.4 to +10.3, with T_{DM2} ages from 0.6 to 1.1 Ga while the meta-lithic tuff zircon $\varepsilon Hf_{(T)}$ values vary from +10.5 to −13.9, with T_{DM2} ages from 0.7 to 2.2 Ga. The formation age of the meta-volcanic rocks coincides with extension magmatic event (365-330 Ma) from the prolonged southern Paleo-Tethys Ocean subduction. The roll-back of Paleo-Tethys oceanic slab may have caused the upwelling of asthenosphere which resulted in the melting of the continental crust.

Keywords: Geology of Western Peninsular Malaysia; Sibumasu; Gondwana tectonic; Zircon U-Pb geochronology; Zircon Lu-Hf isotope

VOLKANISME PALEOZOIK AWAL KE TENGAH

DI BARAT SEMENANJUNG MALAYSIA

ABSTRAK

Kajian ini melaporkan data analisis unsur-unsur major dan unsur-unsur surih serta analisis usia isotop U-Pb dan isotop Lu-Hf zirkon bagi batuan meta-volkanik Paleozoik Awal–Tengah di Barat Semenanjung Malaysia yang terdiri daripada meta-volkanik Gerik-Dinding, intrusi meta-dolerit and meta-volkanik Rephens. Batuan meta-volkanik Paleozoik awal ini diwakili oleh meta-volkanik Gerik-Dinding, yang terbentuk semasa usia Ordovisi Awal ke Ordovisi Tengah (480-460 Ma). Meta-volkanik ini mempunyai persamaan dengan batuan riolit kalk-alkali tinggi yang dicirikan dengan kelimpahan unsur Th, U, dan unsur-unsur nadir bumi ringan (LREEs) serta jelas menunjukkan penyusutan unsur Nb, Ta, Ti, dan P yang biasanya diperhatikan pada ciri-ciri geokimia batuan igneus arka. Perbezaan nilai $\varepsilon Hf_{(T)}$ zirkon meta-volkanik dari +0.85 hingga -15.7, dengan usia T_{DM2} dari 1.3 hingga 2.4 Ga menggambarkan batuan meta-volkanik ini terhasil daripada leburan separa kerak benua Mesoproterozoik Tengah ke Paleoproterozoik Tengah dengan sedikit bahan daripada batuan mantel. Dicadangkan bahawa meta-volkanik Gerik-Dinding ini terbentuk dalam sekitaran tektonik delaminasi litosfera berikutan penebalan kerak hasil daripada pelanggaran fragmen benua-mikro Asia (AMF) dengan Gondwana Timur pada sempadan Lautan Proto-Tethys. Intrusi tidak sekata meta-dolerit yang dicerap di Barat Semenanjung Malaysia boleh dikaitkan dengan formasi meta-sedimen Paleozoik Awal dan dianggarkan berusia Kambria Lewat sehingga Silures Awal (500-430 Ma). Meta-dolerit ini dicirikan dengan nisbah unsur La/Nb (<2), Th/Ce dan Th/La yang rendah serta menunjukkan anomali negatif unsur Nb-Ta yang sangat kecil pada plot diagram labah-labah yang dinormalkan dengan nilai mantel primitif, yang mana tidak menunjukkan ciri-ciri geokimia zon subduksi. Corak data

geokimia unsur-unsur surih disokong dengan plot diskriminasi tektonik menunjukkan bahawa magma meta-dolerit ini mungkin terhasil dalam sekitaran tektonik ekstensi kerak aktif atau sekitaran magmatic antara-plet. Episod delaminasi litosfera (475-460 Ma) di Gondwana Timur berikutan pelanggaran benua dengan AMF dan penebalan litosfera mungkin telah menyebabkan ekstensi kerak pada batas Lautan Proto-Tethys Gondwana Timur, seterusnya membolehkan magma meta-dolerit untuk menerobos ke dalam kerak benua yang telah nipis. Batuan meta-volkanik Paleozoik Tengah diwakili oleh meta-volkanik Rephens yang terbentuk semasa Karbon Awal (~342 Ma dan ~354 Ma). Dua jenis batu meta-volkanik Rephens dicerap: (1) meta-andesit dan (2) meta-tuf litik. Kedua-dua batu meta-volkanik ini mempunyai ciri-ciri geokimia unsur surih yang menggambarkan asalan tektonik subduksi (penyusutan unsur Nb, Ti, dan P). Nilai $\varepsilon Hf_{(T)}$ zirkon meta-andesit menunjukkan julat dari +3.4 hingga +10.3, dengan usia T_{DM2} dari 0.6 ke 1.1 Ga manakala nilai $\varepsilon Hf_{(T)}$ zirkon meta-tuf litik menunjukkan variasi dari +10.5 ke -13.9, dengan usia T_{DM2} dari 0.7 hingga 2.2 Ga. Usia pembentukan kedua-dua jenis batu meta-volkanik ini selaras dengan episod ekstensi kerak (365-330 Ma) hasil daripada subduksi Lautan Paleo-Tethys yang berterusan ke arah selatan. Kemungkinan semasa episod ekstensi, episod penggolekkan plet Lautan Paleo-Tethys ke belakang mungkin telah menyebabkan kenaikan astenosfera yang seterusnya mengakibatkan peleburan kerak benua.

Kata Kunci: Geologi Barat Semenanjung Malaysia; Sibumasu; Tektonik Gondwana; Usia isotop U-Pb zirkon; Isotop Lu-Hf zirkon

ACKNOWLEDGEMENTS

This work is partly sponsored by UM/MOHE High Impact Research Grant (UMC/HIR/MOHE/SC/27). The completion of this thesis could not have been possible without the participation and assistance of so many people whose names may not all be enumerated. Their contributions are sincerely appreciated and gratefully acknowledged. However, I would like to express my sincere appreciation particularly to the following:

- My supervisor, Professor Dr. Azman Abdul Ghani for his guidance and support. His comments and suggestions have contributed to the success of this research.
- University Malaya Department of Geology Assistant Science Officer, Mr. Zamrut Daunar for his help and guidance during thin section preparation.
- The former and current staff at Department of Geology, University Malaya for their various forms of support during my graduate study.
- National Taiwan University and Academia Sinica geochemistry lab managers, Professor Dr. Sun-Lin Chung and Dr. Hao-Yang Lee, and assistants, Ms. Terri Tang, Ms. Chiu-Hong Chu and Ms. Chien-Hui Hung for their support with the major and trace elements analysis and zircon U-Pb and Lu-Hf analysis.
- National Taiwan University Scholars Dr. Xiao Ran Zhang, Dr. Ping Ping Liu, Ms. Yu-Hsiang Chien, Dr. Shan Li and Dr. Yu-Ming Lai (currently National Taiwan Normal University) for scientific discussions.
- My colleagues, Mr. Muhammad Hatta Roselee, Mr. Muhammad Hafifi Badruldin, Mr. Muhammad Afiq Muhammad Ali, Mr. Galih Yudha Kuswandaru, Mr. Rezal Rahmat, Ms. Azmiah Jamil, Ms. Fatin Nur Diana for beneficial scientific discussion throughout the thesis works. Thanks for the friendship and memories.
- My parents, Mr. Quek Weng Kim and Mrs. Tan Wat Jin for their continuous encouragement, moral and financial support.

TABLE OF CONTENTS

LIST OF FIGURES

LIST OF TABLES

LIST OF APPENDICES

CHAPTER 1: INTRODUCTION

1.1 Research Introduction

Present-day Western Peninsular Malaysia, together with Western Yunnan, the Shan States of Burma, Northwest Thailand, Peninsular Burma and Thailand and Northwest Sumatra, share comparable geological history and are situated on a mass of continental crust known as the Sibumasu Terrane (Figure 1.1). The Sibumasu Terrane was one of the main terranes along East Gondwana Proto-Tethys margin in the Early Paleozoic, a significant period in the final assembly of East Gondwana (Meert, 2003; Cawood and Buchan, 2007). Reconstruction of the East Gondwana Proto-Tethys margin during the Early Paleozoic (530-470 Ma) reveal a series of terranes (e.g. Sibumasu, Lhasa, Himalaya, Qiangtang and Asian micro-continental fragments) which are at present located in South Asia, East Asia and South East Asia (Cawood et al., 2007; Zhu et al., 2012; Lin et al., 2013; Hu et al., 2015; G. Li et al., 2015; Li et al., in press) (Figure 1.2). The unique Cambrian Gondwanaland faunas with northwest Australian affinities of the Sibumasu Terrane indicate that it was adjacent to northwest Australia during Early Paleozoic (Burrett and Stait, 1986; Torsvik and Cocks, 2009; Metcalfe, 2013b).

Most works suggested a subduction zone was present at the East Gondwana Proto-Tethys margin, and the widespread Early Paleozoic magmatism associated with these terranes in the margin was related to the subduction of the Proto-Tethys Ocean under the margin and the collision accretion of outboard Asian micro-continental fragments onto the margin (Cawood et al., 2007; Liu et al., 2009; Zhu et al., 2012; Hu et al., 2013, 2015; Li et al., 2016, Zhao et al., 2017). Although previously there are other studies that proposed that these magmatic rocks were produced in a post-collision extensional setting in reaction to the final assembly of Gondwana supercontinent (Murphy and Nance, 1991; Miller et al., 2001; Xu et al., 2005, 2014; Song et al., 2007; Hu et al., 2010; Liu et al.,

2012; Lin et al., 2013; Pan et al., 2012; Yang et al., 2012), evidences from new structural geology and zircon data are inclined to support the Proto-Tethys subduction hypothesis for the magmatism origin (Hu et al., 2015).

The studies of Early Paleozoic magmatic rocks related to the evolution of East Gondwana Proto-Tethys margin on Sibumasu Terrane are mostly limited to Western Yunnan (Y. Wang et al., 2013; Dong et al., 2013; Xing et al., 2015; Zhao et al., 2017) and north of Peninsular Thailand (Lin et al., 2013; Kawakami et al., 2014). Although there are several field reports of probable Early Paleozoic meta-volcanic rocks in Western Peninsular Malaysia (Jones, 1970, 1973; Hutchison, 1973a), studies in Peninsular Malaysia during the past decade are generally focused on the subsequent Mesozoic crustal forming orogeny event. Complete geochemical data and absolute isotope age for the Early Paleozoic meta-volcanic rocks are still lacking.

During Middle Paleozoic, the Paleo-Tethys Ocean began to open at the East Gondwana margin and was already a wide ocean around the equator during Middle Devonian (Metcalfe, 2011, 2013b). At the same time, the Paleo-Tethys Ocean was being consumed at a north-dipping subduction beneath the Hun superterrane (Stampfli and Borel, 2002), Kazakhstan (Metcalfe, 2011), and North China (Pan et al., 2004). Recent reliable study discovered Middle Paleozoic magmatism (Zhu et al., 2013) and arc-related detrital zircons (Guo et al., 2016) in the Western Qiangtang Terrane and Southern Lhasa Terrane, which indicate that a subduction zone could have existed along the southern rim of the Paleo-Tethys Ocean. The Sibumasu Terrane, which was still attached to the East Gondwana margin and aligned with the Western Qiangtang Terrane and Southern Lhasa Terrane along the southern rim of the Paleo-Tethys Ocean may have undergone similar tectonic events. However, existing data on the Sibumasu Terrane are restricted and detailed petrological studies on suspected Middle Paleozoic magmatic rocks would be vital in order to resolve this problem.

Considering that the absence of absolute age and comprehensive petrological data impede the understanding of the correlation between the Early to Middle Paleozoic volcanism of Western Peninsular Malaysia and other Early to Middle Paleozoic East Gondwana margin tectonic elements identified in the evolution of Southeast Asia and East Asia, a detailed study on the Western Peninsular Malaysia meta-volcanic rocks has been undertaken. Our in-situ zircon U-Pb geochronology method provide the first robust evidence for the presence of Early to Middle Paleozoic volcanism in Western Peninsular Malaysia. Here, we report new petrography, whole-rock geochemical data, zircon U-Pb ages and Lu-Hf isotope data for the Early to Middle Paleozoic meta-volcanic rocks. The data will be used to discuss the petrogenesis of meta-volcanic rocks, in addition to the tectonic evolution of the Western Peninsular Malaysia part of Sibumasu Terrane at East Gondwana margin during the Early Paleozoic and Middle Paleozoic.

1.2 Aims and Objectives of the Study

This research is primarily intended to understand the petrogenesis and tectonic setting of the Early to Middle Paleozoic meta-volcanic rocks in Western Peninsular Malaysia, consisting of Gerik-Dinding meta-volcanic, meta-dolerite intrusions and Rephens meta-volcanic. In-depth understanding of these geological units were generally lacking from previous literature. Below are the research objectives of this thesis:

1. To study the petrography and geochemistry of the meta-volcanic rocks.
2. To determine the absolute age and source of the meta-volcanic rocks through zircon U-Pb isotope geochronology and in-situ zircon Lu-Hf-isotope.
3. To interpret the possible geotectonic conditions for the meta-volcanic rocks using immobile element geochemistry and synthesize the Early to Middle Paleozoic tectonic history of Western Peninsular Malaysia by correlating this data with other identified similar tectonic elements from regional tectonic setting.

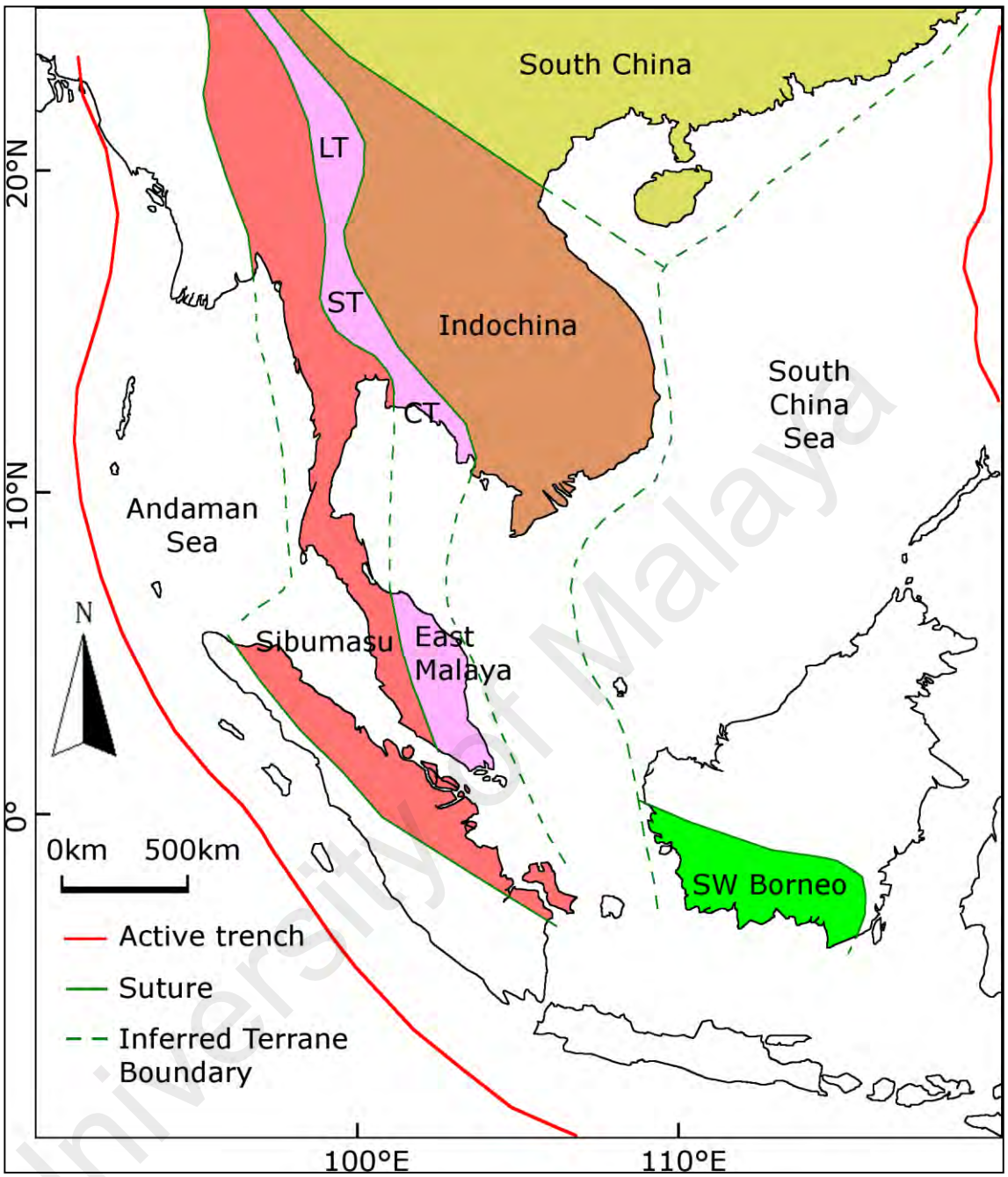

Figure 1.1: Present-day distribution of continental blocks, fragments and terranes derived from Gondwana in Southeast Asia. LT = Lincang Terrane, ST = Sukhothai Terrane and CT = Chanthaburi Terrane. Diagram is modified after Metcalfe (2013).

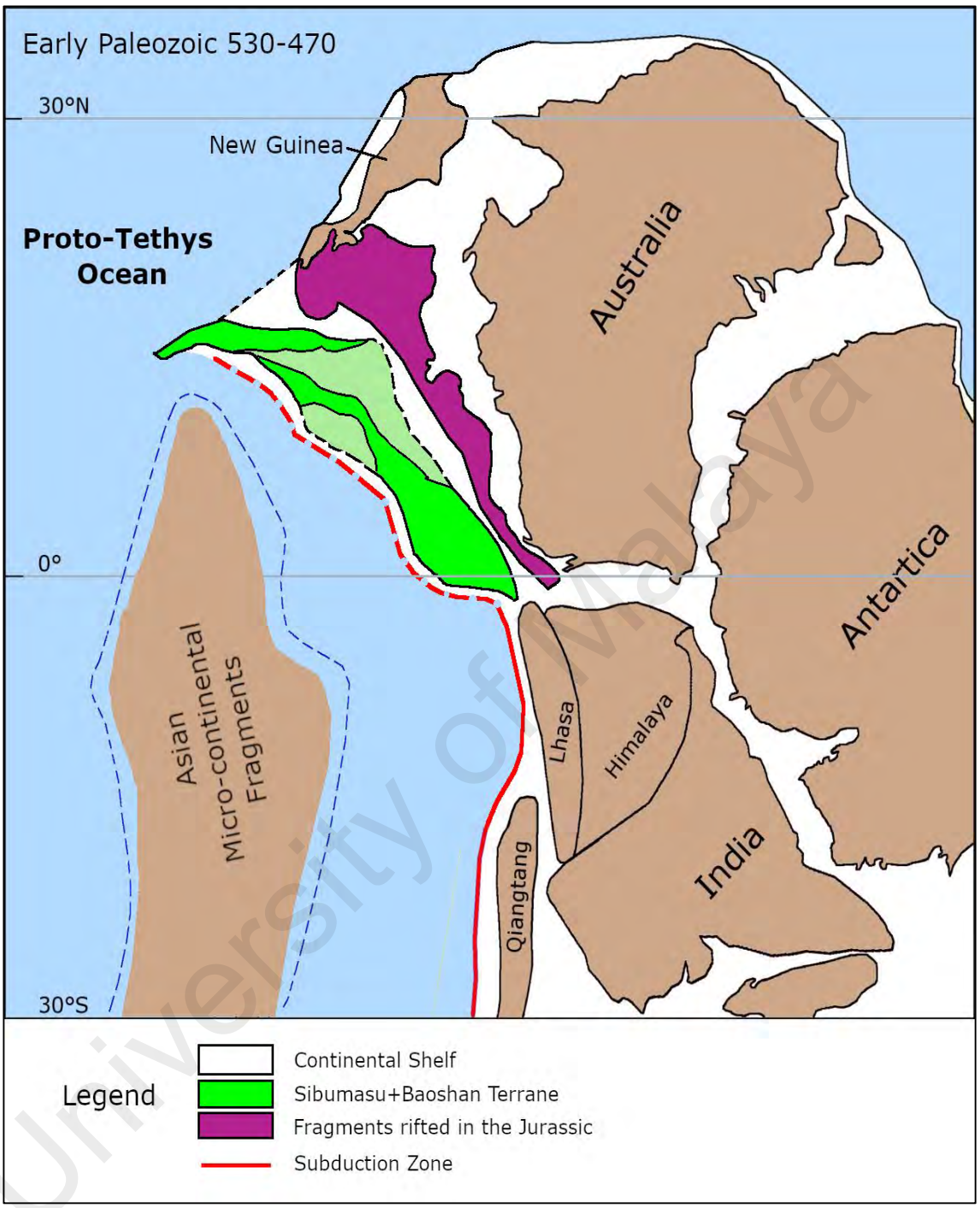

Figure 1.2: Early Paleozoic (530-470 Ma) paleogeographic reconstruction of the East Gondwana margin showing the terranes on its margin. Sibumasu, Lhasa and Qiangtang terranes are located at the north of the margin. Diagram is modified after Hu et al. (2015) and G. Li et al. (2015). Fragments inboard of Sibumasu which rifted later in the Jurassic from the Australian Gondwana margin are from Ali and Aitchison (2012), Ali et al. (2013) and Hall (2012).

1.3 General Geology

The Southeast Asia continental blocks are comprised of a collection of allochthonous continental fragments and volcanic arcs joined together during the Late Paleozoic and Mesozoic as a results of separation of continental fragments from the East Gondwana margin and successive opening and closure of the Tethyan Ocean basins (Metcalfe, 2000). Malaysia, covering a land area of 329,613 km^2, is situated in the heart of the Southeast Asia (Figure 1.2). Malaysia contains two regions: Peninsular Malaysia (131,532 km^2) which lies on the southeastern end of Asia continent, and the states of Sabah (73,631 km^2) and Sarawak (124,450 km^2) on the northwestern coast of Borneo Island. Peninsular Malaysia consists of two distinct tectonic blocks derived from the East Gondwana margin, the Sibumasu Terrane and the Indochina-East Malaya Block (Metcalfe, 1996, 2011, 2013a, 2013b) (Figure 1.3). The western half of the peninsula represents part of the Sibumasu Terrane, while the eastern half of the peninsula represents part of the Indochina-East Malaya Block.

In Peninsular Malaysia, the two tectonic blocks are separated by the Bentong-Raub suture zone (Figure 1.3), which is primarily composed of mélange with sheared mud/silt matrix containing a variety of clasts, including oceanic ribbon-bedded cherts, metamorphosed mudstones and rhythmites, limestone, sandstone, conglomerate and volcaniclastic rocks, and several isolated and small bodies of serpentinite (Hutchison, 1975; Metcalfe, 2000, 2013a, 2013b). The Bentong-Raub suture zone is interpreted to contain a segment of the closed Eastern Paleo-Tethys Ocean (Metcalfe, 2000, 2011, 2013a, 2013b; Sone and Metcalfe, 2008). The closing of the Eastern Paleo-Tethys Ocean was widely accepted to have initiated by the Late Paleozoic to Early Mesozoic subduction under the Indochina-East Malaya Block and subsequent Late Triassic continental collision with the Sibumasu Terrane (Sevastjanova, et al. 2011; Metcalfe, 2002, 2013a, 2013b, Ng et al., 2015b).

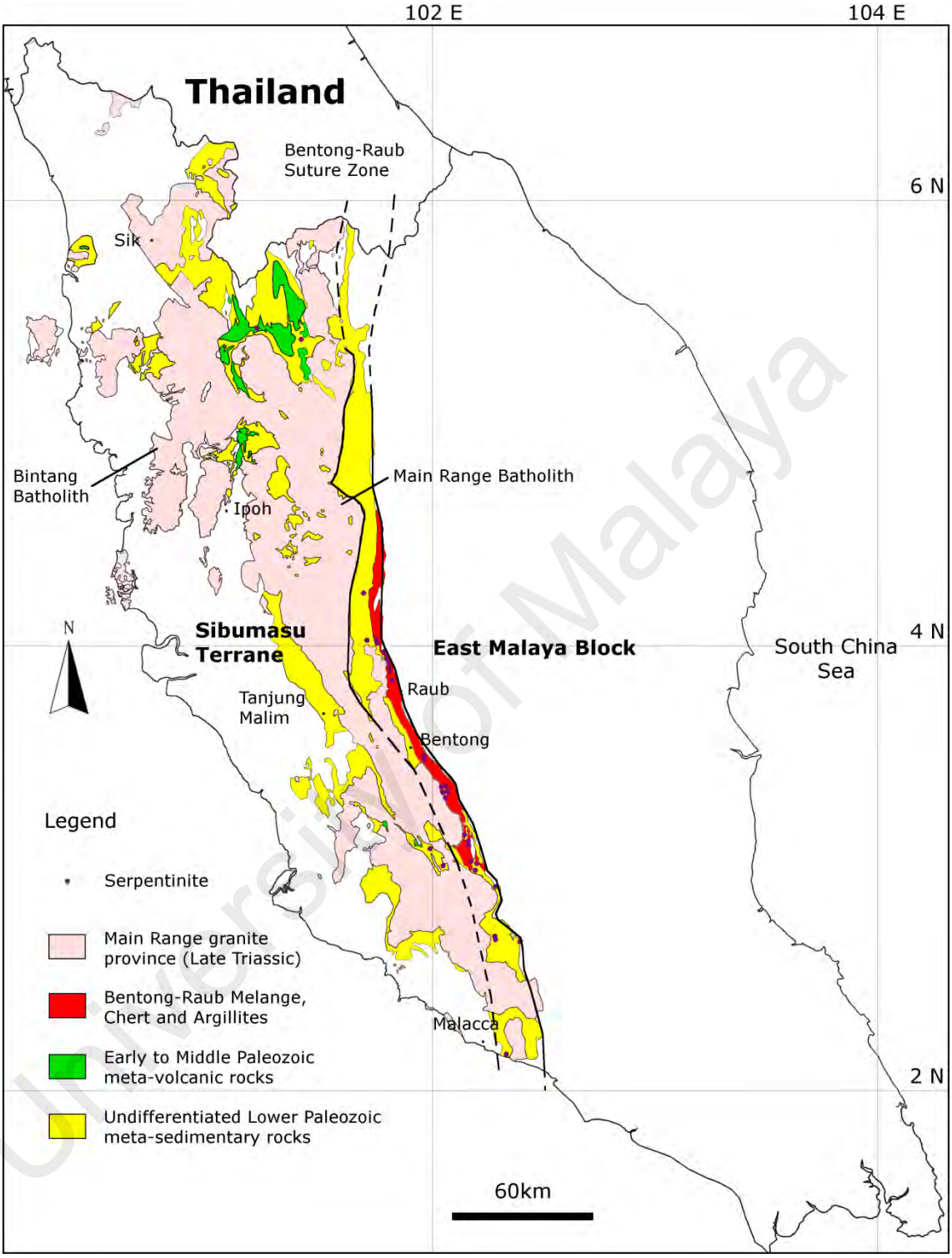

Figure 1.3: Map showing the geology of Western Peninsular Malaysia. The map shows the granitoids of the Main Range granite province, Bentong-Raub suture rocks, Early to Middle Paleozoic meta-volcanic rocks and undifferentiated Lower Paleozoic meta-sedimentary rocks. Only the Sibumasu Terrane part is shown. Diagram is modified after Hutchison (1973a, 1973b).

Peninsular Malaysia contains numerous mountain ranges running parallel from north to south along the peninsula (Figure 1.4). The largest mountain range in Peninsula is the Titiwangsa Mountain Range (a part of the Tenasserim Hills system) and may possess peaks around 2000 m high (Tjia, 1973). Mountains in the Titiwangsa Mountains Range and west peninsula are mainly granite of the Late Triassic (201-227 Ma) Main Range granite province (Figure 1.3). The petrogenesis of the Main Range granite province is related to the Late Triassic Sibumasu Terrane and Indochina-East Malaya Block collision event (Searle et al., 2012; Oliver et al., 2014; Ghani et al., 2013; Ng et al., 2015a, 2015b; Quek et al., 2015, 2017; Jamil et al., 2016). The Main Range batholith and Bintang batholith represent two main intrusive phases within the Main Range granite province. The Early to Middle Paleozoic meta-volcanic rocks studied in this thesis are primarily exposed at the western flank of the Main Range batholith and eastern flank of the Bintang batholith (Figure 1.3).

Most studied Early Paleozoic meta-sedimentary rocks of the Western Peninsular Malaysia include a series of well-defined, weakly metamorphosed sedimentary deposits that was initiated in the Late Cambrian and can be traced to the Early Devonian (Jones 1973). They are suggested to show Gondwana biogeographic affinities (Sevastjanova et al. 2011) and can be traced up to Myanmar and Yunnan, China in the north (Jones 1973). Presence of Early Permian glacio-marine diamictites indicate that Western Peninsular Malaysia was attached to the East Gondwana margin until its separation during the Early Permian (Metcalfe, 1996)[1]. Associated with the Early Paleozoic meta-sedimentary rock belt are acid to intermediate Early to Middle Paleozoic meta-volcanic rocks and meta-dolerite intrusions (Jones 1970, 1973). The meta-volcanic rocks primarily outcrop at the north while the meta-dolerite intrusions occur as isolated outcrops (Jones 1970, 1973).

[1] Although Metcalfe (1996) supported this with tectono-stratigraphical similarities between Sibumasu and the Canning Basin of NW Australia, the distance between them before the Permian would have been very large and comparison with much further northeast in the NW Shelf would be more appropriate.

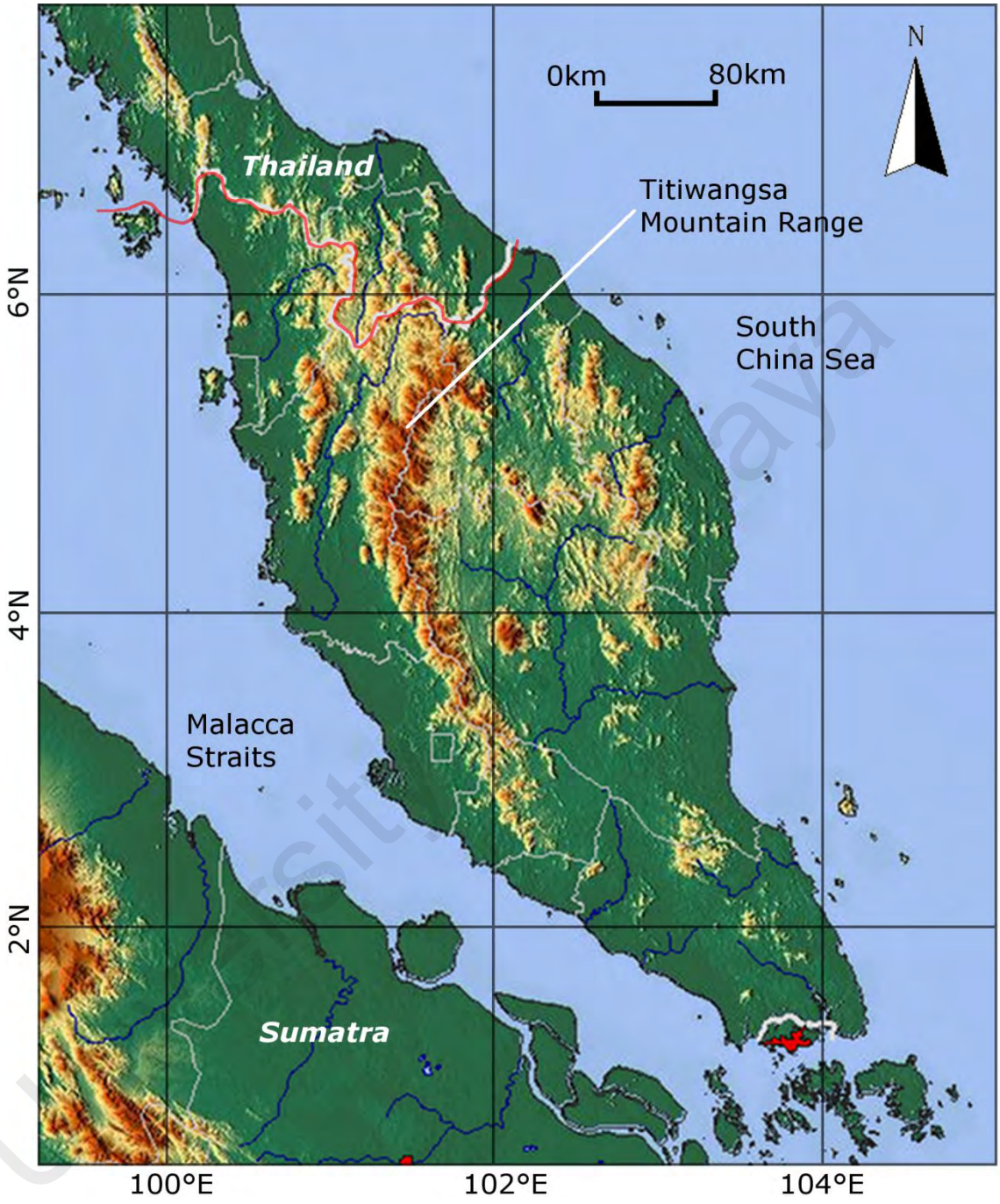

Figure 1.4: Topography map of Peninsular Malaysia**.** Numerous mountain ranges can be seen running parallel from north to south along the peninsula.

CHAPTER 2: LITERATURE REVIEW

2.1 Introduction

This chapter will discuss the previous literature on the Early to Middle Paleozoic volcanism and meta-dolerite intrusions in Western Peninsular Malaysia, as well as the East Gondwana margin tectonics during Early to Middle Paleozoic

2.2 Volcanism in Western Peninsular Malaysia

The volcanic rocks in Western Peninsular Malaysia can be generally separated into Early to Middle Paleozoic and Late Triassic. The Early to Middle Paleozoic volcanic rocks are represented by the Early Paleozoic Gerik-Dinding meta-volcanic rocks (Jones, 1970, 1973; Hutchison, 1973a) (Figure 2.1) and the Middle Paleozoic Rephens meta-volcanic rocks (Shu, 1989) (Figure 2.1). The Gerik-Dinding meta-volcanic rocks are well exposed at the northern end of Western Peninsular Malaysia, while the Rephens meta-volcanic rocks are restricted to the southern end of Western Peninsular Malaysia. Based on apparent stratigraphic position, the relative age of the Gerik-Dinding meta-volcanic rocks is suggested to be Ordovician (Jones, 1970, 1973), while the relative age for Rephens meta-volcanic rocks is suggested to be somewhere between Devonian to Carboniferous (Shu, 1989).

The Late Triassic volcanic rocks are represented by the Genting Sempah volcanic rocks (Figure 2.1), which is associated with the Late Triassic Main Range granite province granitoid (Liew, 1983; Ghani and Singh, 2005; Ng et al., 2015a, 2015b). The two main rock types present in Genting Sempah volcanic rocks are rhyolite and orthopyroxene rhyodacite (Liew, 1983; Ghani and Singh, 2005). Ghani and Singh (2005) reported the rhyolite to be a hypidiomorphic holocrystalline rock consisting of phenocrysts of quartz, plagioclase, biotite and alkali-feldspar set in an aphanitic glassy

groundmass. On the other hand, the orthopyroxene rhyodacite contain phenocrysts of quartz, plagioclase, biotite, alkali-feldspar and orthopyroxene set in a slightly coarser-grained groundmass consisting of quartz and alkali feldspar. Geochemically, both rhyolite and orthopyroxene rhyodacite are peraluminous, high-K calc-alkaline and display S-type affinities (Ghani and Singh, 2005). Ng et al. (2015b) zircon U-Pb analysis on the Genting Sempah volcanic rocks dated the volcanic rocks at ~226 Ma.

2.2.1 Early Paleozoic Gerik-Dinding meta-volcanic rocks

The outcrops of the Early Paleozoic Gerik-Dinding meta-volcanic rocks are located to the west of the Bentong-Raub suture zone, at the western foothills of Main Range batholith and eastern foothills of Bintang batholith. The occurrence of the Gerik-Dinding meta-volcanic rocks was first reported by Jones (1970) in Gerik, Perak. Jones (1970) estimated the maximum thickness of Gerik-Dinding meta-volcanic rocks strata to be around 1830 m. Sub-schistose to schistose texture present on the meta-volcanic rock is imposed by several regional metamorphism events which post-date the volcanism. In general, the metamorphism grade of the Gerik-Dinding meta-volcanic rocks is no higher than greenschist facies, although higher temperature metamorphic minerals (e.g. garnet and andalusite) may develop as a result of contact metamorphism with the younger Late Triassic Main Range granite province granitoid. Meta-sedimentary rocks deposited contemporaneously with the Gerik-Dinding meta-volcanic rocks and metamorphosed lithic tuff indicates that the meta-volcanic rocks were formed by several episodes of explosive volcanism under sub-aerial to marine condition (Jones, 1970; Jones, 1973). No lava flows have been documented with certainty, but fragments of scoriaceous rhyolite resembling flow material and metamorphosed rocks strongly resembling a rhyolite have been recognized (Jones, 1970; Hutchison, 1973a).

Jones (1970) divided the Gerik-Dinding meta-volcanic rocks in the Gerik area into two types: meta-lithic tuff and meta-crystal tuff. The meta-lithic tuff can be divided into calcareous, shaly and sandy, depending on the sedimentary material within the tuff. On the other hand, the meta-crystal tuff is made up of entirely pyroclastic content. The meta-crystal tuff is the most widespread volcanic rock type within Gerik area. The meta-crystal tuff matrix is fine-grained and is composed of quartz, mica, chlorite and iron oxide. Fragments and phenocryst crystals of quartz, K-feldspar and plagioclase are found within the meta-crystal tuff. Meta-volcanic rock outcrops reported in Sg. Siput area by Jones (1973) and Dinding area by Yew (1971) were later recognized as a part of the Gerik-Dinding meta-volcanic rocks by Hutchison (1973a). Recent petrographic analysis by Ghani (2009) described the meta-volcanic rock from Dinding area as a light gray rock with black streaks and small clots of biotite. Petrographic observation of the Dinding meta-volcanic rocks indicates angular to euhedral phenocryst crystals of quartz and feldspar within a fine-grained flow banded matrix.

2.2.2 Middle Paleozoic Rephens meta-volcanic rocks

The outcrops of the Middle Paleozoic Rephens meta-volcanic rocks are located to the west of the Bentong-Raub suture zone, at the south-western foothills of Main Range batholith. The occurrence of the Middle Paleozoic Rephens meta-volcanic rocks was first reported by Shu (1989) in Kuala Kelawang, Negeri Sembilan. The effects of thermal metamorphism are evident in the Rephens meta-volcanic rocks. Shu (1989) described the Rephens meta-volcanic rocks to consist of at least three volcanic rock type: rhyolite-like volcanic rock, meta-lithic tuff and meta-crystal tuff. The most common Rephens meta-volcanic rock type in the area is the meta-lithic tuff. The rhyolite-like volcanic rock has a completely recrystallized quartz and biotite groundmass with quartz, K-feldspar and plagioclase phenocrysts. On the other hand, the meta-lithic tuff is described as light gray

to dark gray meta-volcanic rock with quartz, feldspar and graphitic material present as its phenocrysts. The further thermal metamorphosed meta-lithic tuff is described as dark gray spotted hornfels with random andalusite crystals. The matrix of the meta-lithic tuff is microcrystalline, generally consisting of quartz, biotite, muscovite and sericite.

2.3 Meta-dolerite intrusions in Western Peninsular Malaysia

Meta-dolerite intrusions of small dimensions are found scattered in the Western Peninsular Malaysia. Although the age of the meta-dolerite cannot be definitely known, Hutchison (1973b) suggested the meta-dolerite intruded earlier than the Late Triassic Main Range granite province (pre-orogenic) and is distinct from the post-granite dolerite dikes in the Eastern Peninsular Malaysia. The meta-dolerite intrusions are hypabyssal and generally take the form of dikes, sills and other small bodies (Jones, 1973). In many reported cases, the meta-dolerite outcrops are interpreted as isolated outcrops as the field relations between two outcrops are extremely difficult to trace (Hutchison, 1973b). The meta-dolerite intrusions were first reported by Roe (1951a, 1951b) in the Fraser Hill area and in the Kuala Selangor and Rasa areas. The meta-dolerite outcrops often have very low relief and are found within or along the side of the rivers. The best exposure of meta-dolerite intrusion is found at Serendah, Kuala Selangor and Rasa area, where the outcrop can be traced for 2.5 km (Roe, 1951b). Roe (1951a, 1951b) suggest that the minor actinolite-epidote and diopside schist associated with the meta-dolerite outcrops are a product from more intense regional metamorphism of the meta-dolerite. Hutchison (1973b) reported the meta-dolerite often contain clinopyroxene with actinolite replacement and secondary epidote. It is suggested the metamorphism grade of all the meta-dolerite in Western Peninsular Malaysia is no higher than greenschist facies.

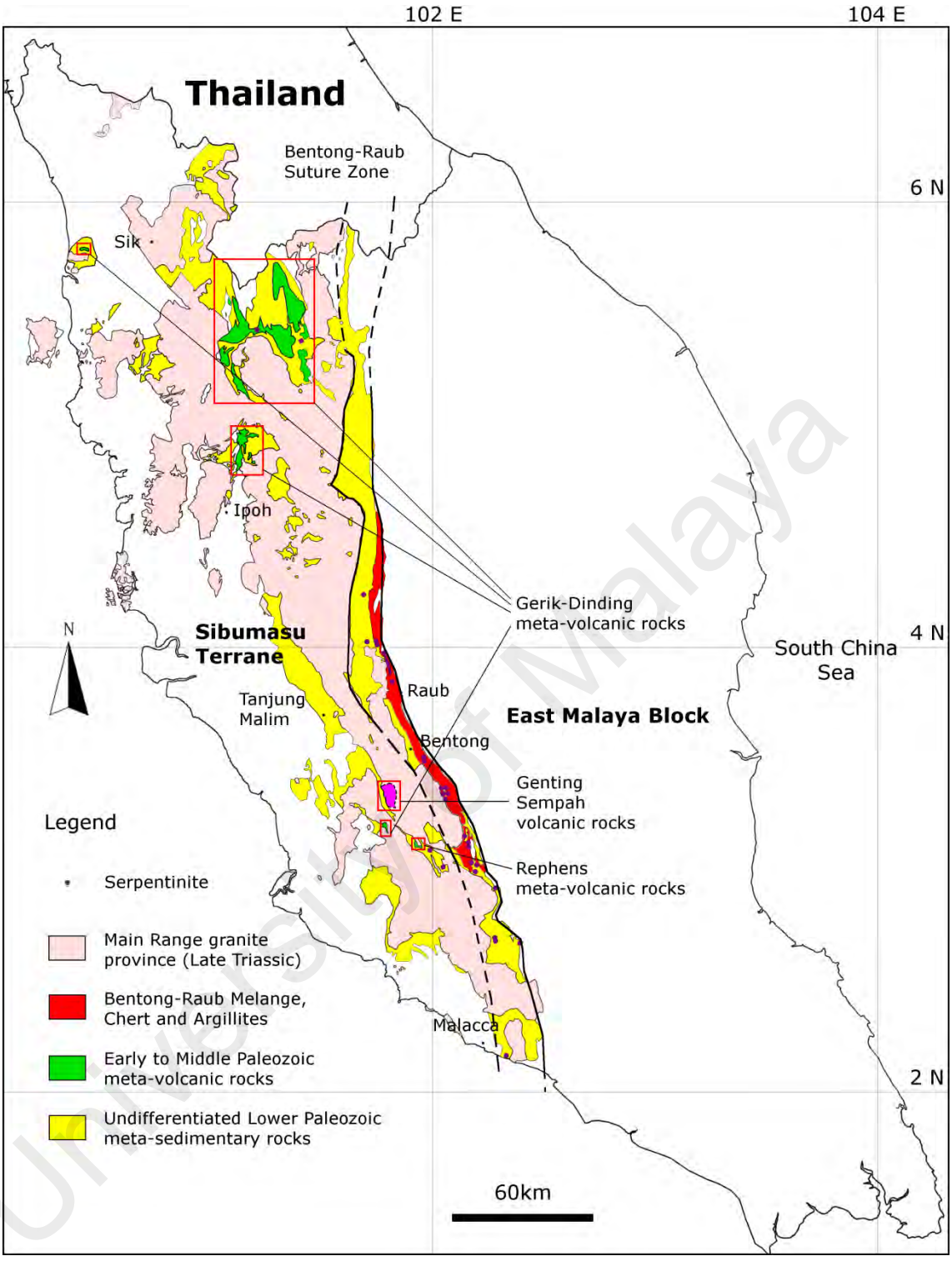

Figure 2.1: The distribution of Western Peninsular Malaysia volcanic rocks. The Gerik-Dinding meta-volcanic rocks are primarily located at the north while the Rephens meta-volcanic rocks are located at the south.

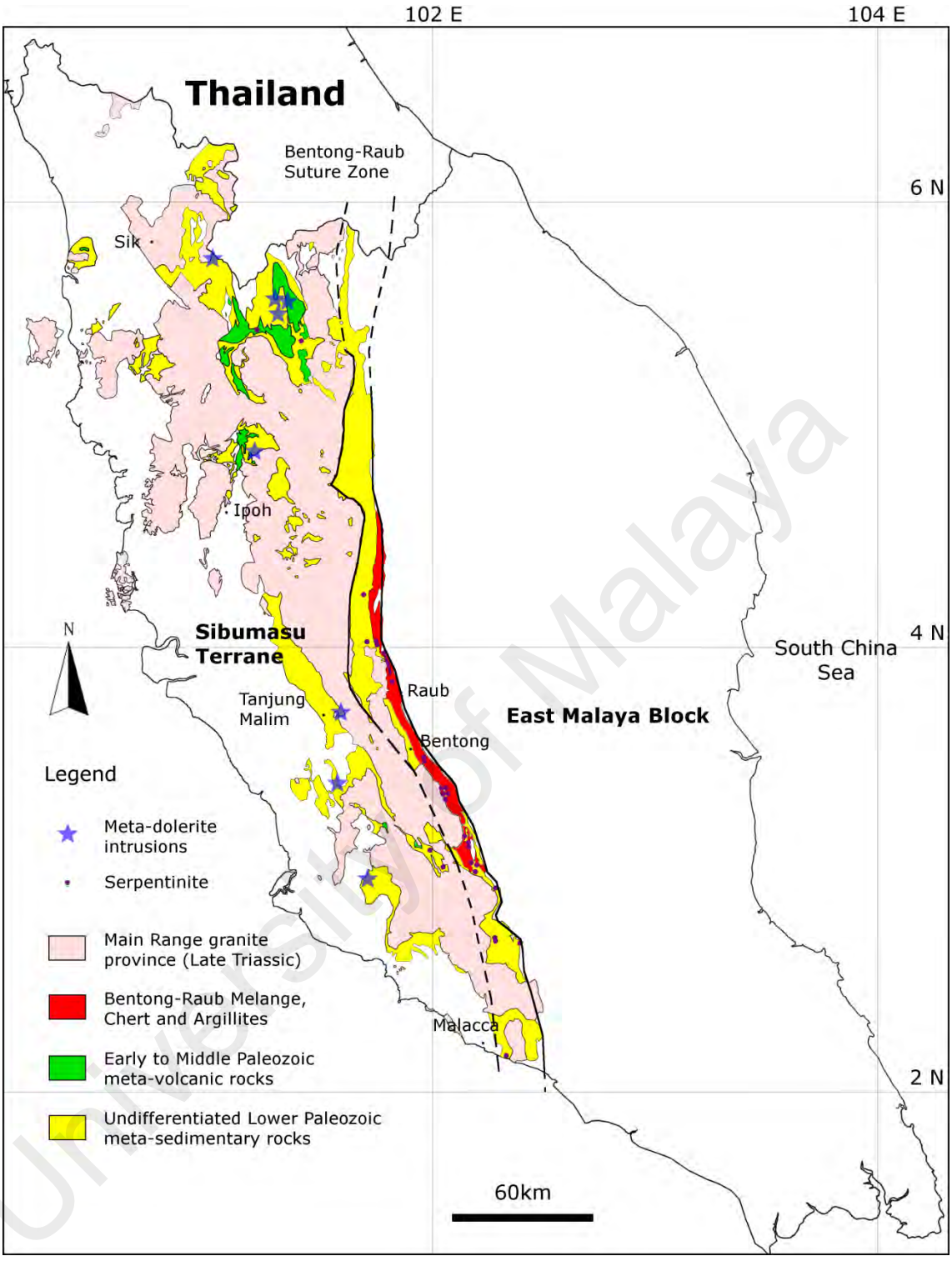

Figure 2.2: The distribution of Western Peninsular Malaysia meta-dolerite. The meta-dolerite is mainly distributed on the foothills of the Main Range batholith.

2.4 East Gondwana tectonics during Early to Middle Paleozoic

Western Peninsular Malaysia, together with Western Yunnan, the Shan States of Burma, Northwest Thailand, Peninsular Burma and Thailand and Northwest Sumatra, are situated on the Sibumasu Terrane, one of the main terranes along the East Gondwana Proto-Tethys margin during Early Paleozoic. The tectonic scenario of the Early Paleozoic magmatism in the series of terranes at the Proto-Tethys margin of East Gondwana (Figure 2.3) has been a highly contested issue for a long time. While Murphy and Nance (1991) suggest they represent a magmatic result of the Gondwana breakup, Meert and Van der Voo (1997) interpreted them as an artifact of collision during the final assembly of Gondwana. Yin and Harrison (2000) were the first to propose that some of the Early Paleozoic magmatic rocks are the product of a subduction zone dipping beneath the Proto-Tethys margin of East Gondwana. Cawood et al. (2007) further elaborated the proposal to suggest a Cambrian-Ordovician Andean-type orogenic event on the Proto-Tethys margin of East Gondwana. The magmatic arc at the margin was active from 530 to 490 Ma and was associated with andesitic and basaltic volcanism. The arc activity overlaps with and is succeeded by regional deformation, crustal melting and S-type granite emplacement that extended to 470 Ma, an age determined through Sensitive High-Resolution Ion Microprobe (SHRIMP) U-Pb isotope analysis on the S-type Lesser Himalayan granite zircons (Cawood et al., 2007).

Cawood et al. (2007) suggestion was supported by Hu et al. (2013) and Ding et al. (2015) reports of Cambrian meta-rhyolite (510-525 Ma) with subduction geochemical signatures in the Lhasa Terrane, and Chen et al. (2004, 2007), Song et al. (2007), Liu et al. (2009), Dong et al. (2013) and Y. Wang et al. (2013) reports of the occurrence of numerous Early Palaeozoic granitoid rocks (490-470 Ma) in the Tengchong-Baoshan region (South Sibumasu Terrane during Early Paleozoic). While studying the Cambrian (ca. 492 Ma) meta-volcanic rocks from a bimodal volcanic suite in the Lhasa Terrane,

Zhu et al. (2012) suggest that the emplacement of the bimodal volcanic rocks and the development of the Cambrian-Ordovician angular unconformity in the central Lhasa Terrane can be attributed to slab break-off of the Proto-Tethys Ocean lithosphere following the collisional accretion of Asian micro-continental fragments located outboard of the magmatic arc. By re-interpreting previous data, the NE Australia Kalkarindji continental flood basalts (Glass and Phillips, 2006; Evins et al., 2009) and the NW High Himalaya Mandi basalts (Miller et al., 2001) from East Gondwana margin, Zhu et al. (2012) suggested the Proto-Tethys Ocean lithosphere underwent slab roll back at ca. 510 Ma before the slab break-off at ca. 492 Ma.

While studying the Early Paleozoic (470-460 Ma) granite magmatism in the Baoshan region, Li et al. (2016) combined their data with data from the other periphery blocks in East Gondwana margin and proposed that the Early Paleozoic post-arc magmatism in the East Gondwana margin were produced in successive stages. Zhao et al. (2016) supported Li et al. (2016) proposal and suggested two stages of a flare-up (ca. 490 Ma and 460 Ma) of the Early Paleozoic magmatism represent different tectonic regimes (slab break-off and lithospheric delamination) along the margin of East Gondwana. The Late Cambrian (ca. 500 Ma) magmas in East Gondwana were probably formed in response to the Proto-Tethys oceanic slab rollback. Subsequently, the slab break-off of the subducting Proto-Tethys Ocean lithosphere may have occurred at 500-490 Ma. The break-off of this slab resulted in asthenospheric upwelling and the underplating of mafic magma, thus inducing partial melting of crustal materials. After that, the crust and lithosphere were thickened at 490-475 Ma. The Middle to Late Ordovician (475-450 Ma) magmas are results from the delamination of an already thickened crust and lithospheric mantle leading to the partial melting of crustal materials. The Proto-Tethys accretionary orogeny was suggested to end at ca. 450 Ma.

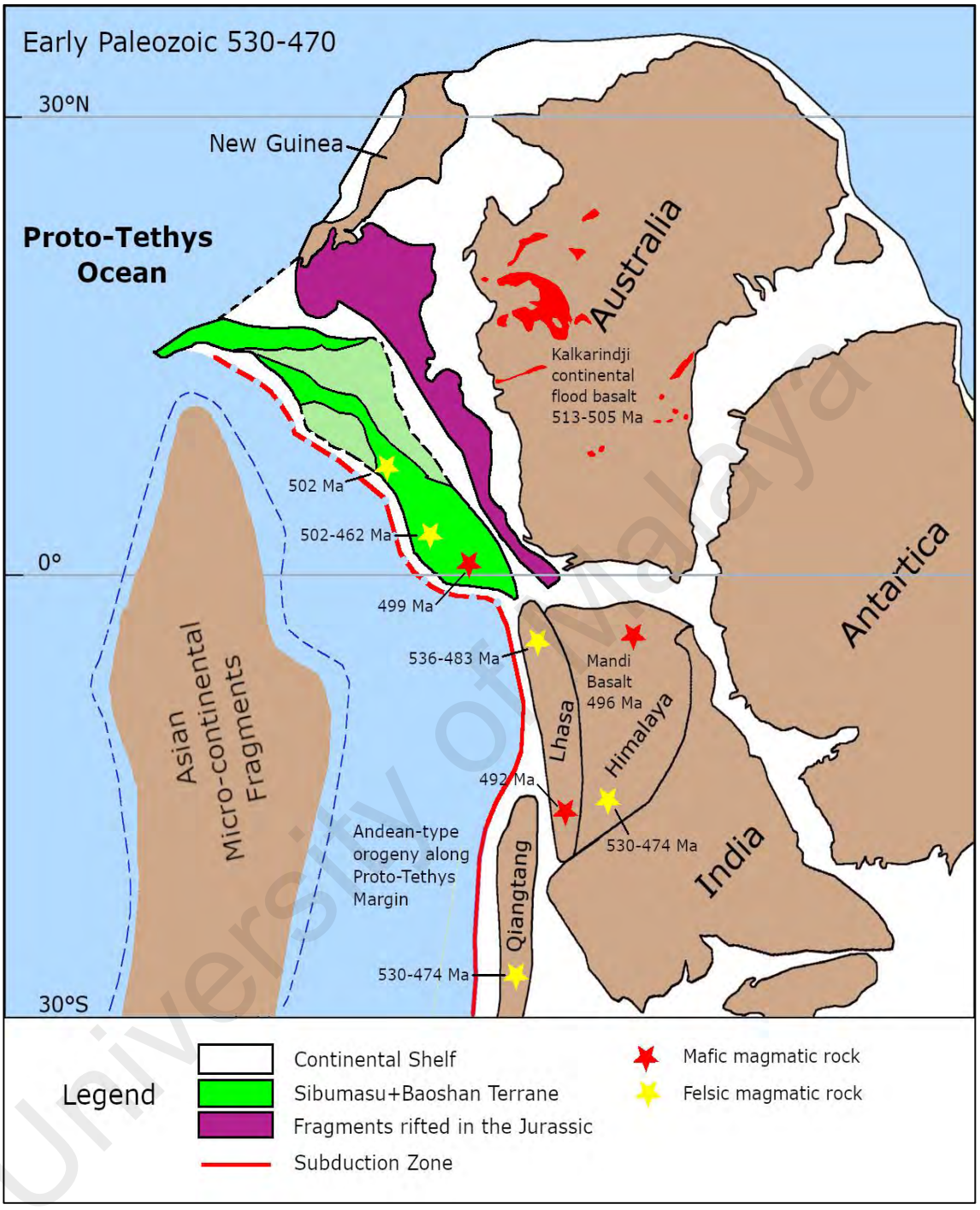

Figure 2.3: The Early Paleozoic (530-470 Ma) reconstruction of East Gondwana margin showing the locations and ages of Early Paleozoic granitoids and volcanic rocks. Isotopic age data sources: Australia (Glass et al., 2006); Burma (Mitchell et al., 2012); and Sibumasu (Metcalfe, 1998; Lin et al., 2013). The source of other isotopic age is listed in Table 2.1

Table 2.1: Source of other Early Paleozoic magmatic age data

Tectonic Terrane	Age (Ma)	Dating method	Reference
Mafic volcanic rocks			
Lhasa	492	Zircon U-Pb	Zhu et al. (2012)
Himalaya	496	Cpx-Plg Sm-Nd	Miller et al. (2001)
Baoshan	499	Zircon U-Pb	Yang et al. (2012)
Silicic volcanic rocks			
Lhasa	492	Zircon U-Pb	Zhu et al. (2012)
	536		Pan et al. (2012)
	525, 511, 510		Hu et al. (2013)
	501		Ji et al. (2009)
	512		Ding et al. (2015)
Granitoids			
Southern Qiangtang	476-471	Zircon U-Pb	Pullen et al. (2011)
	486,480,481		Hu et al. (2015)
Lhasa	510		Gehrels et al. (2011)
	507		Li et al. (2008)
	508		Lee et al. (2000)
Himalaya	484	Monazite U-Pb	Godin et al. (2001)
	484-476	Zircon U-Pb	Gehrels et al. (2003)
	478, 477		Cawood et al. (2007)
	530		Lee and Whitehouse (2007)
	506		Quigley et al. (2008)
	499		Shi et al. (2010)
	499-473		X. X. Wang et al. (2011)
	512-474		Gehrels et al. (2006a)
	484-476		Gehrels et al. (2006b)
	499-490		Zhang et al. (2008)
Baoshan	502-499		Liu et al. (2009)
	472, 466		Chen et al. (2007)
	486-480		Dong et al. (2013)
	473-460		Y. Wang et al. (2013)

After ~450 Ma, the East Gondwana margin was characterized by passive margin evolution (Cawood et al., 2007) that persisted until the Early Devonian, at which time the Paleo-Tethys Ocean began to open. The Paleo-Tethys ocean was already a wide ocean around the equator during the Devonian to Triassic (Metcalfe, 2011, 2013b) and was being consumed at a north-dipping subduction beneath the Hun superterrane (Stampfli and Borel, 2002), Kazakhstan (Metcalfe, 2011), and North China (Pan et al., 2004) in the Devonian. Zhu et al. (2013) suggest the calc-alkaline and metaluminous Late Devonian granitoids (367–364 Ma) revealed in the Western Qiangtang and southern Lhasa subterranes (Mu et al., 2005; Dong et al., 2010b; Pullen et al., 2011) indicate that a subduction zone may have existed along the southern rim of the Paleo-Tethys Ocean. Subsequent Early Carboniferous magmatism (ca. 350 Ma) with geochemical features resulting from varying degrees of mixing between melts derived from the anatexis of mature continental crustal materials and mantle materials (Li et al., 2006) may represent an extensional magmatic event (perhaps from slab roll back), which eventually resulted in the opening of a back-arc oceanic basin. At present, however, the geochemistry and isotope data of Late Devonian to Early Carboniferous magmatic rocks from East Gondwana is still extremely limited (Zhu et al., 2013).

2.5 Chapter Summary

1. The Western Peninsular Malaysia Early to Middle Paleozoic volcanic rocks are represented by the Early Paleozoic Gerik-Dinding meta-volcanic rocks and the Middle Paleozoic Rephens meta-volcanic rocks. The Gerik-Dinding meta-volcanic rocks are well exposed at the northern end of Western Peninsular Malaysia, while the Rephens meta-volcanic rocks are restricted to the southern end of Western Peninsular Malaysia. Based on apparent stratigraphic position, the relative age of the Gerik-Dinding meta-volcanic rocks is suggested to be Ordovician, while the relative age for Rephens meta-

volcanic rocks is suggested to be somewhere between Devonian to Carboniferous. The Gerik-Dinding meta-volcanic rocks in Gerik area can be divided into two types: meta-lithic tuff and meta-crystal tuff. The meta-lithic tuff can be divided into calcareous, shaly and sandy, depending on the sedimentary material within the tuff. On the other hand, the meta-crystal tuff is made up entirely of pyroclastic content. The Rephens meta-volcanic rocks consist of at least three volcanic rock types: rhyolite-like volcanic rock, meta-lithic tuff and meta-crystal tuff.

2. Meta-dolerite intrusions of small dimensions are found scattered in the Western Peninsular Malaysia. These meta-dolerite intrusions are hypabyssal and generally take the form of dikes, sills and other small bodies. Minor actinolite-epidote and diopside schist associated with the meta-dolerite outcrops are a product from more intense regional metamorphism of the meta-dolerite
3. Previous studies suggest that the Early Paleozoic magmatic rocks at the Proto-Tethys margin of East Gondwana were related to the collisional accretion of Asian micro-continental fragments that took place as a result of oceanic subduction (530 to 490 Ma) along the margin. Published data suggest the long-lived early Paleozoic peraluminous magmatism on the margin was activated as a consequence of Proto-Tethys Ocean slab rollback (>500 Ma), slab breakoff (500-490 Ma), lithospheric thickening (490-475 Ma), and lithospheric delamination (475-450 Ma).
4. Due to limited data, the Late Devonian to Early Carboniferous magmatism along the East Gondwana margin is still not well understood. Geochemical evidence suggests a subduction zone may have existed along the southern rim of the Paleo-Tethys Ocean during this period. An extensional magmatic event, perhaps from slab roll back, is suggested to occur subsequently.

CHAPTER 3: RESEARCH METHODOLOGY

3.1 Introduction

The laboratory analyses equipments, methods and materials used in this research will be described in detail in this chapter. All of the rock samples used in this study was personally collected by the author from the field area. The whole-rock major and trace geochemistry and the zircon U-Pb and Lu-Hf isotope analyses were carried out by the author with the assistance of laboratory assistants at Department of Geosciences, National Taiwan University at Taipei, Taiwan and Institute of Earth Sciences, Academia Sinica at Nankang, Taiwan. Only one zircon U-Pb and Lu-Hf isotope analyses were carried out with the help of trained personnel at Arizona LaserChron Center, The University of Arizona, Arizona, United States.

3.2 Sampling Locations

The meta-volcanic rocks from Western Peninsular Malaysia were collected for whole-rock major and trace geochemistry, zircon U-Pb dating and Lu-Hf isotopic analysis (Figure 3.1). The meta-dolerite from Western Peninsular Malaysia was only collected for whole-rock major and trace elements geochemistry analysis, as they did not yield adequate amount of zircons for analysis (Figure 3.2). The coordinates of the meta-volcanic samples collected for zircon U-Pb isotope dating and Lu-Hf isotopic analysis are listed in Table 3.1. The sample locations for geochemistry analyses are listed in Appendix A. The reference coordinate system used for the meta-volcanic sample locations is World Geodetic System 84 (WGS84). To ensure the quality of the interpretation for this study, only non-weathered rock samples were collected for analysis. The sampling process was generally done along the road cut outcrops, rock quarries and headwaters of rivers. Any rock samples that demonstrate heavy weathering were excluded from the study.

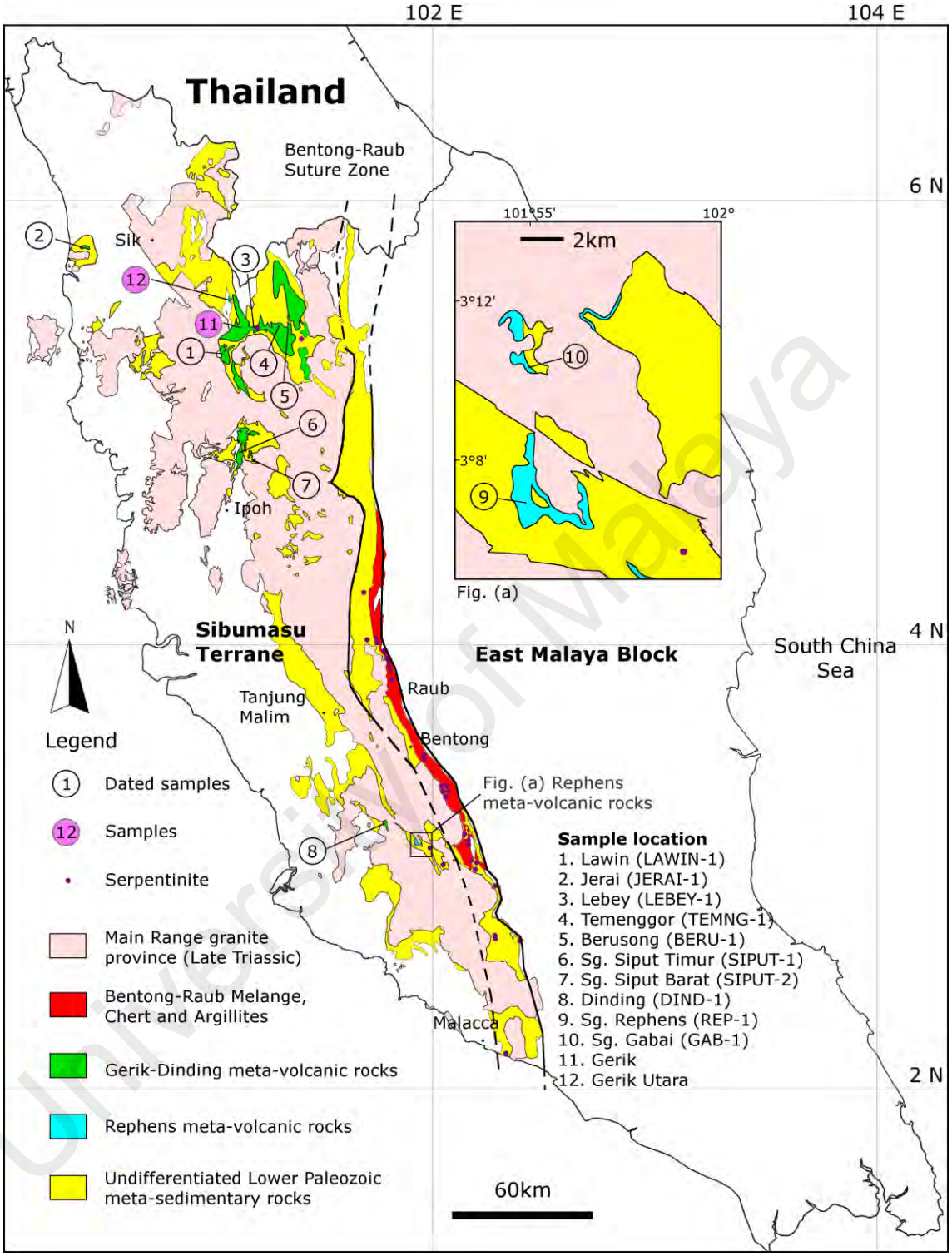

Figure 3.1: The locations of the meta-volcanic rocks samples. The samples are collected for whole-rock major and trace element geochemistry analysis, zircon U-Pb isotope dating and zircon Lu-Hf isotopic analysis.

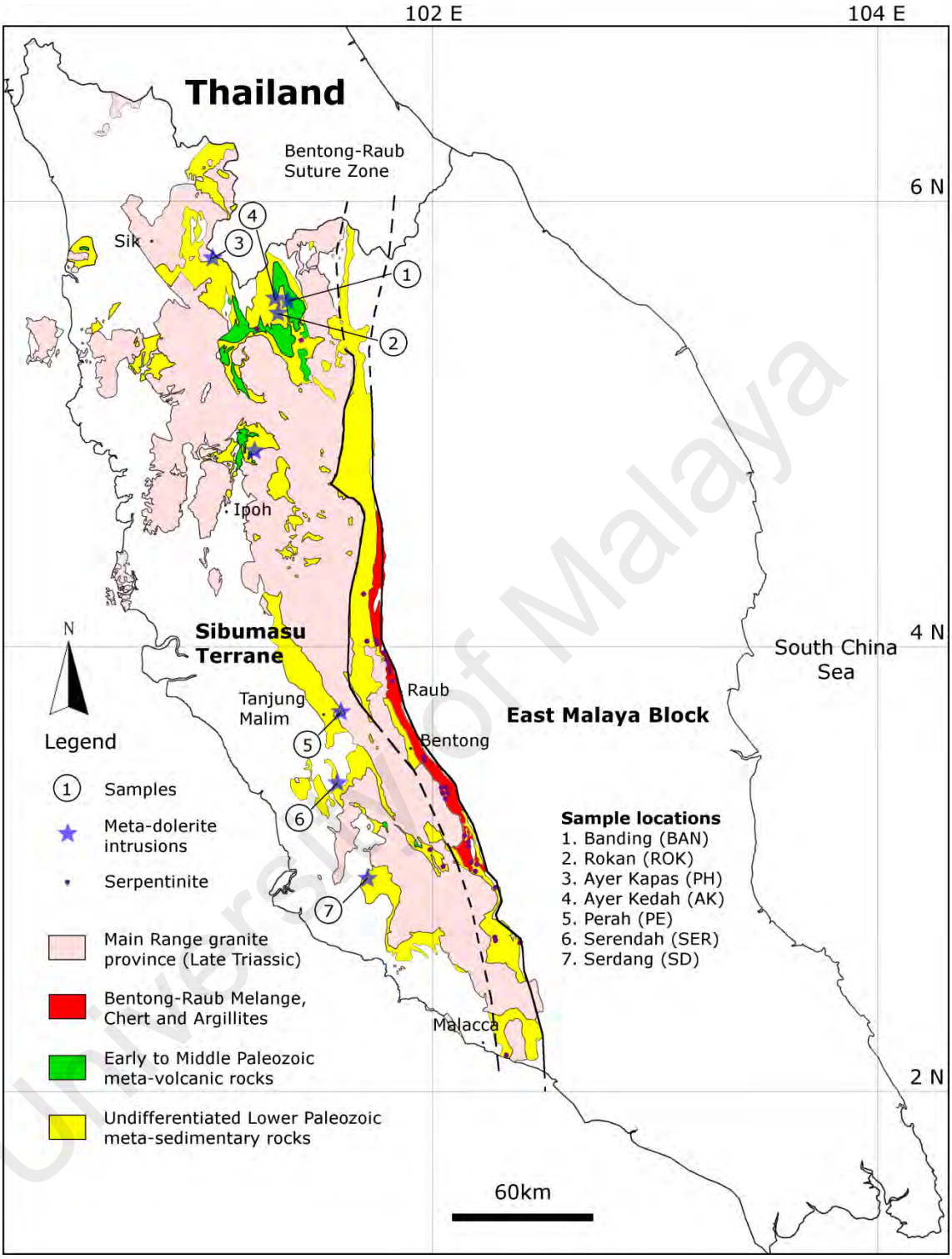

Figure 3.2: The locations of the meta-dolerite samples. The samples are collected for whole-rock major and trace element geochemistry analysis.

Table 3.1: Coordinate of meta-volcanic samples for zircon U-Pb isotope dating

No.	Sample	GPS Coordinate	Rock type	Meta-volcanic rock group
1	LAWIN-1	5.306558N, 101.056318E	Meta-crystal tuff	
2	JERAI-1	5.795970N, 100.437220E	Meta-rhyolite	
3	LEBEY-1	5.433640N, 101.207919E	Meta-crystal tuff	
4	TEMNG-1	5.408730N, 101.299290E	Meta-rhyolite	Gerik meta-volcanic rocks
5	BERU-1	5.393630N, 101.339990E	Meta-rhyolite	
6	SIPUT-1	4.981640N, 101.177450E	Meta-rhyolite	
7	SIPUT-2	4.854770N, 101.134040E	Meta-crystal tuff	
8	DIND-1	3.204780N, 101.777505E	Meta-crystal tuff	
9	REP-1	3.116280N, 101.915670E	Meta-andesite	Rephens meta-volcanic rocks
10	GAB-1	3.173900N, 101.916000E	Meta-lithic tuff	

3.3 Laboratory Analysis

The selected meta-volcanic and meta-dolerite samples for further geochemical and zircon isotope laboratory analyses will first be made into petrographic thin section for petrography analyses to ensure the hand sample identifications are correct. Petrography analyses are performed visually by the author using a Leica DM LM/P/11888500 polarizing optical microscope with 5× to 40 × magnification powers at the Department of Geology, University Malaya. The mineralogy and rock texture recognition of the samples are guided by published references such as MacKenzie et al. (1982).

3.3.1 XRF (X-ray Fluorescence) Spectrometry

The XRF spectrometry is a non-destructive chemical analysis method. It is well suited for obtaining major oxide values (SiO_2, Al_2O_3, CaO, Fe_2O_3, K_2O, MgO, Na_2O, P_2O_5, TiO_2 and MnO) from the rock samples. To prepare the rock samples for XRF spectrometer analysis, rock samples (~1 kg) are first crushed into smaller pieces (~5 to 10 mm) using a jaw crusher with tungsten carbide plates and ground into fine rock powder (>0.1 mm) using a mild steel swing mill. The pulverizing and grinding procedure are carried out by the author at the Department of Geology, University Malaya. The prepared rock powder

is then fused with dried borate fluxing material (dilithium tetraborate, $Li_2B_4O_7$) in a Pt-Au (95% Pt, 5% Au) crucible using an automated fusion machine (Tokyo Kagaku Co. Ltd. TK-4100 Bead & Fuse-Sampler, Figure 3.3a) in the Department of Geosciences, National University of Taiwan. The dilution ratio of flux to sample weight is 10:1. Finally, the completed borate fusion glass bead analyzed in the XRF spectrometer for major elements (in wt. %) using prepared reference materials.

The major oxide analysis of the fusion glass beads is completed using the Rigaku RIX-2000 XRF spectrometer in the Department of Geosciences, National University of Taiwan (Figure 3.3b). The analytical procedures were the same as those described by Pang et al. (2012), yielding analytical uncertainties better than ±5% (2σ) for all major elements (Yang et al., 2005). A basaltic sample from Penghu Island, Taiwan (PH-1) is analyzed at the beginning and at the end of the batch sample analysis (~20 samples) for consistency check (Table 3.2). The loss on ignition (LOI) of the samples was determined separately by routine procedure in Department of Geology, University Malaya. About 1.0 g of sample in powder form is placed into a platinum crucible and weighted. The sample is heated at 950ºC in a heating furnace for 1 hour. After 1 hour, the sample is removed from the furnace and cooled for about 10 minutes. The weight of the crucible with sample after the sintering and cooling process is recorded. The value of LOI (in weight %) can be determined by using the formula below:

$$LOI = 100\% \times ((a - b) / (a - c))$$

a is the weight of the crucible with sample before sintering (in grams)

b is the weight of the crucible with sample after sintering (in grams)

c is the weight of the empty crucible (in grams)

Figure 3.3: Machines used for XRF spectrometry. (a) Tokyo Kagaku Co. Ltd. TK-4100 Bead & Fuse-Sampler (National Taiwan University). (b) Rigaku RIX-2000 XRF spectrometer (National Taiwan University)

Table 3.2: The obtained value of PH-1 during the XRF operation

Oxide	PH-1-A	PH-1-B	PH-1-A1	PH-1-B1	Standard Deviation (SD), σ	Relative Standard Error (%)
SiO_2	44.84	44.85	45.04	44.81	0.105	0.23
TiO_2	2.43	2.43	2.48	2.49	0.032	1.30
Al_2O_3	13.67	13.62	13.55	13.49	0.079	0.58
Fe_2O_3	12.22	12.26	12.45	12.39	0.108	0.88
MnO	0.18	0.18	0.18	0.18	0.000	0.00
MgO	9.48	9.44	9.54	9.38	0.067	0.71
CaO	10.38	10.33	10.51	10.45	0.079	0.76
Na_2O	2.43	2.46	2.29	2.28	0.093	3.94
K_2O	1.52	1.51	1.52	1.51	0.006	0.38
P_2O_5	0.60	0.60	0.59	0.59	0.006	0.97
Total	**97.75**	**97.67**	**98.14**	**97.55**		

3.3.2 ICP-MS (Inductively Coupled Plasma-Mass Spectrometry)

The ICP-MS is a destructive chemical analysis method. It is well suited for obtaining trace element (including rare earth elements) values from the rock samples. However, the samples will need to undergo digestion and dilution procedure before the analysis. The sample preparation procedure for ICP-MS analysis was carried out by the author in a clean room of Department of Geosciences, National University of Taiwan. The technique used here is a type of multi-acid digestion followed by dilution. Instead of rock powder, the glass beads used for XRF analysis were used for the ICP-MS analysis. The glass beads were crushed, weighed for ~40 mg and digested with HNO_3 (1:1) and super-pure HF in screw-top Teflon Savillex beakers at 100°C for 2 hours. The digested samples were evaporated to dryness and digested again by HNO_3 (1:2) at 100 °C overnight. An internal standard solution of 10 ppb Rh and Bi in 2% HNO_3 was added. The internal standard was used for monitoring signal shift during ICP-MS measurements. The spiked dissolutions were diluted by 2% HNO_3 by 1500 times.

The prepared sample solutions were analyzed at Department of Geosciences, National Taiwan University using an Agilent 7500cx ICP-MS (Figure 3.4a). The precision of the

result is generally within ±5% (2σ) (Lee et al., 2012; Ng et al., 2015a) for all trace elements. Most of the analyzed elements show readings that are below detection limit when blanks were analyzed. The external standards used in the analyses were USGS standards AGV-2, BHVO-2, BCR-2 and DNC-1. The recommended values and the analytical results of the external USGS standards are shown in Table 3.3 and 3.4.

3.3.3 Zircon U-Pb Isotope Geochronology

The zircon separation process was carried out with the help of trained personnel. Rock samples selected for zircon extraction first undergo the gravity mineral separation process (Wilfley table) to generate a heavy mineral separate. After that, the zircons are separated from other high-density minerals such as: titanite, garnet, monazite, pyrite, and Fe-Ti oxides. The second step is outlined in detail below:

1. Removal of ferromagnetic minerals with a hand magnet
2. Separation of paramagnetic minerals from zircon with a Frantz magnetic separator
3. Separation of minerals according to density using heavy liquids (diiodomethane)
4. Removal of "soft" minerals with a Wig-L-Bug shaker
5. Removal of pyrite, apatite by acid washing

The separated zircons were mounted on an epoxy mount. The mount making process was carried out by the author at the Department of Geosciences, National University of Taiwan. One zircon mount was made by trained personnel at Arizona LaserChron Center, The University of Arizona. At the Department of Geosciences, National University of Taiwan, the zircon grains were cast in an epoxy mount using Struers EpoFix Kit (3.75 ml resin and 0.5 ml hardener for one mount), and was carefully polished using water-based diamond suspension (Stuers DiaPro Nap B 1 μm) to section the zircon crystals for analysis. Finished zircon mounts were documented using transmitted and reflected light microscopes.

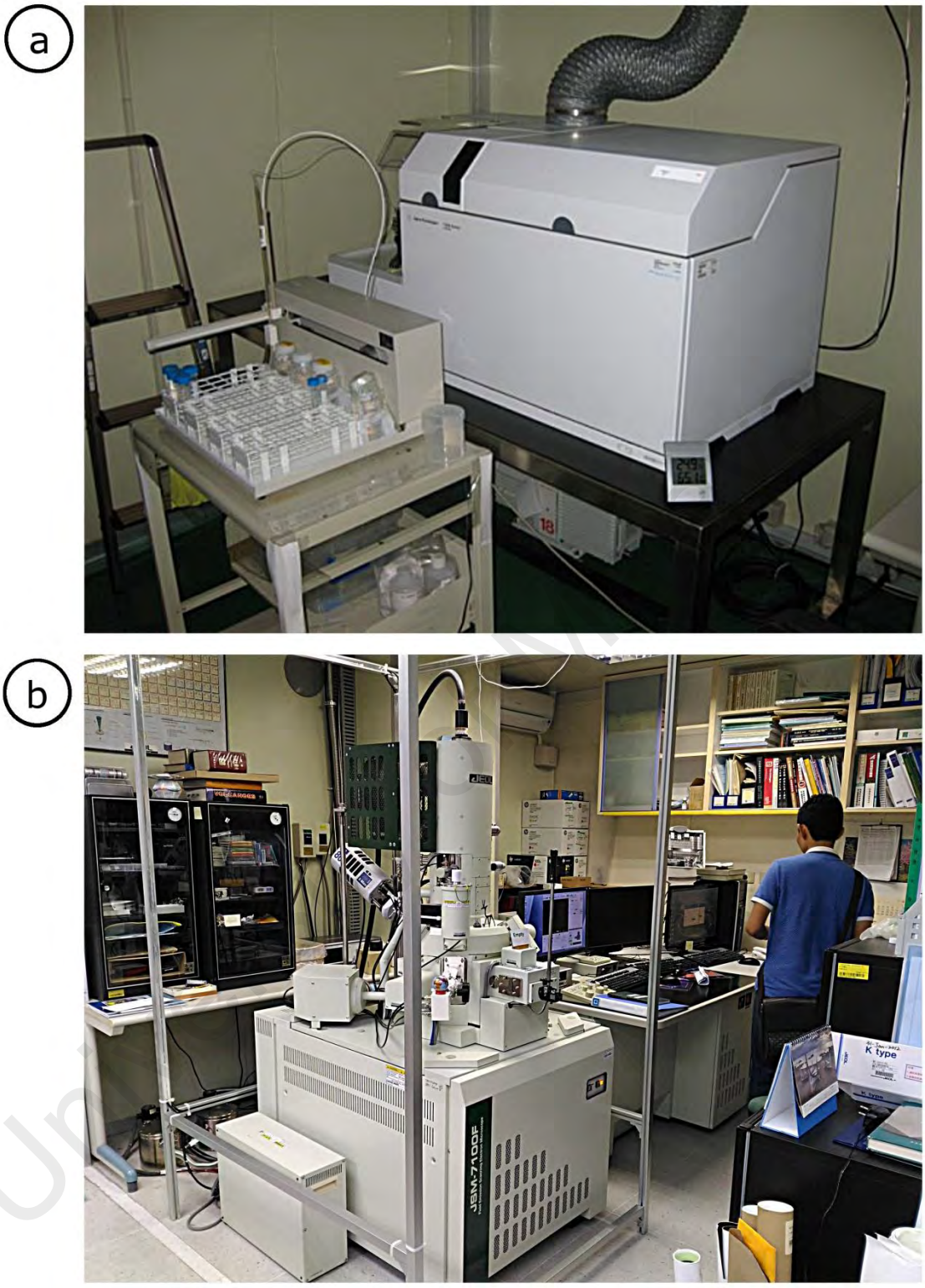

Figure 3.4: Machines used for ICP-MS and zircon imaging. (a) Agilent 7500cx ICP-MS (National Taiwan University). (b) JEOL JSM-7100F SEM (Academia Sinica)

Table 3.3: The recommended values of the external USGS standards

Element	AGV-2 (ppm)	2σ	BCR-2 (ppm)	2σ	BHVO-2 (ppm)	2σ	DNC-1 (ppm)
Cr	16.2	0.7	15.9	0.4	287	3	285
Ba	1134	8	684	5	131	1	118
Co	15.5	0.5	37.3	0.4	44.9	0.3	54.7
Cs	1.17	0.02	1.16	0.023	0.100	0.002	0.3
Ga	20.4	0.2	22.1	0.2	21.4	0.2	15
Hf	5.14	0.06	4.97	0.03	4.47	0.03	1.05
Nb	14.1	0.2	12.4	0.2	18.1	0.2	2
Rb	67.8	0.7	46.0	0.6	9.26	0.10	4.5
Sr	660	6	337	7	394	2	145
Ta	0.87	0.02	0.79	0.02	1.15	0.02	0.098
Th	6.17	0.06	5.83	0.05	1.22	0.02	0.24
U	1.89	0.02	1.68	0.02	0.41	0.04	0.05
V	119	1	418	5	318	2	148
W	0.55	0.09	0.47	0.05	0.25	0.04	0.2
Zr	232	2	187	2	171	1	41
Y	19.1	0.8	36.1	0.4	25.9	0.3	17.7
La	38.2	0.4	25.1	0.2	15.2	0.1	3.53
Ce	69.4	0.6	53.1	0.3	37.5	0.2	8.19
Pr	8.17	0.08	6.83	0.04	5.34	0.03	1.1
Nd	30.5	0.5	28.3	0.4	24.3	0.3	4.86
Sm	5.51	0.08	6.55	0.05	6.02	0.06	1.4
Eu	1.55	0.02	1.99	0.02	2.04	0.01	0.6
Gd	4.68	0.06	6.81	0.08	6.21	0.04	2
Tb	0.65	0.01	1.08	0.03	0.94	0.01	0.39
Dy	3.55	0.03	6.42	0.06	5.28	0.03	2.75
Ho	0.68	0.01	1.31	0.01	0.99	0.01	0.65
Er	1.83	0.01	3.67	0.04	2.51	0.01	1.9
Tm	0.262	0.004	0.534	0.006	0.335	0.003	0.33
Yb	1.65	0.01	3.39	0.04	1.99	0.03	1.97
Lu	0.251	0.003	0.505	0.008	0.275	0.002	0.31
Ni	18.9	0.4	12.6	0.3	120	1	247

*preferred values from Jochum et al. (2005)

Table 3.4: Analytical results of external USGS standards

Element	Most abundant isotope	n	Average AGV-2 (ppm)	RSE (%)	n	Average BCR-2 (ppm)	RSE (%)
Cr	53	5	17.0	2.62	4	14.4	3.85
Ba	137	8	1136	2.02	6	679	3.02
Co	59	8	15.6	1.15	6	36.9	1.43
Cs	133	8	1.18	1.30	6	1.15	1.46
Ga	69	7	20.6	1.89	6	21.8	2.97
Hf	179	8	5.20	1.42	6	4.88	0.63
Nb	93	8	14.1	0.96	6	12.4	1.01
Rb	85	8	66.7	2.41	6	46.4	1.17
Sr	88	8	649	1.91	6	341	1.17
Ta	181	8	0.84	0.68	6	0.78	1.01
Th	232	8	6.14	1.10	6	5.83	1.16
U	238	8	1.91	2.52	6	1.67	1.31
V	51	8	114	4.86	6	415	0.54
W	184	7	0.52	3.94	5	0.48	2.34
Zr	90	8	233	1.48	6	184	1.22
Y	89	8	19.7	2.17	6	35.9	1.44
La	139	8	37.4	3.53	6	24.8	1.80
Ce	140	8	68.5	3.39	6	52.3	1.71
Pr	141	8	8.04	3.46	6	6.73	1.73
Nd	146	8	30.0	3.31	6	28.3	1.57
Sm	147	8	5.47	2.76	6	6.54	1.27
Eu	153	8	1.58	2.27	6	1.96	1.24
Gd	157	8	4.64	4.66	6	6.74	1.06
Tb	159	8	0.65	2.02	6	1.06	0.70
Dy	163	8	3.49	2.03	6	6.40	1.21
Ho	165	8	0.67	1.86	6	1.31	1.11
Er	166	8	1.81	2.01	6	3.66	0.93
Tm	169	8	0.255	2.62	6	0.537	0.90
Yb	172	8	1.65	2.02	6	3.39	0.82
Lu	175	8	0.250	1.45	6	0.506	1.37
Ni	60	7	18.2	3.26	4	12.9	4.14

*RSE = Relative standard error

Table 3.4 continued

Element	Most abundant isotope	n	Average BHVO-2 (ppm)	RSE (%)	n	Average DNC-1 (ppm)	RSE (%)
Cr	53	7	280	1.94	5	284	4.07
Ba	137	4	130	1.35	4	101	1.02
Co	59	7	44.7	0.54	6	55.2	0.90
Cs	133	4	0.121	4.24	4	0.2	2.63
Ga	69	5	21.8	1.43	5	14	3.00
Hf	179	7	4.44	0.91	6	0.98	3.64
Nb	93	7	18.4	0.89	6	2	4.08
Rb	85	7	9.33	2.00	4	3.7	1.67
Sr	88	7	399	1.82	6	143	1.58
Ta	181	7	1.16	1.40	6	0.084	4.97
Th	232	7	1.20	1.81	4	0.24	3.00
U	238	7	0.43	1.25	4	0.06	3.91
V	51	7	330	1.19	6	135	4.51
W	184	4	0.29	4.15	3	0.2	4.53
Zr	90	7	170	1.45	6	35	4.53
Y	89	7	26.4	1.59	6	17.3	1.75
La	139	7	15.2	2.48	6	3.57	2.85
Ce	140	7	37.4	2.24	6	7.91	3.27
Pr	141	7	5.29	2.39	6	1.1	3.48
Nd	146	7	24.3	2.15	6	4.79	2.40
Sm	147	7	6.07	2.41	6	1.4	2.54
Eu	153	7	2.03	2.20	6	0.6	4.28
Gd	157	7	6.24	1.65	6	2	3.96
Tb	159	7	0.95	1.38	6	0.38	3.60
Dy	163	7	5.34	1.76	6	2.71	2.93
Ho	165	7	1.00	2.07	6	0.62	3.28
Er	166	7	2.54	1.41	6	1.9	2.86
Tm	169	7	0.340	1.75	6	0.30	2.25
Yb	172	7	2.01	1.42	6	1.95	3.42
Lu	175	7	0.277	1.88	6	0.30	4.02
Ni	60	7	118	2.33	6	248	0.59

*RSE = Relative standard error

After the zircon mounts were coated with carbon, cathodoluminance (CL) images of all the zircon were acquired by the author using a JEOL JSM-7100F scanning electron microscope (SEM) (Figure 3.4b) at Institute of Earth Sciences, Academia Sinica. The zircon mount made in Arizona LaserChron Center, The University of Arizona was analyzed at the same location with the help of trained personnel using a Photo Machines analyte G2 laser ablation system coupled with ThermoFinnigan Element2 ICP-MS, and following the procedure developed by Gehrels et al. (2008) and Johnston et al. (2009). The zircon mounts made in the National University of Taiwan were analyzed using a New Wave UP 213 laser ablation (LA) system coupled with Agilent 7500s quadrupole ICP-MS (Figure 3.5a), following analytical procedures described by Chiu et al. (2013). The laser ablation was performed with a helium carrier gas to reduce the deposition of ablated material onto the sample surface, which can significantly improve transport efficiency and thus increase the signal intensities. The routine laser ablation conditions include spot size of 35 μm, energy output of 41% with densities of 6.36 J/cm^2 and repetition rate of 5 Hz. Data acquisition time for each spot was about 100 s, i.e. 50 s gas blank followed with 50 s ablation.

The GJ-1 zircon was used as a standard for instrumental drift correction, which yielded a concordia $^{206}Pb/^{238}U$ age of 601.3 Ma (Figure 3.6a and b, Appendix A) during the experiments. This age is very close to the standard age of 601.86 Ma by LA-ICP-MS analyses provided in Horstwood et al. (2016). Two reference zircons analyzed during the experiments for consistency check, 91500 and Plešovice yielded $^{206}Pb/^{238}U$ age of 1061.5 Ma (Figure 3.7a and b, Appendix A) and 336.3 Ma (Figure 3.8a and b, Appendix A) respectively. Both ages are very close to the standard age (91500: 1063.51 Ma; Plešovice: 337.16 Ma) provided in Horstwood et al. (2016). All U-Pb isotopic concentrations were calculated using the GLITTER 4.4.4 data reduction software for laser ablation microprobe by Geochemical Evolution and Metallogeny of Continents (GEMOC).

Common lead correction was done using the procedure suggested by Andersen (2002). During this procedure, discordant analyses were filtered out. The weighted mean U-Pb ages and concordia plots were carried out using Isoplot v. 4.15 (Ludwig, 2003).

3.3.4 Zircon Lu-Hf Isotope

Lu-Hf analyses were conducted at the exact same spots or the same age domains for the U-Pb age dating as guided by CL images. Lu-Hf analyses were performed on the zircon mount made in Arizona LaserChron Center, The University of Arizona with the assistance of trained personnel using a Nu Plasma HR ICP-MS, coupled to a Photon Machines Analyte G2 laser equipped with a LelEX cell, and following the procedure described in Gehrels and Pecha (2014). Lu-Hf analyses on the rest of the zircon mounts were performed using a Nu Plasma multi-collector (MC) ICP-MS, coupled to a Photon Machines Analyte G2 laser ablation system (Figure 3.5b), housed at the Institute of Earth Sciences, Academia Sinica. Laser spot analyses were done using a spot diameter of 50 μm at an energy output of 100% with densities of 5.75 J/cm^2 and 8 Hz repetition rate. Following a 30 s of blank acquisition, typical ablation times were around 60-90 s. $^{176}Hf/^{177}Hf$ results of the Mud Tank zircon standards during analysis of this study are 0.282496 ± 0.0000051 (2σ, n= 22) (Appendix B), which are similar to the values given by Woodhead and Hergt (2005) for solution analysis (0.282507 ± 0.000006; n = 5) and laser ablation microprobe (LAM) (MC) ICPMS analysis (0.282504 ± 0.000044; n = 158). A detailed description of the analyses is given in Lan et al. (2009). MC-ICPMS instrumental conditions and data acquisition followed those reported by Griffin et al. (2000, 2004). The $\varepsilon Hf_{(T)}$ values and model ages used in the figures were calculated using the decay constant (1.867×10^{-11} per year) proposed by Söderlund et al. (2004). The two-stage model ages (T_{DM2}) are calculated by assuming that the $^{176}Lu/^{177}Hf$ of the average continental crust is 0.015 (Griffin et al., 2004).

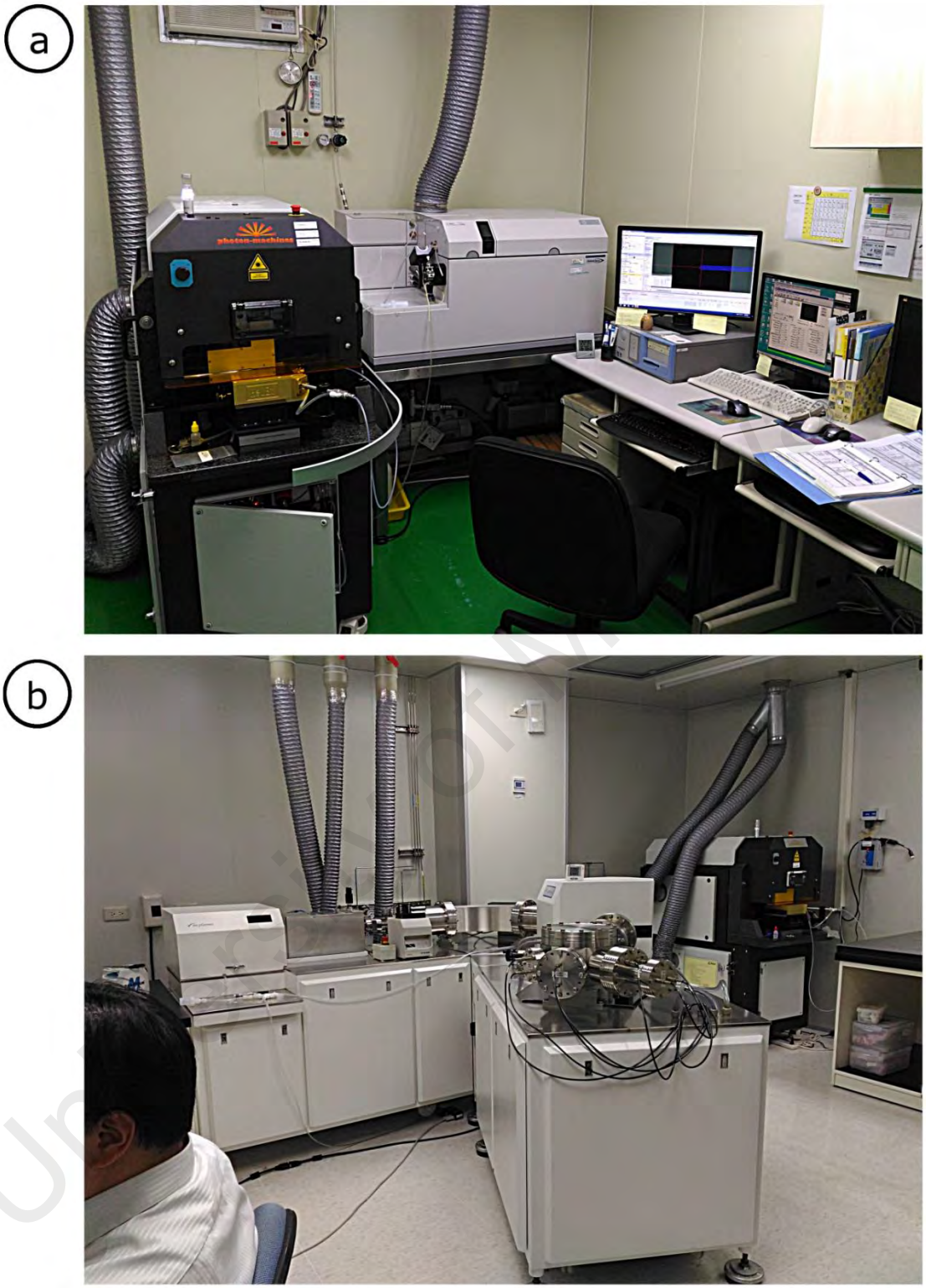

Figure 3.5: Machines used for zircon U-Pb and Lu-Hf isotope analysis. (a) Agilent 7500s quadrupole ICP-MS, coupled to a New Wave UP 213 laser ablation system (National Taiwan University). (b) Nu Plasma multi-collector (MC) ICP-MS, coupled to a Photon Machines Analyte G2 laser ablation system (Academia Sinica)

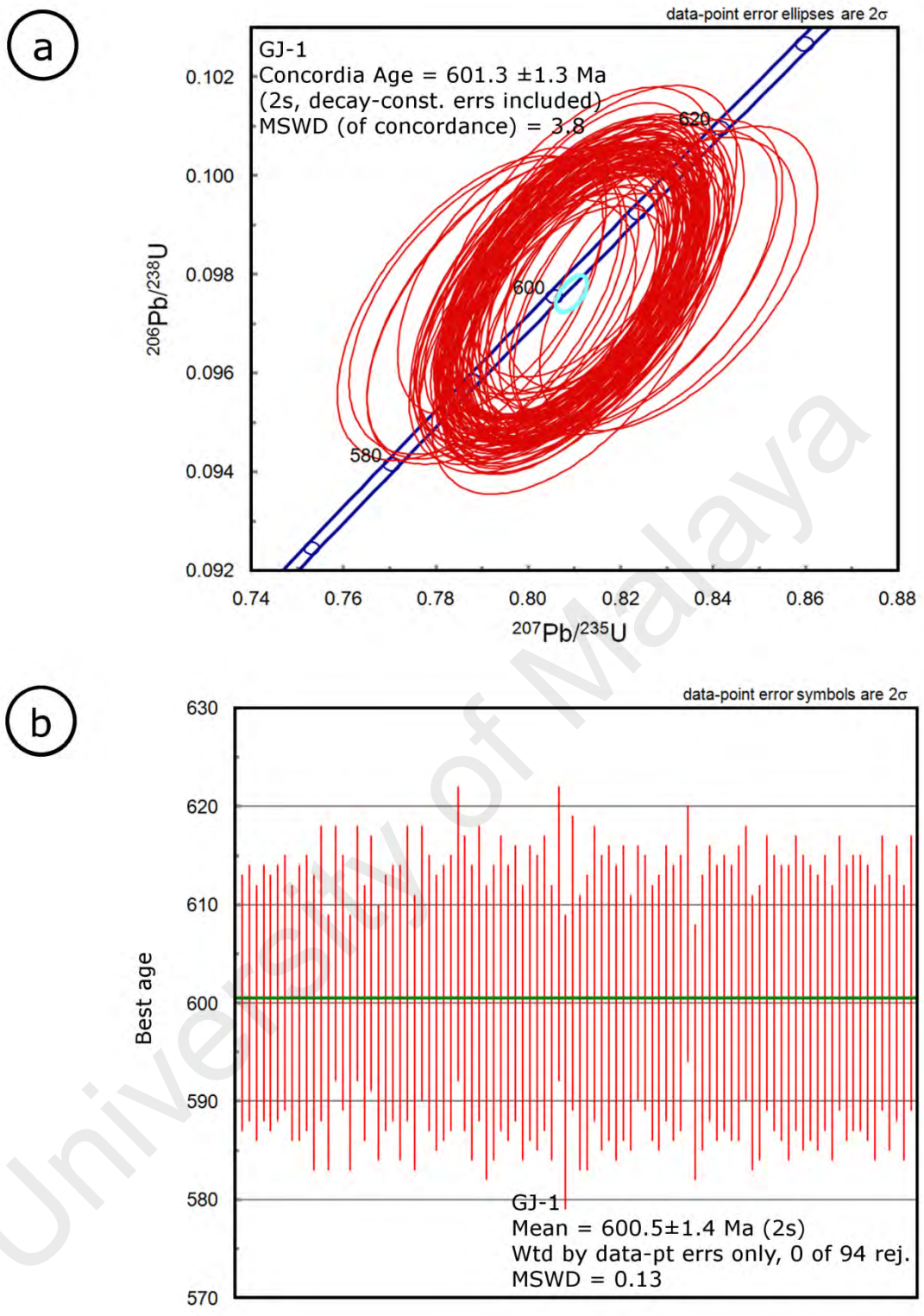

Figure 3.6: Concordia and weighted average plots for reference zircon GJ-1. (a) Concordia plot. (b) Weighted average plot. (Reference zircon GJ-1 standard age: 601.86 Ma) (Horstwood et al., 2016).

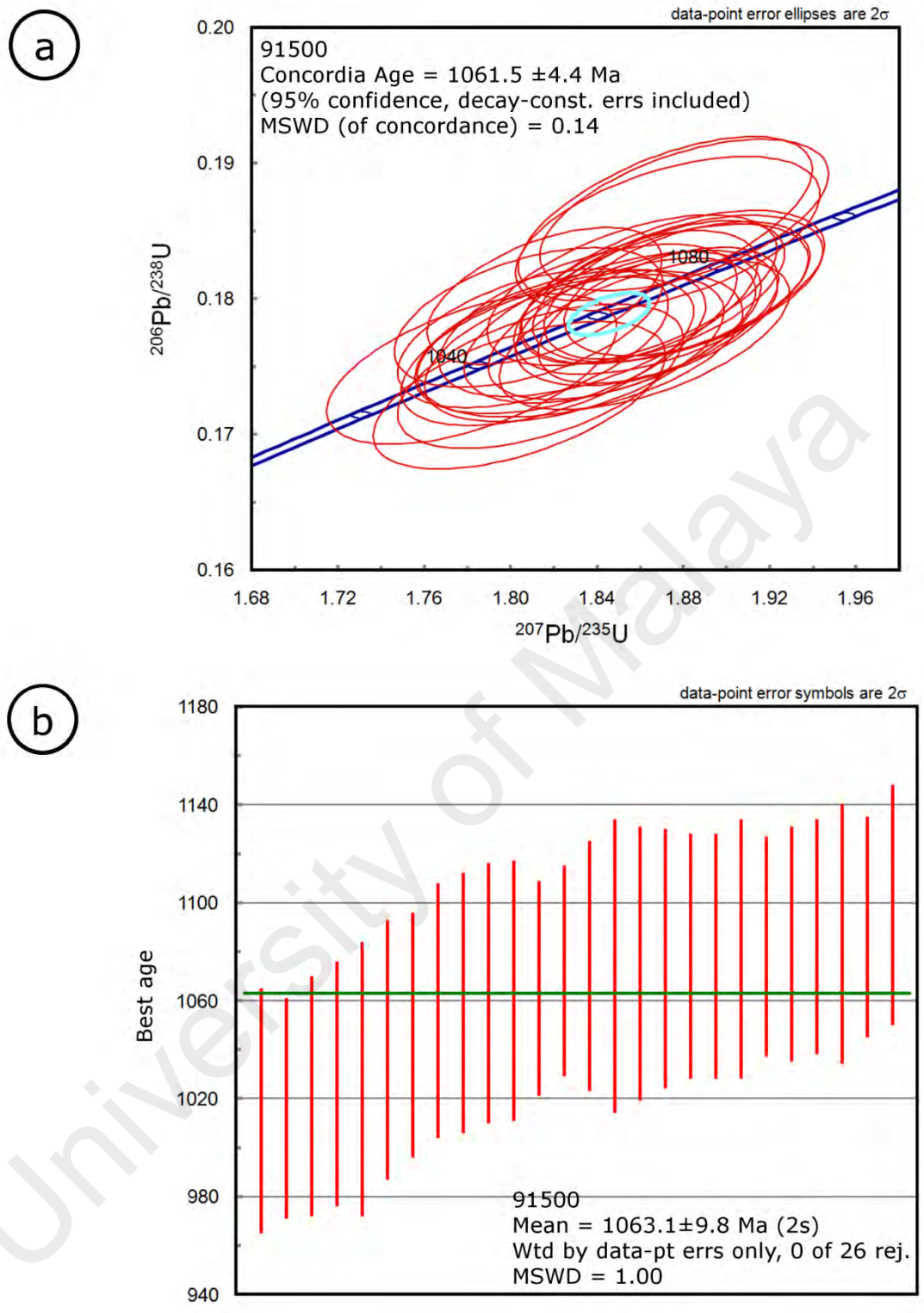

Figure 3.7: Concordia and weighted average plots for reference zircon 91500. (a) Concordia plot. (b) Weighted average plot. (Reference zircon 91500 standard age: 1063.51 Ma) (Horstwood et al., 2016).

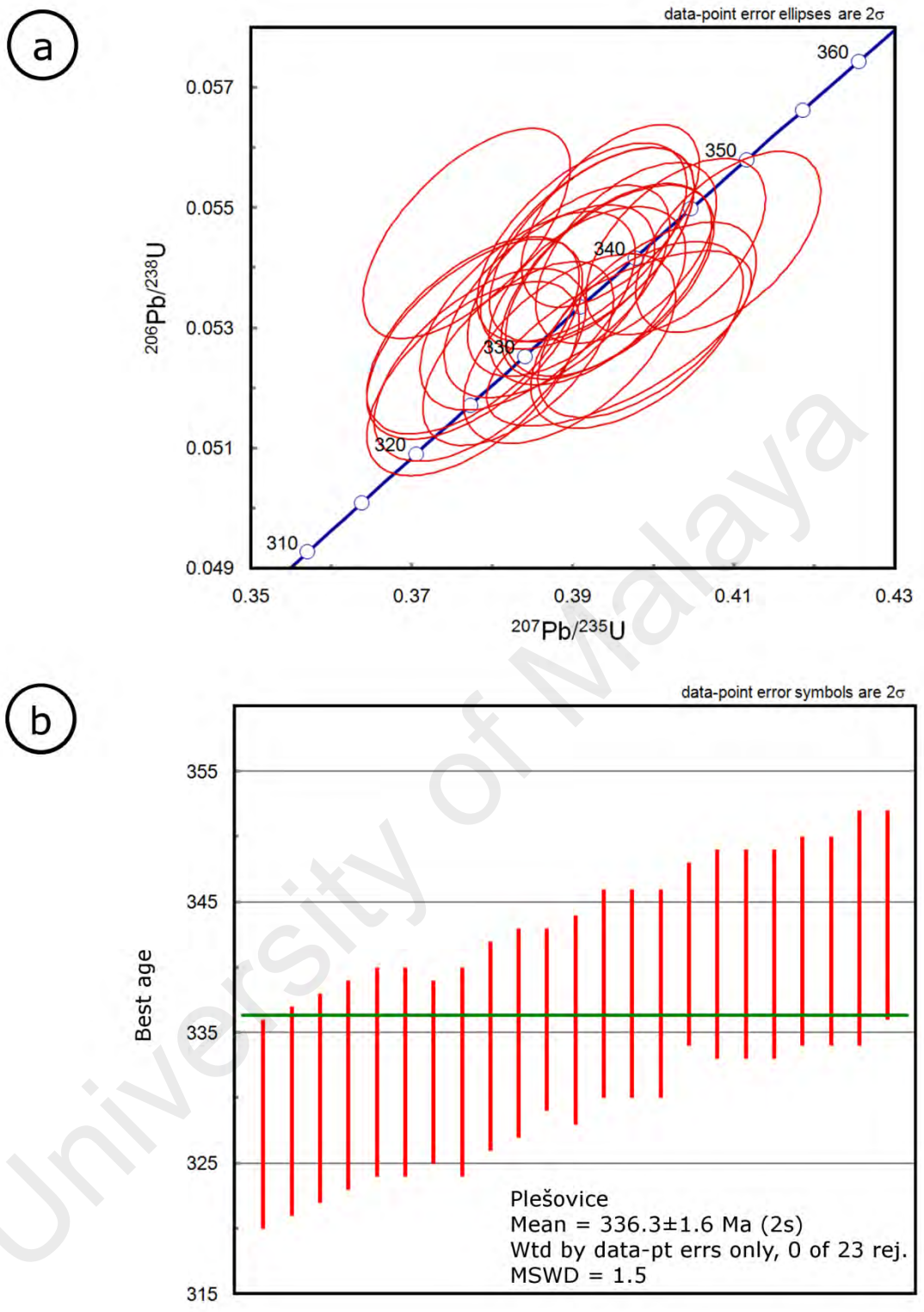

Figure 3.8: Concordia and weighted average plots for reference zircon Plešovice. (a) Concordia plot. (b) Weighted average plot. (Reference zircon Plešovice standard age: 337.16 Ma) (Horstwood et al., 2016).

3.5 Chapter Summary

1. Major element compositions of the rock samples were determined by X-ray fluorescence (XRF) using a Rigaku RIX 2000 spectrometer at the Department of Geosciences, National Taiwan University, Taiwan, and following the analytical procedures described by Pang et al. (2012). The analytical uncertainties are generally better than 5% for all major elements.
2. Trace element compositions of the rock samples were determined by inductively coupled plasma-mass spectrometry (ICP-MS) using an Agilent 7500cx ICP-MS at the Department of Geosciences, National Taiwan University, Taiwan, and following the analytical procedures described by Lee et al. (2012). The precision of the result is generally within ±5% (2σ) for all trace elements.
3. The zircon U-Pb isotope of LAWIN-1 sample was analyzed at the Lasechron Center of The University of Arizona, Tucson, Arizona, using a Photo Machines Analyte G2 laser ablation system coupled with ThermoFinnigan Element2 ICP-MS, and following the analytical procedure developed by Gehrels et al. (2008). The zircon Lu-Hf isotope was analyzed at the using a Nu Plasma HR ICP-MS, coupled to a Photon Machines Analyte G2 laser equipped with a LelEX cell, and following the procedure described in Gehrels and Pecha (2014).
4. The remaining samples' zircons U-Pb isotope were analyzed at the Department of Geosciences, National Taiwan University, Taiwan, using a New Wave UP-213 laser ablation system coupled with Agilent 7500s ICP-MS, and following analytical procedures described by Chiu et al. (2013). The zircons Lu-Hf isotope were analyzed at the Institute of Earth Sciences, Academia Sinica, Taiwan, using a Photon Machines Analyte G2 laser ablation system coupled with Nu Plasma multi-collector (MC) ICP-MS, and following analytical procedures described by Lan et al. (2009).

CHAPTER 4: RESULTS

4.1 Introduction

This chapter will describe the results from field (macroscopically) and petrographic observation (microscopically), geochemical analysis and zircon isotope analysis.

4.2 Field observation and petrography

4.2.1 Gerik-Dinding meta-volcanic rocks

The Gerik-Dinding meta-volcanic rocks are well exposed along the western flank of the Main Range batholith. The meta-volcanic rocks can be separated into at least three rock types: meta-lithic tuff, meta-crystal tuff and meta-rhyolite. Meta-lithic tuff contains a considerable quantity of terrigenous material (argillaceous, calcareous and siliceous materials) (Figure 4.1a). In contrast, the meta-crystal tuff made up of entirely pyroclastic content (Figure 4.1b and 4.2a). The meta-crystal tuff is characteristically crystalline and massive, showing no signs of bedding or structure. They are typically grayish to greenish in color and its groundmass is composed entirely of fine-grained material with quartz and white feldspar phenocrysts. In some areas, the intensity of shearing is sufficient to convert part of the meta-crystal tuff into porphyroblastic schist with metamorphic flaser texture (Figure 4.2b). The occurrence of volcanic rock strongly resembling meta-rhyolite has been found at Jerai, Temenggor and Sungai Siput. Even though the volcanic rock has been metamorphosed, the swirling layers of different color with aligned phenocrysts strongly resemble flow banding structures.

Meta-lithic tuff generally shows welded texture. The fine-grained groundmass can be described as poorly crystallized mosaic quartz, chlorite, graphite and muscovite. Meta-lithic tuff with carbonaceous content is easily recognized as they contain large (1-2 mm) carbonaceous fragments aligned parallel to the foliation of the rock (Figure 4.3a). The

meta-crystal tuff groundmass is mostly chlorite, quartz, feldspar, sericite and epidote. The phenocrysts of the meta-crystal tuff are K-feldspar (perthite & sanidine?), quartz and plagioclase. While most of the collected meta-crystal tuff samples have a heavily chloritized fine-grained groundmass (Figure 4.3b) without any unique rock fabrics, a small quantity of meta-crystal tuff is observed to preserve its original welded (Figure 4.3c) and non-welded texture (Figure 4.3d). Quartz phenocrysts in the meta-crystal tuff frequently show rounded, embayed margin (Figure 4.3e). K-feldspar phenocrysts in the meta-crystal tuff may show micro-graphic texture (Figure 4.3f). Occasionally, glass fragments are present in the meta-crystal tuff (Figure 4.5a). Alteration of some feldspar grains to calcite suggests the present of calcic feldspar (Figure 4.4a). Notable accessory minerals in the meta-crystal tuff are zircon, apatite, leucoxene, tourmaline (Figure 4.4b), orthopyroxene (Figure 4.4c), clinopyroxene (Figure 4.4d), amphibole (Figure 4.4e and 4.4f), epidote and garnet.

The meta-rhyolite is a fine-grained porphyritic volcanic rock with phenocrysts of quartz (50%) (Figure 4.6a), K-feldspar (45%) (Figure 4.6b), plagioclase (~4%) and orthopyroxene (< 1%) (Figure 4.6c). The size of the phenocrysts (up to 3 mm) in meta-rhyolite is noticeably larger than the phenocrysts (1-2 mm) in meta-crystal tuff. Quartz and K-feldspar phenocrysts in the meta-rhyolite are commonly resorbed (with embayed margin) and may be shattered. The meta-rhyolite groundmass can be strongly sheared (Figure 4.6d) and comprises 60% to 70 % of the rock. The groundmass is usually cryptocrystalline and speckled with irregular quartz, feldspar and biotite crystals. Only a number of meta-rhyolite samples show almost glassy groundmass (Figure 4.5b). Accessory minerals in the meta-rhyolite are zircon, apatite, amphibole and leucoxene. Glomeroporphyritic clusters of quartz, K-feldspar, biotite and plagioclase (Figure 4.6e and 4.6f) in the meta-rhyolite suggest a lava or shallow intrusion origin (Dusel-Bacon et al., 1998). Such glomerocryst are not present in the meta-crystal tuff.

Figure 4.1: Hand specimen of meta-lithic tuff and meta-crystal tuff. (a) Meta-lithic tuff from Gerik area. The meta-tuff contains a considerable amount of black carbonaceous materials. The diameter of the coin is 19 mm. (b) Fine-grained meta-crystal tuff from Lawin area. The diameter of the coin is 23 mm.

Figure 4.2: Hand specimens of meta-crystal tuff samples. (a) Sample from Dinding area. (b) Sample from Berusong area with flaser texture. The diameter of coin in both photos is 19 mm.

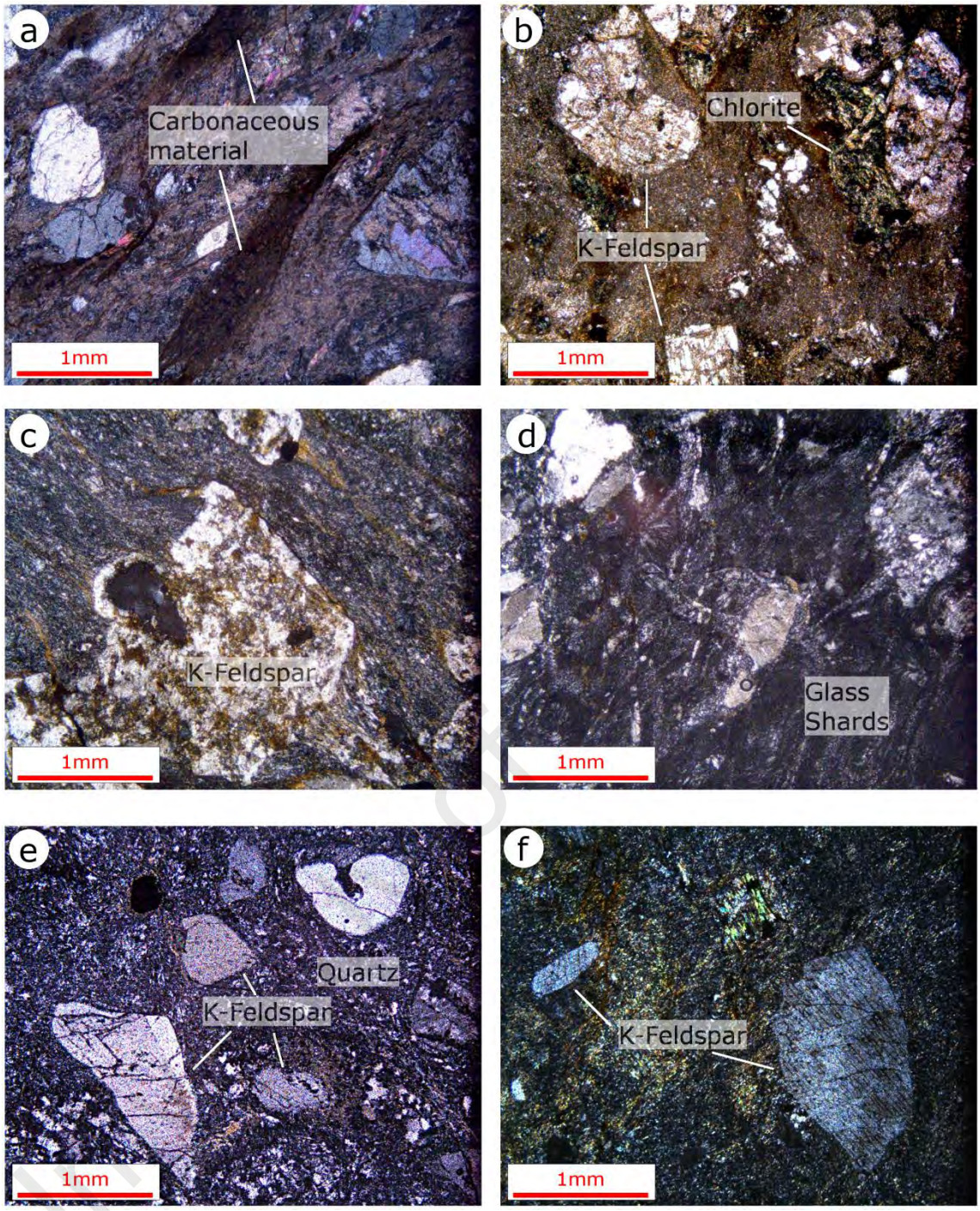

Figure 4.3: Thin section photos showing textures and mineral constituents of Gerik-Dnding meta-volcanic rocks. (a) Photomicrograph of meta-lithic tuff showing the carbonaceous materials. Cross-polarized light (XPL). (b) Photomicrograph of meta-crystal tuff showing the chloritized groundmass. Plane polarized light (PPL). (c) Photomicrograph (XPL) showing welded texture in the meta-crystal tuff groundmass. (d) Photomicrograph (XPL) showing non-welded texture in the meta-crystal tuff groundmass. (e) Photomicrograph (XPL) of meta-crystal tuff showing embayment margin on quartz. (f) Photomicrograph (XPL) of meta-crystal tuff showing visible micro-graphic texture on K-feldspar.

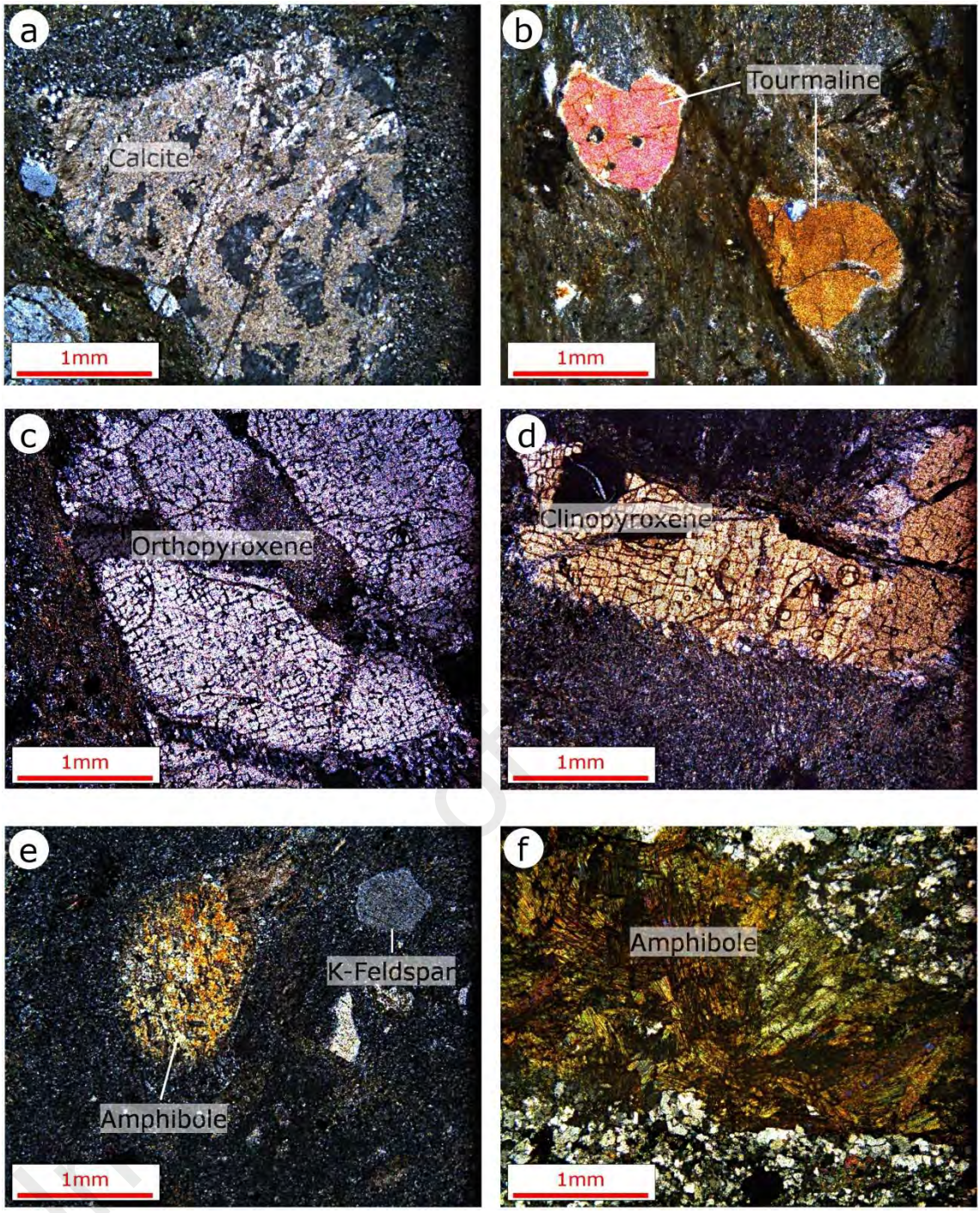

Figure 4.4: Thin section photos showing various accessory minerals of Gerik-Dinding meta-volcanic rocks (meta-crystal tuff). (a) Photomicrograph (XPL) showing a feldspar grain replaced by secondary calcite. (b) Photomicrograph (XPL) showing tourmaline. (c) Photomicrograph (XPL) showing orthopyroxene. The diagnostic 90° cleavage of pyroxene group is clearly visible. (d) Photomicrograph (XPL) showing clinopyroxene. (e) Photomicrograph (XPL) showing amphibole (actinolite?). (f) Photomicrograph (XPL) showing amphibole (actinolite?).

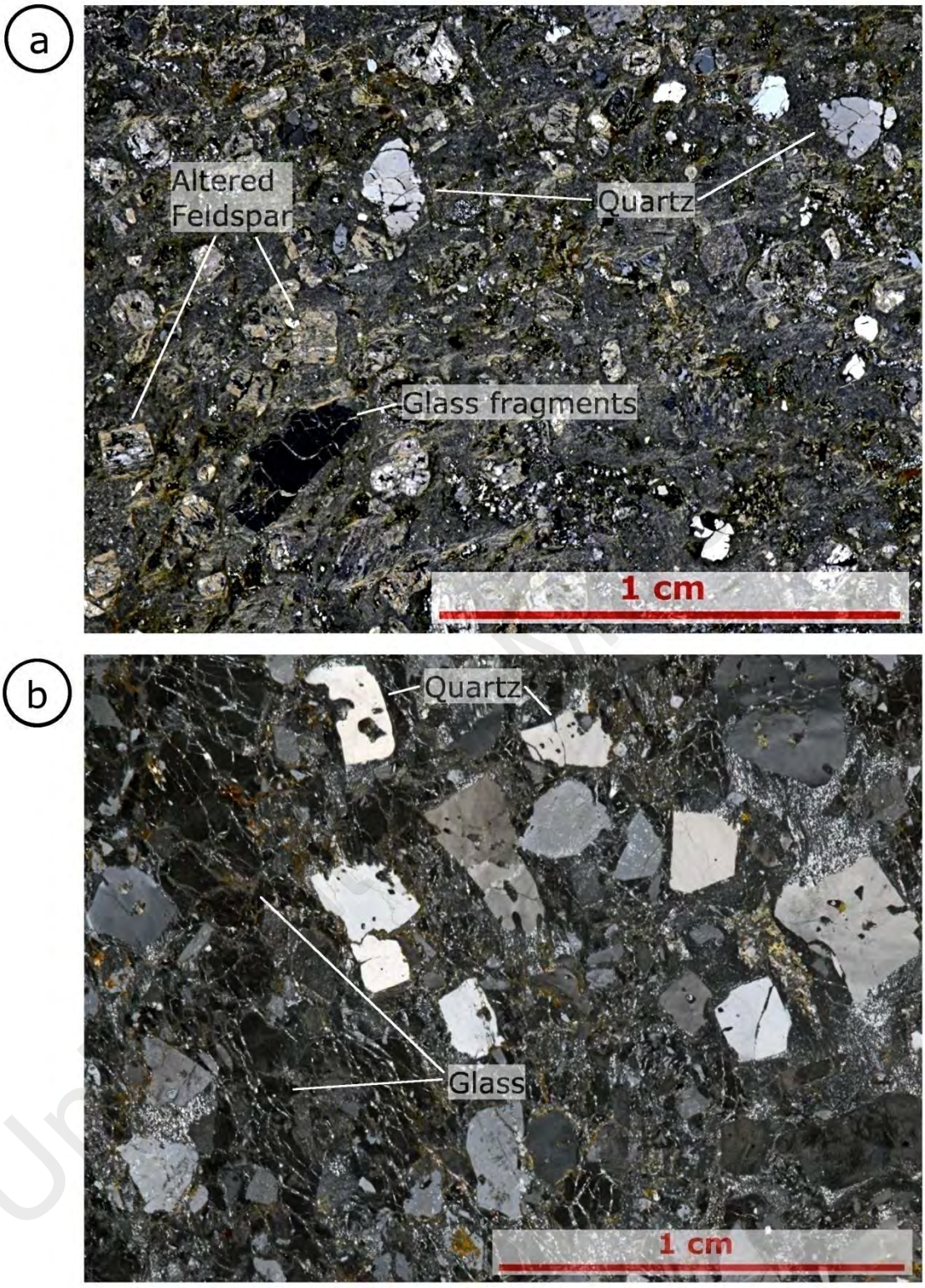

Figure 4.5: Photomicrographs (XPL) showing textures and mineral constituents of the Gerik-Dinding meta-volcanic rocks. (a) Meta-crystal tuff. (b) Meta-rhyolite. Note that the grain size in the meta-rhyolite is coarser than the meta-crystal tuff.

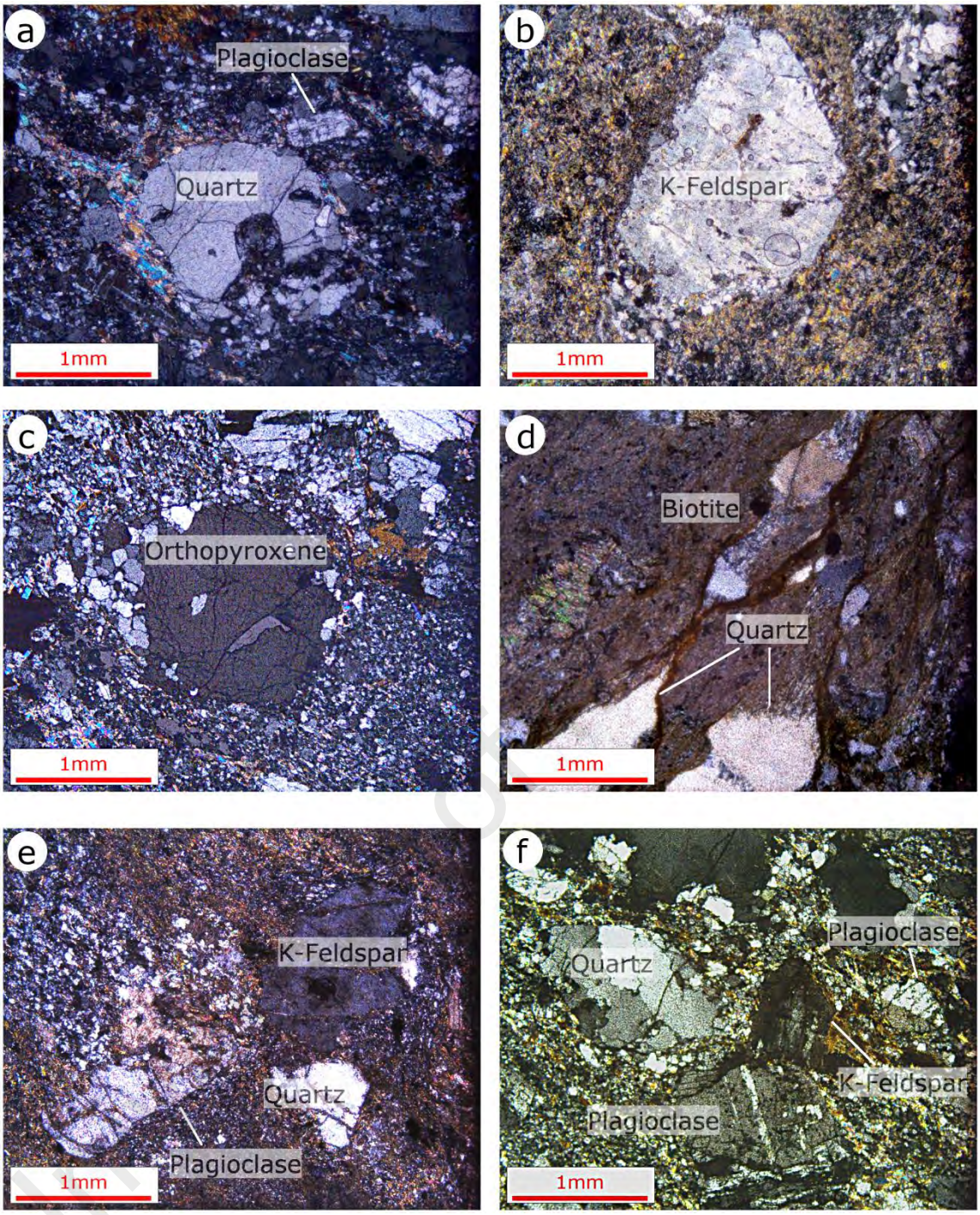

Figure 4.6: Thin section photos showing textures and mineral constituents of the Gerik-Dinding meta-volcanic rocks (meta-rhyolite). (a) Photomicrograph (XPL) showing quartz with embayed margin. (b) Photomicrograph (XPL) showing K-feldspar phenocryst. (c) Photomicrograph (XPL) showing an orthopyroxene, identified through its 1st order gray interference color. (d) Photomicrograph (XPL) showing sheared groundmass composed of quartz and biotite. (e) Photomicrograph (XPL) showing a glomeroporphyritic cluster of quartz, K-feldspar and plagioclase. (f) Another photomicrograph (XPL) showing a glomeroporphyritic cluster of quartz, K-feldspar and plagioclase.

4.2.2 Rephens meta-volcanic rocks

The Rephens meta-volcanic rocks are only exposed at the south-west flank of the Main Range batholith, near Kuala Kelawang area. These meta-volcanic rocks are very close to the Main Range batholith intrusion and have undergone contact metamorphism. Two types of volcanic rocks are found here: meta-andesite and meta-lithic tuff. The meta-andesite is a gray colored and fine-grained indurated meta-volcanic rock (Figure 4.7a). Small (< 0.5 mm) and white colored feldspar crystals are found speckled on the volcanic rock. Rarely, white feldspar phenocrysts (up to 2 mm) may be present. The meta-lithic tuff is a dark-gray spotted siliceous rock with random white colored andalusite crystals (~2-5 mm) (Figure 4.7b). The meta-lithic tuff does not contain any identifiable lithic fragments. The terrigenous materials (argillaceous?) in the meta-lithic tuff appear to be completely converted into andalusite.

In thin section, the meta-andesite consist of small angular phenocrysts of plagioclase, K-feldspar and quartz in a micro-crystalline groundmass of plagioclase, biotite and quartz (Figure 4.8a). The biotite is typically yellowish-brown and shows acicular (needle-like) habit. Quartz phenocrysts are rare in the meta-andesite, and may display embayed margins (Figure 4.8b). The plagioclase in the meta-andesite is often affected by sericitization while the K-feldspar has been kaolinized to some extent. Quartz and stilpnomelane veins (Figure 4.8c) are sometimes present in the meta-andesite. Accessory minerals in the meta-andesite are: tourmaline, epidote, stilpnomelane and iron oxides. The meta-lithic tuff is noted to consist of fine-grained quartz embedded in a slightly schistose groundmass of dense graphite dust with anhedral patches of muscovite (Figure 4.8d and 4.8f). Large euhedral andalusite crystals (~2 mm), identified by its 1st order gray or white interference color are randomly distributed throughout the rock. Staurolite is also present in minor quantities within the meta-lithic tuff (Figure 4.8e); identifiable by its weak pleochroism and 1st order yellow interference color.

Figure 4.7: Hand specimens of meta-andesite and meta-lithic tuff. (a) Meta-andesite from Rephens area. The length of the Swiss knife is 8.5 cm. (b) Meta-lithic tuff from Gabai area. The diameter of the coin is 25 mm. The metamorphism on these rocks may be related to thermal effects of granite magmatism, as the Rephens meta-volcanic rocks are in close proximity with Triassic granite intrusion.

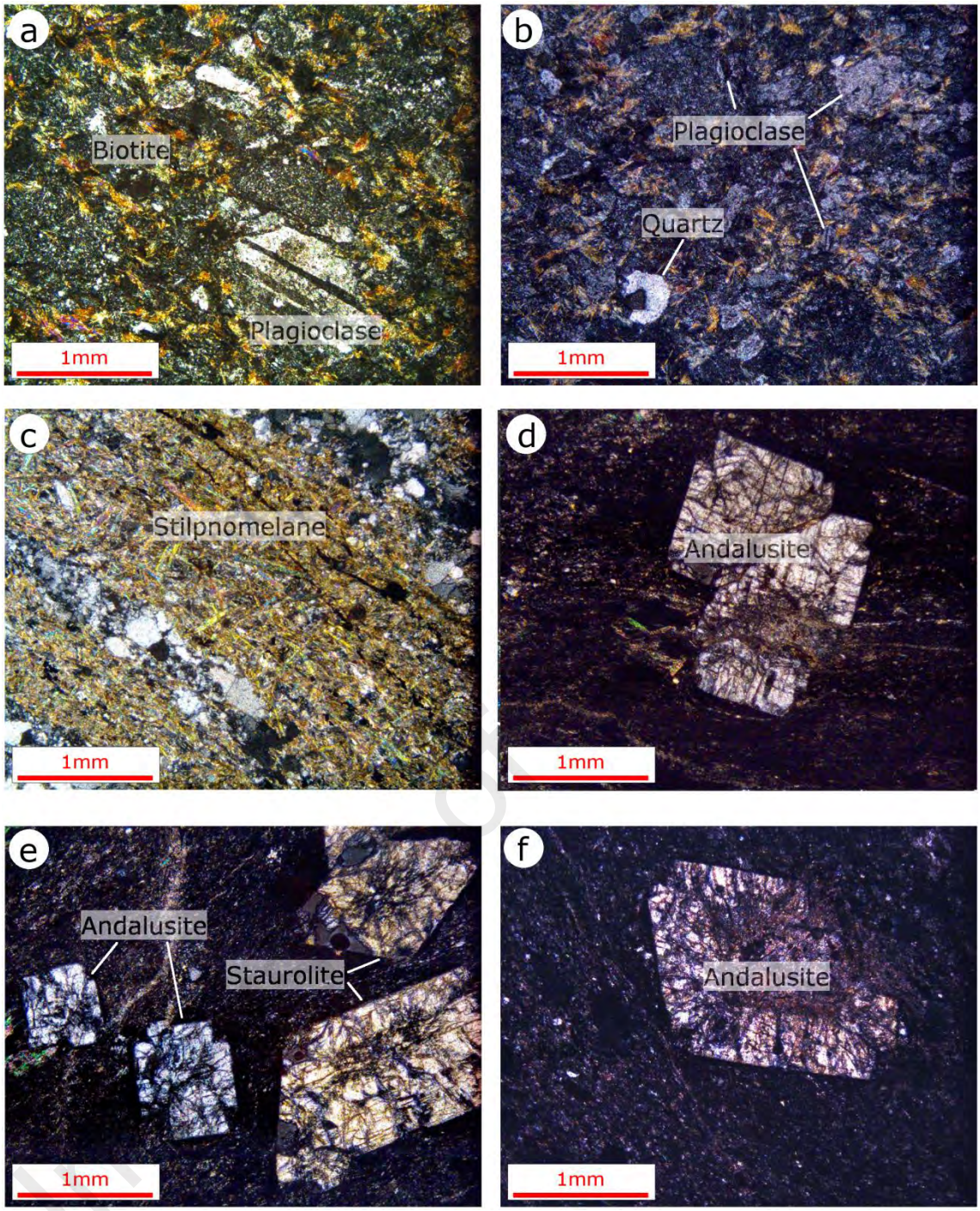

Figure 4.8: Thin section photos showing textures and mineral constituents of the meta-andesite and meta-lithic tuff. (a) Photomicrograph (XPL) showing the typical texture of the meta-andesite with acicular biotite. (b) Photomicrograph (XPL) showing plagioclase and quartz in meta-andesite. (c) Photomicrograph (XPL) showing stilpnomelane in meta-lithic tuff. (d) Photomicrograph (XPL) showing a twinned andalusite crystal in meta-lithic tuff. (e) Photomicrograph (XPL) showing andalusite (chiastolite?) and staurolite in meta-lithic tuff. (f) Photomicrograph (XPL) showing a subhedral basal section of andalusite grain in meta-lithic tuff. The occurrence of andalusite within the meta-lithic tuff indicates a low pressure and low to high-temperature metamorphism.

4.2.3 Meta-dolerite

The meta-dolerite samples collected for this study are intruded into the Early Paleozoic meta-sedimentary formation (Table 4.1 and Figure 4.10b). Sharp contact is present between the meta-dolerite and meta-sedimentary formation. The meta-dolerite is generally dark-green to dark gray in color with fine- to medium-grain size (Figure 4.9a and 4.9b). They are characteristically crystalline and massive, showing no peculiar structures or features. Strongly foliated actinolite-epidote and diopside schist are often found present together with the meta-dolerite in minor quantities (Figure 4.10a). The schist is assumed to have originated from further regional metamorphism of the meta-dolerite. The meta-dolerite outcrops observed in this study generally are in the form of sills. Seeing that there is no observable contact metamorphism between the meta-dolerite intrusions and the country meta-sedimentary rock, it is suggested that the meta-dolerite intrusion was penecontemporaneous; the meta-dolerite was emplaced immediately after the deposition of the sedimentary rock. Due to the humid tropical condition and heavy vegetation in Peninsular Malaysia, most meta-dolerite outcrops are weathered rapidly into red ferruginous laterite/bauxite. Fresh meta-dolerite outcrops are typically confined to stream beds. Such outcrops have low relief and are only exposed and accessible during the dry season (Figure 4.11a and 4.11b).

The meta-dolerite grain size varies with localities. Most of the meta-dolerite has medium grain size. Serendah meta-dolerite (Figure 4.12a) has the coarsest grain size (~0.5 cm) while Banding and Serdang meta-dolerite (Figure 4.12b) have the finest grain size (< 0.1 cm). Although the meta-dolerite is affected by metamorphism, some unaltered parts still retain the original ophitic to sub-ophitic texture (Figure 4.13a). Plagioclase usually exists as lath-shaped crystals while clinopyroxene commonly occurs as twinned crystals. The main minerals in the meta-dolerite are: plagioclase (Figure 4.13b), clinopyroxene (Figure 4.13c), orthopyroxene and iron oxide. Secondary minerals present in the meta-

dolerite are: amphibole, sericite, chlorite, epidote, calcite, antigorite and an iddingsite-like mineral. The amphibole minerals are formed as an alteration of pyroxene group minerals. Trellis-type laminae (or widmanstätten pattern) (Buddington and Lindsey, 1964) may be present in the accessory iron oxide grains in the meta-dolerite (Figure 4.13d). Such laminae are commonly present in magnetite-ilmenite intergrowths from the slow rate of cooling (Mondal and Baidya, 2015).

Meta-dolerite affected by ductile deformation display mylonitic texture (Figure 4.13e and 4.13f). While these rocks may retain the original mineralogy, the original ophitic texture has been completely obliterated. The plagioclase in these rocks commonly displays a sigmoid shape. Meta-dolerite affected by uralitization exhibit blastophitic texture, where traces of the original ophitic texture still remain. Plagioclase is normally sericitized (into sericite) or saussuritized (into chlorite and epidote) (Figure 4.14a to 4.14d) and pale-green amphibole form pseudomorphs after clinopyroxene (together with chlorite and white mica). Strong alteration on plagioclase may affect its identification as they are darkened under cross nichols light. On the other hand, meta-dolerite affected by brittle deformation display cataclastic texture. The original ophitic texture and mineralogy of the meta-dolerite were not preserved in these rocks, with the exception of a few clinopyroxenes which display heavily altered rims (Figure 4.14e and 4.14f).

Table 4.1: Meta-sedimentary formations intruded by meta-dolerite

No.	Meta-dolerite localities	Associated meta-sedimentary formation	Age
1.	Banding	Papulut quartzite	Late Cambrian to Late Ordovician
2.	Rokan		
3.	Ayer Kedah		
4.	Ayer Kapas	Kroh formation	Late Ordovician to Early Devonian
5.	Perah	Terolak formation	Ordovician to Silurian
6.	Serendah		
7.	Serdang	Hawthornden schist	Ordovician to Early Silurian

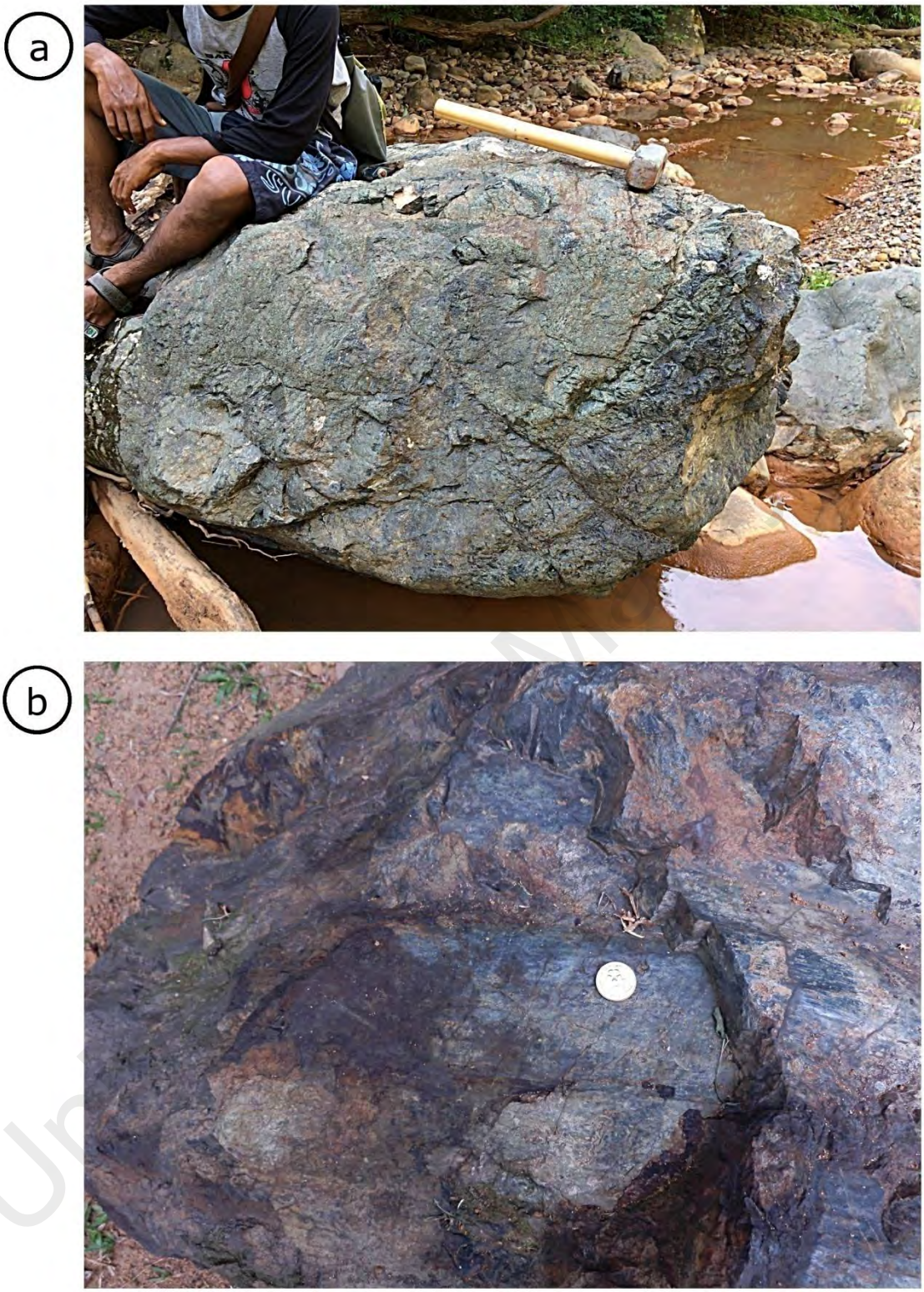

Figure 4.9: Field photographs showing the meta-dolerite. (a) Meta-dolerite from Ayer Kedah area. The length of the hammer is 40 cm. (b) Meta-dolerite from Serdang area. The diameter of the coin is 23 mm.

Figure 4.10: Field photographs showing the meta-dolerite and Papulut quartzite. (a) Meta-dolerite from Banding area. (b) Papulut quartzite outcrop from Ayer Kedah area. The length of hammer in both photos is 40 cm.

Figure 4.11: Field photographs showing the outcrop of the meta-dolerite. (a) Meta-dolerite from Ayer Kapas area. The length of the hammer is 1.1 m. (b) Meta-dolerite area from Rokan area. The length of the hammer is 40 cm.

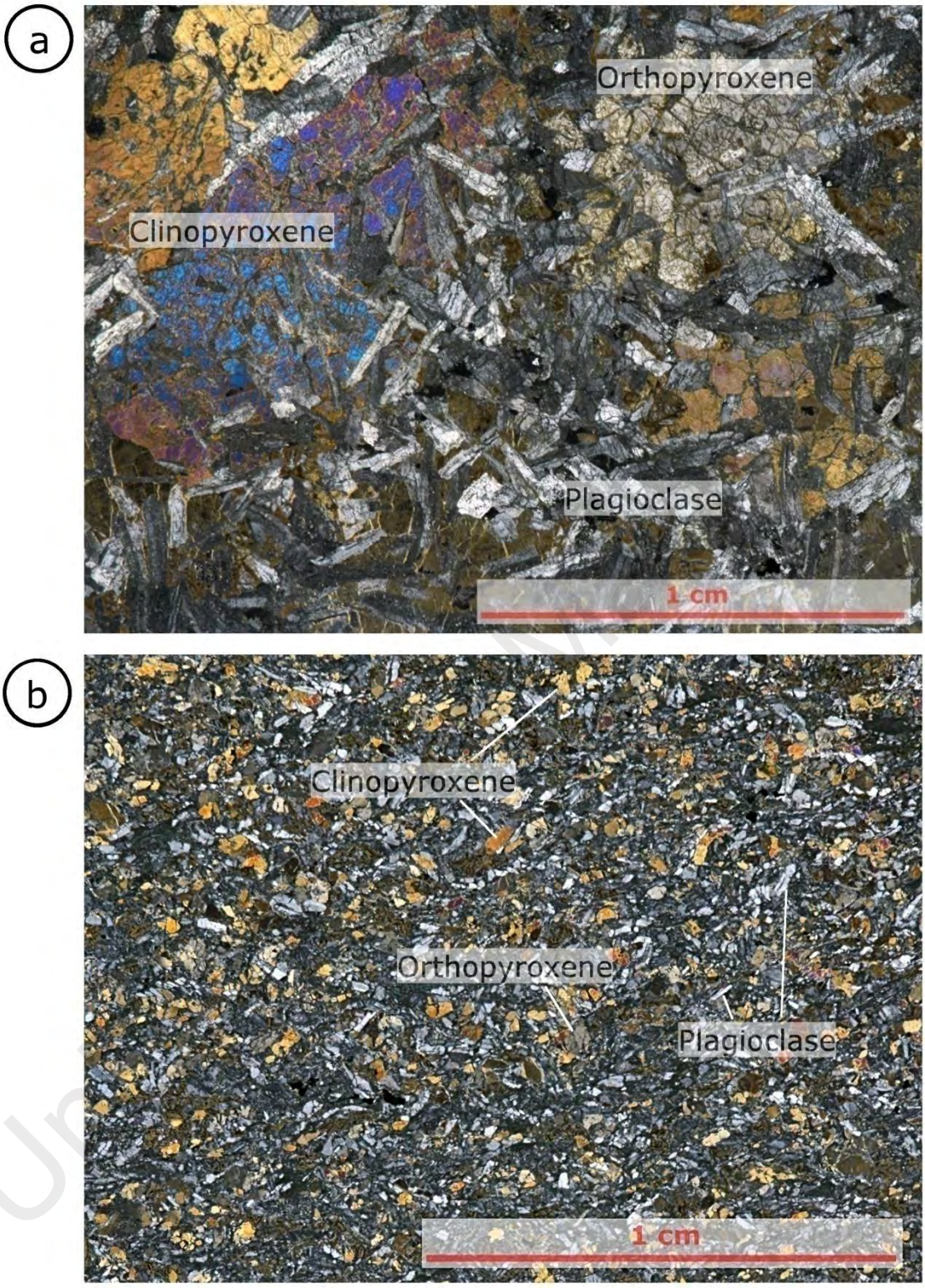

Figure 4.12: Photomicrographs (XPL) showing textures and mineral constituents of the meta-dolerite. (a) Coarse-grained meta-dolerite from Serendah area. (b) Fine-grained meta-dolerite from Serdang area.

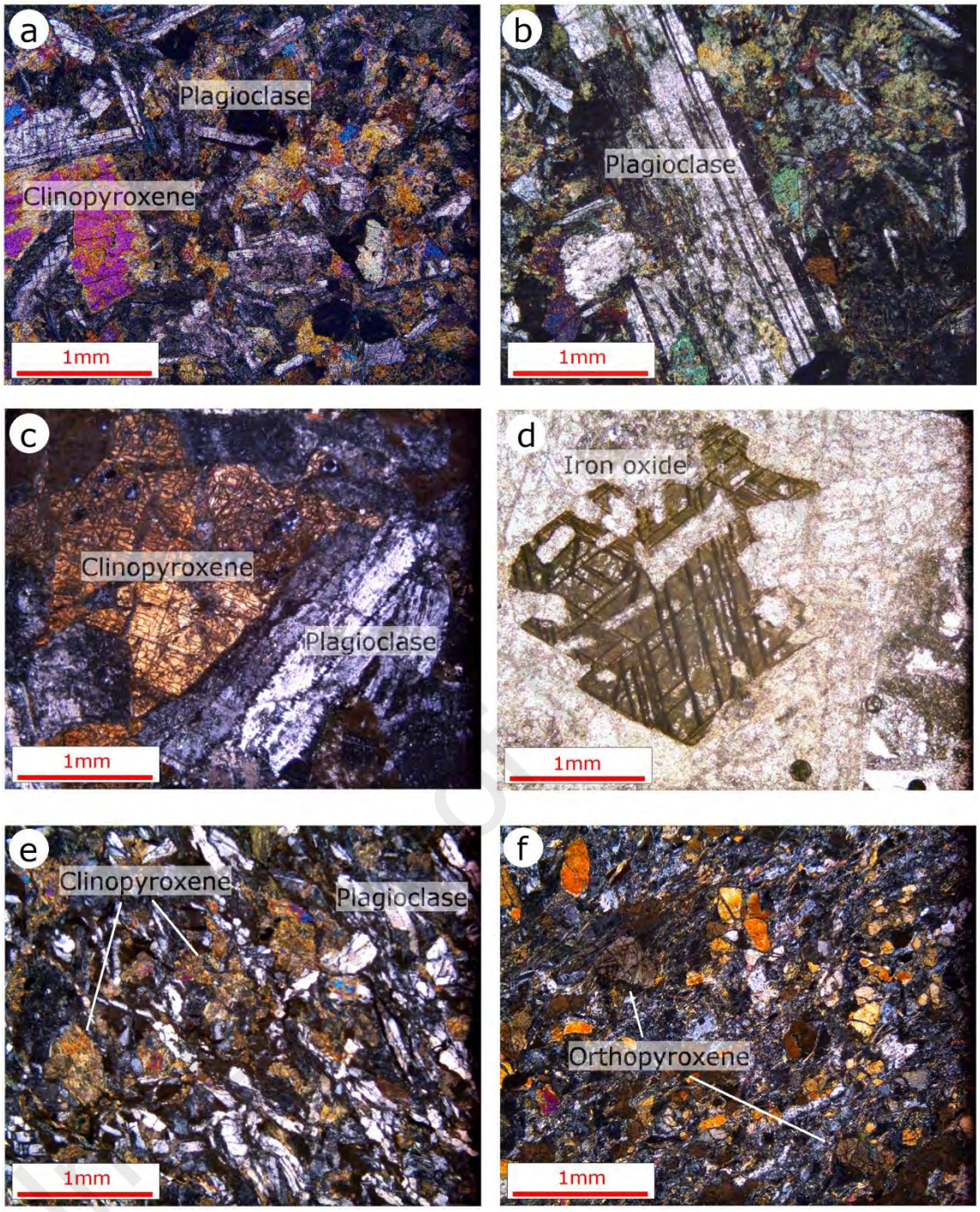

Figure 4.13: Thin section photos showing textures and mineral constituents of the meta-dolerite. (a) Photomicrograph (XPL) showing the typical ophitic texture of unaltered meta-dolerite. (b) Photomicrograph (XPL) showing a plagioclase phenocryst grain. (c) Photomicrograph (XPL) showing clinopyroxene (identified through 2nd order interference color and inclined extinction) and sericitized plagioclase phenocryst. (d) Photomicrograph (PPL) showing Trellis-type laminae on iron oxide grains in the meta-dolerite. (e) Photomicrograph (XPL) showing the mylonitic texture of ductile deformed meta-dolerite. (f) Another photomicrograph (XPL) showing intensely flattened plagioclase and pyroxene in a fine-grained streaked matrix (mylonitic texture) of ductile deformed meta-dolerite.

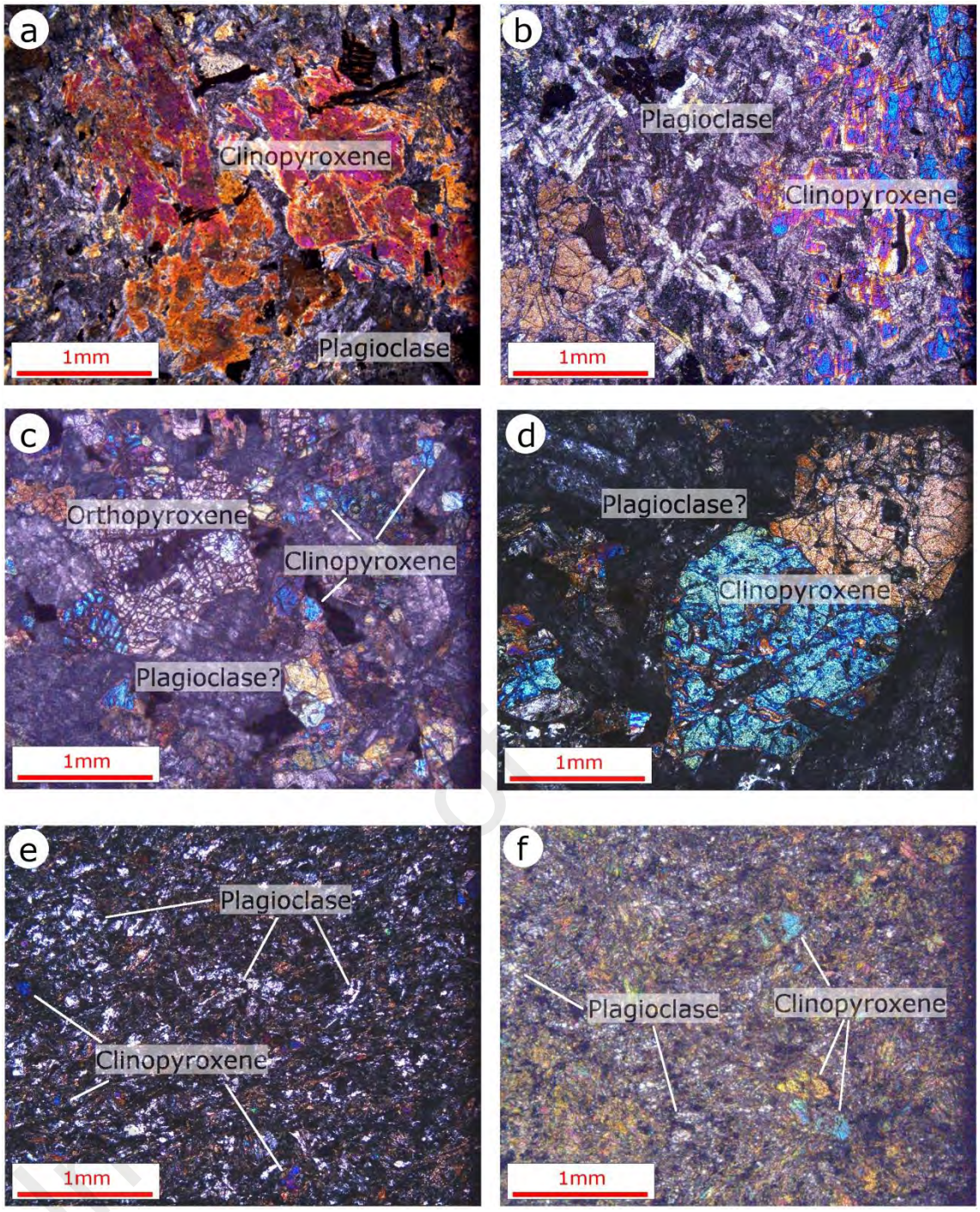

Figure 4.14: Thin section photos showing textures and mineral constituents of the meta-dolerite. Note that the groundmass minerals in all samples are altered due to post-magmatic events. (a to d) Photomicrograph (XPL) showing the alteration on the plagioclase of the meta-dolerite. Traces of the original ophitic texture are still noticeable. (e and f) Photomicrograph (XPL) showing cataclastic texture on deformed meta-dolerite. The original ophitic texture is not preserved.

4.3 Whole-rock major and trace elements geochemistry

Field and petrographical observations indicate that both meta-volcanic rocks and the meta-dolerite underwent greenschist facies metamorphism and possible variable alteration, during which the concentrations of fluid-mobile elements (e.g., K, Na, Cs, Rb, Ba, and Sr) are most likely changed. Only immobile elements (e.g., high-field-strength elements (HFSEs), rare-earth elements (REEs), transition elements, Th, Ti and P) were relatively unaffected by these processes (Li et al. 2002; Hu et al., 2013); thus they are appropriate for use in the classification and investigation of petrogenesis and tectonic setting for the meta-volcanic rocks and meta-dolerite. Major and trace element data for Gerik-Dinding meta-volcanic rocks, Rephens meta-volcanic rocks and meta-dolerite are listed in Appendix C, D and E respectively.

4.3.1 Gerik-Dinding meta-volcanic rocks

Forty-three Gerik-Dinding meta-volcanic samples (meta-crystal tuff and meta-rhyolite) were analyzed for whole-rock major and trace element compositions. The meta-volcanic rocks display a varied range of SiO_2 (60.68 to 82.56 wt. %), TFe_2O_3 (0.52 to 6.78 wt. %) and MgO (0.09 to 2.21 wt. %) values with metaluminous to peraluminous A/CNK values (0.89 to 2.90). The loss on ignition (L.O.I) for the meta-volcanic rocks is generally low (< 5.0 wt. %), with values varying from 0.47 to 3.98 wt. %. Samples with SiO_2 > 80 wt. % are found to contain higher quartz crystal fragments in petrography. The meta-volcanic rocks are classified using the immobile element ratio discrimination diagrams Nb/Y vs. Zr/Ti after Pearce (1996). Results suggest that they are comparable to rhyolite (Figure 4.15a). The Th vs. Co classification diagram after Hastie et al. (2007), which is also effective in discriminating between altered volcanic rocks (Hu et al., 2013), shows the meta-volcanic rocks plot within the rhyolite/dacite and high-K calc-alkaline and shoshonite series fields (Figure 4.15b).

The meta-volcanic rocks total REE content varies from 103.6 to 371.3 ppm. The chondrite (Bonyton, 1984) normalized REE variation diagram for the meta-volcanic rocks are shown in Figure 4.16a. The meta-volcanic rocks demonstrate moderate to strong light rare-earth elements (LREEs) enrichment (La_N/Yb_N = 2.8 - 13.0, where N denotes normalization to the chondrite values) and a relatively flat heavy rare-earth elements (HREEs) pattern. The Eu-anomalies (Eu/Eu*) of the meta-volcanic rocks are generally negative (<1) but the values are highly variable, from 0.04 to 0.71. Some samples have much greater negative Eu-anomalies than most due to plagioclase fractionation. According to Bachmann (2008), rhyolite and granite with weak Eu-anomalies are derived from cold-wet-oxidized magmas, typically found in subduction zones. Since upper continental crust is generally formed by subduction-related processes (Condie, 1997), patterns of samples with weak Eu-anomalies are similar to those of the upper crust (Rudnick and Fountain, 1995).

In the primitive mantle (Sun and Mcdonough, 1989) normalized trace element variation diagram (Figure 4.16b), all samples exhibit similar trace element patterns. The meta-volcanic rocks are marked by enrichment in Th, U, Zr, and Hf and depletion in Nb, Ta, Ti, and P. Such Nb–Ti–P anomalies are typically observed in subduction-related rocks (Saunders et al., 1991). In general, the meta-volcanic rocks trace element patterns are consistent with those of the upper crust (Rudnick and Fountain, 1995), however, some samples may exhibit stronger P, Eu and Ti depletion. The selective depletion of P and Ti indicates that one or more mineral phases (e.g. garnet) removed Ti and P selectively without causing larger depletion in other HFSE (Saunders et al., 1991).

The familiar diagram of Pearce (1983), which used Th/Yb vs. Ta/Yb ratios to discriminate mafic volcanic rocks from various types of tectonic settings, was recently revised by Gorton and Schandl (2000) to accommodate felsic to intermediate volcanic rocks. The new Th/Yb vs. Ta/Yb and Th/Hf vs. Ta/Hf tectonic discrimination diagrams

introduced in Schandl and Gorton (2002) research are based on immobile elements and are effective for the investigation of altered silicic volcanic rocks. On the Th/Yb vs. Ta/Yb diagram (Figure 4.17a), the meta-volcanic rocks plot within the active continental margin field (ACM), which features typical arc-related settings. On the Th/Hf vs. Ta/Hf diagram (Figure 4.17b), the meta-volcanic rocks plot above the dividing line that separates the active continental margin field from within plate volcanic zones field (WPVZ), producing similar interpretation as the first diagram.

4.3.2 Rephens meta-volcanic rocks

Seven Rephens meta-volcanic samples (four meta-andesite and three meta-lithic tuff) were analyzed for whole-rock major and trace element compositions. The meta-andesite exhibit intermediate SiO_2 content (56.95 to 62.41 wt. %) while the meta-lithic tuff exhibits felsic SiO_2 content (67.17 to 71.48 wt. %). The meta-andesite is metaluminous with A/CNK values ranging from 0.68 to 0.71 whereas the meta-lithic tuff is peraluminous with A/CNK values ranging from 3.59 to 4.18. The meta-andesite also shows higher CaO, Fe_2O_3t and MgO values compared to the meta-lithic tuff. The L.O.I for the meta-volcanic rocks is generally low, with values from 0.57 to 3.87 wt. %. The meta-volcanic rocks are classified using the immobile element ratio volcanic discrimination diagrams SiO_2 vs. Zr/TiO_2 (Figure 4.18a) after Winchester and Floyd (1977). Results suggest that the meta-andesite are equivalent to andesite while the meta-lithic tuff is comparable to rhyolite/dacite. The Th vs. Co classification diagram (Figure 4.18b) after Hastie et al. (2007) also displays similar classification results. The meta-andesite plots within the calc-alkaline series while the meta-lithic tuff plots within the high-K calc-alkaline and shoshonite series.

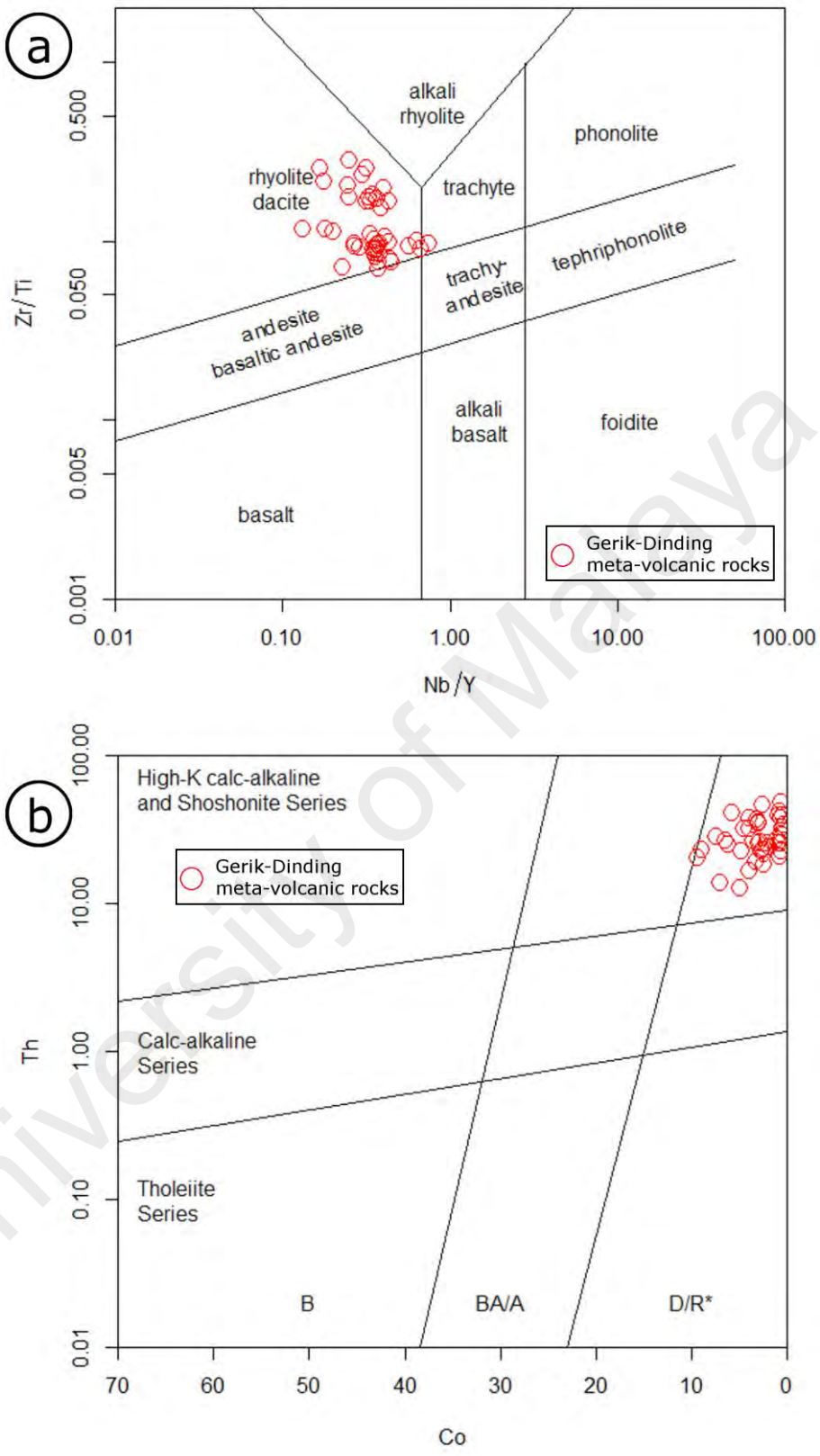

Figure 4.15: Classification plots for Gerik-Dinding meta-volcanic rocks. (a) Zr/Ti vs. Nb/Y plot (Pearce, 1996). (b) Th vs. Co plot (Hastie et al., 2007).

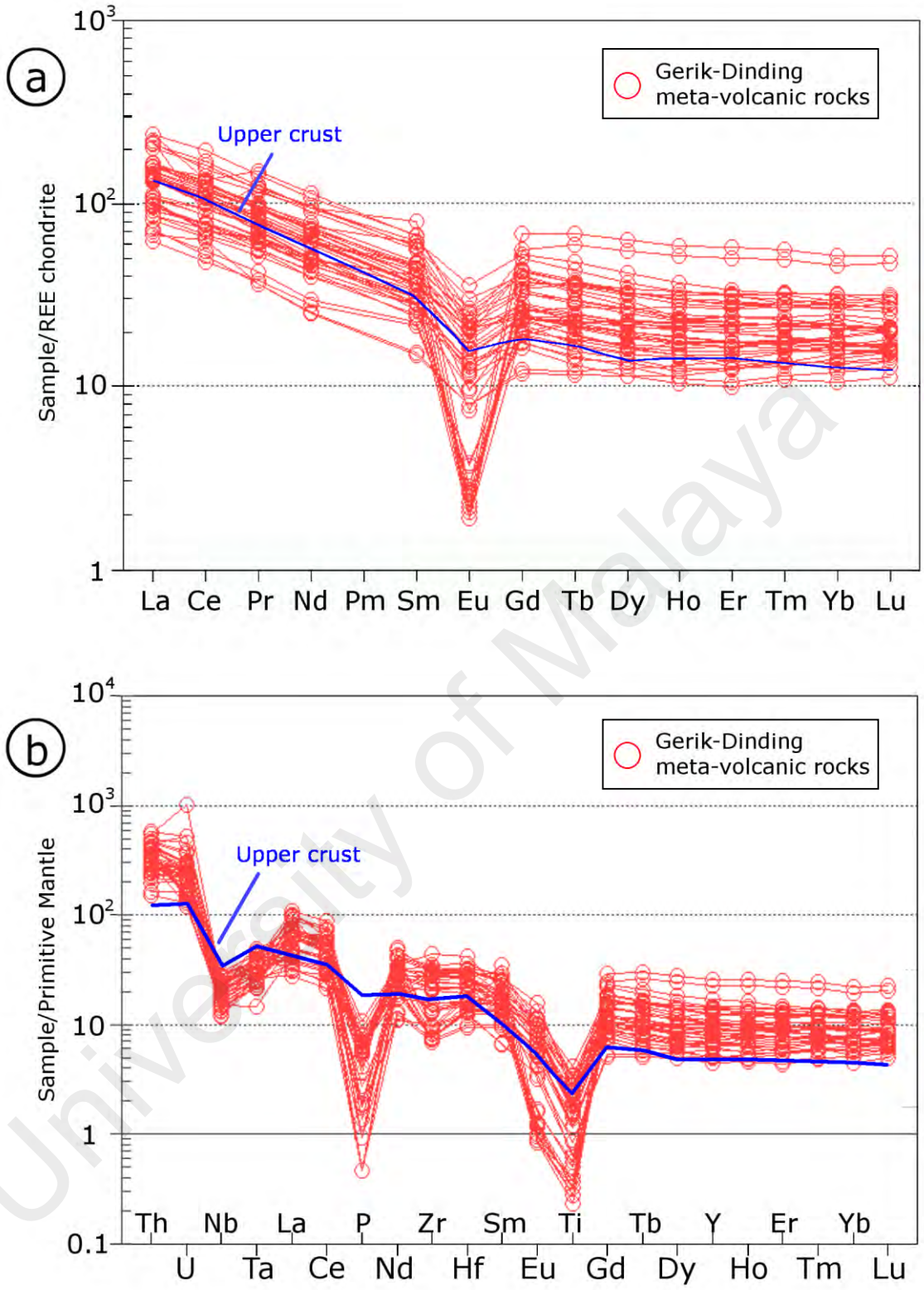

Figure 4.16: Trace element spider plots for Gerik-Dinding meta-volcanic rocks. (a) Chondrite-normalized REE spider plot. REE abundances for chondrites are from Boynton (1983). (b) Primitive mantle-normalized spider plot. Trace element abundances for primitive mantle are after Sun and McDonough (1989). Upper crust patterns are from Rudnick and Fountain (1995).

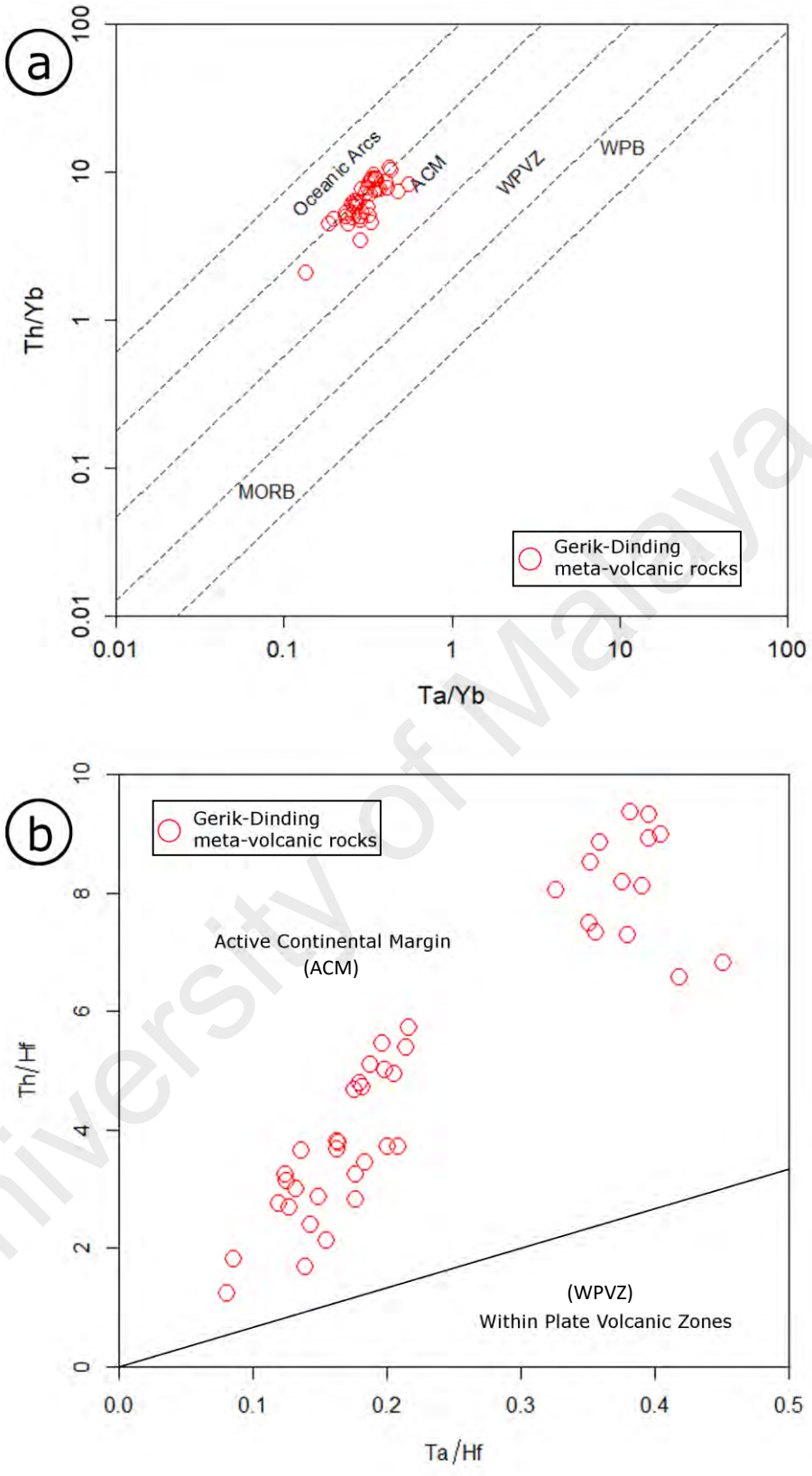

Figure 4.17: Geotectonic discrimination diagrams for silicic to intermediate volcanic rocks (Gerik-Dinding meta-volcanic rocks). Both diagrams are after Schandl and Gorton (2002). (a) Ta/Hf vs. Th/Hf plot. (b) Ta/Yb vs. Th/Yb plot.

The chondrite (Bonyton, 1984) normalized REE variation diagram for the meta-volcanic rocks are shown in Figure 4.19a. The meta-lithic tuff (average: 239.6 ppm) has higher total REE content compared to the meta-andesite (average: 100.9 ppm). Both meta-andesite (La_N/Yb_N = 5.6-8.7) and meta-lithic tuff (La_N/Yb_N = 5.8-6.7) demonstrate elevated LREE content. While meta-andesite shows no visible Eu-anomalies (Eu/Eu* = 0.92 - 1.00), the meta-lithic tuff displays negative Eu-anomalies (Eu/Eu* = 0.49 - 0.67). The REE abundances of the meta-andesite are similar to those of middle crust while the REE abundances of the meta-lithic tuff are comparable to those of the upper crust (Rudnick and Fountain, 1995). In the primitive mantle (Sun and Mcdonough, 1989) normalized trace element variation diagram (Figure 4.19b), though the meta-andesite exhibit lower trace element abundance compared to meta-lithic tuff, both rock types exhibit similar trace element patterns. The meta-volcanic rocks are marked by enrichment in Th, U, Zr, and Hf and depletion in Nb, Ta, Ti, and P. Such Nb–Ti–P anomalies are typically observed in subduction-related rocks (Saunders et al., 1991). The meta-andesite trace element patterns are analogous to the middle crust while the meta-lithic tuff trace element patterns are consistent with those of the upper crust (Rudnick and Fountain, 1995). The comparison of Rephens meta-volcanic rocks chondrite and trace element patterns with several stages of crust curves suggest that melting of different parts of the crust were involved. On the Th/Yb vs. Ta/Yb (Figure 4.20a) and Th/Hf vs. Ta/Hf (Figure 4.20b) immobile element tectonic discrimination diagrams for volcanic rocks after Schandl and Gorton (2002), both meta-volcanic rock types plot within the active continental margin field (ACM) field.

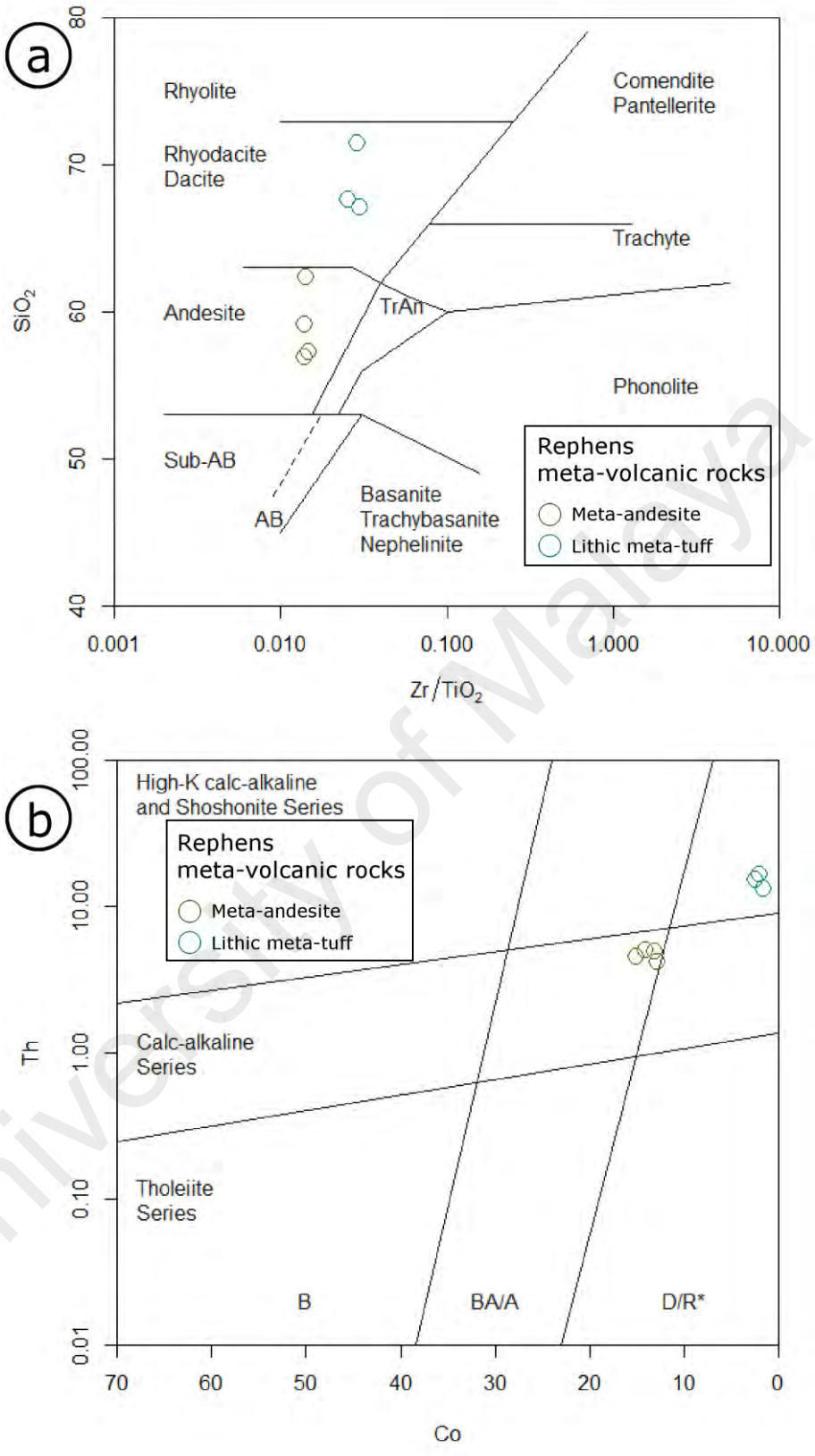

Figure 4.18: Classification plots for Rephens meta-volcanic rocks. (a) SiO_2 vs. Zr/TiO_2 plot (Winchester and Floyd, 1977), (b) Th vs. Co plot (Hastie et al., 2007).

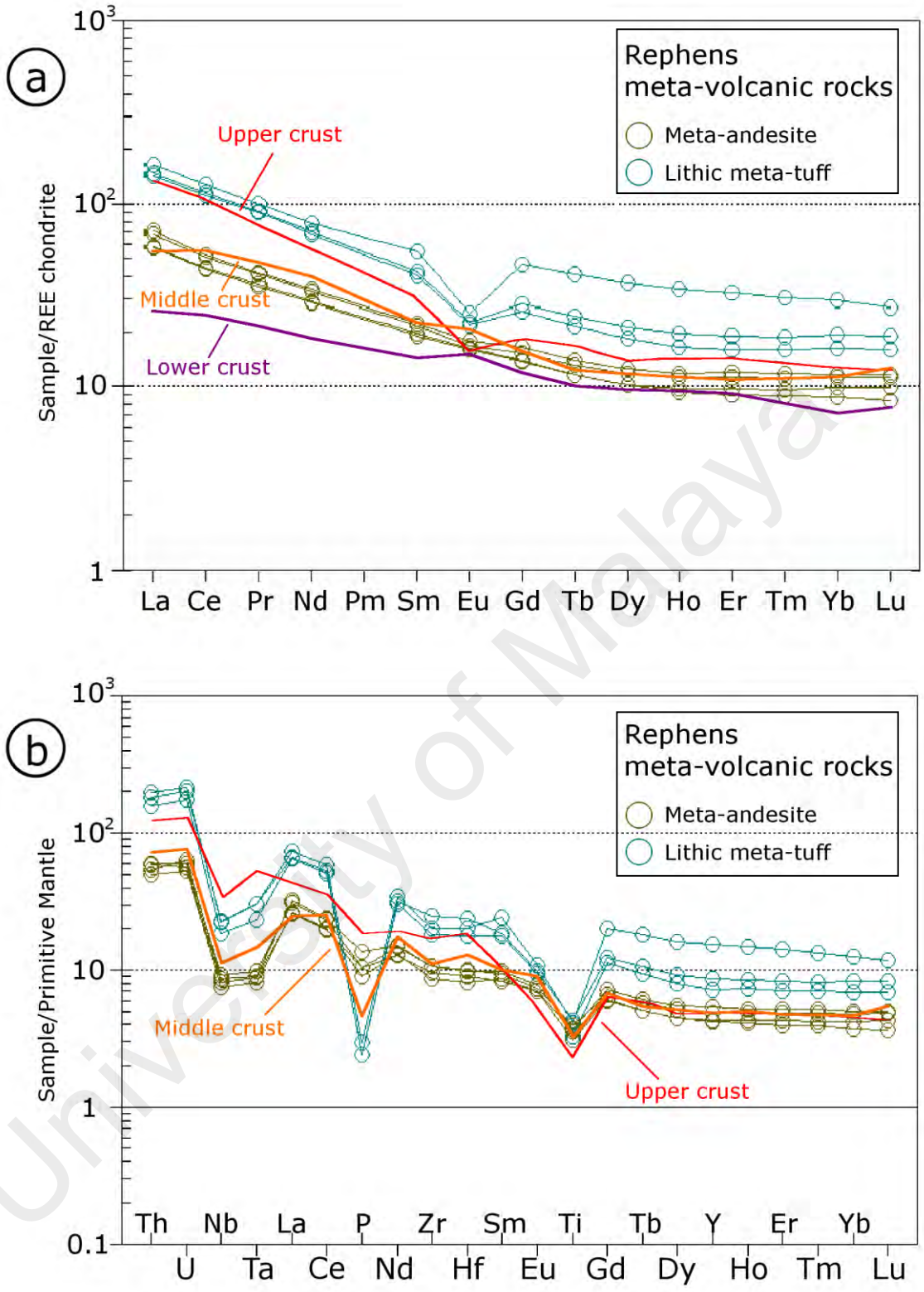

Figure 4.19: Trace element spider plots for Rephens meta-volcanic rocks. (a) Chondrite-normalized REE spider plot. REE abundances for chondrites are from Boynton (1983). (b) Primitive mantle-normalized spider plot. Trace element abundances for primitive mantle are after Sun and McDonough (1989). The upper crust, middle crust and lower crust patterns are from Rudnick and Fountain (1995).

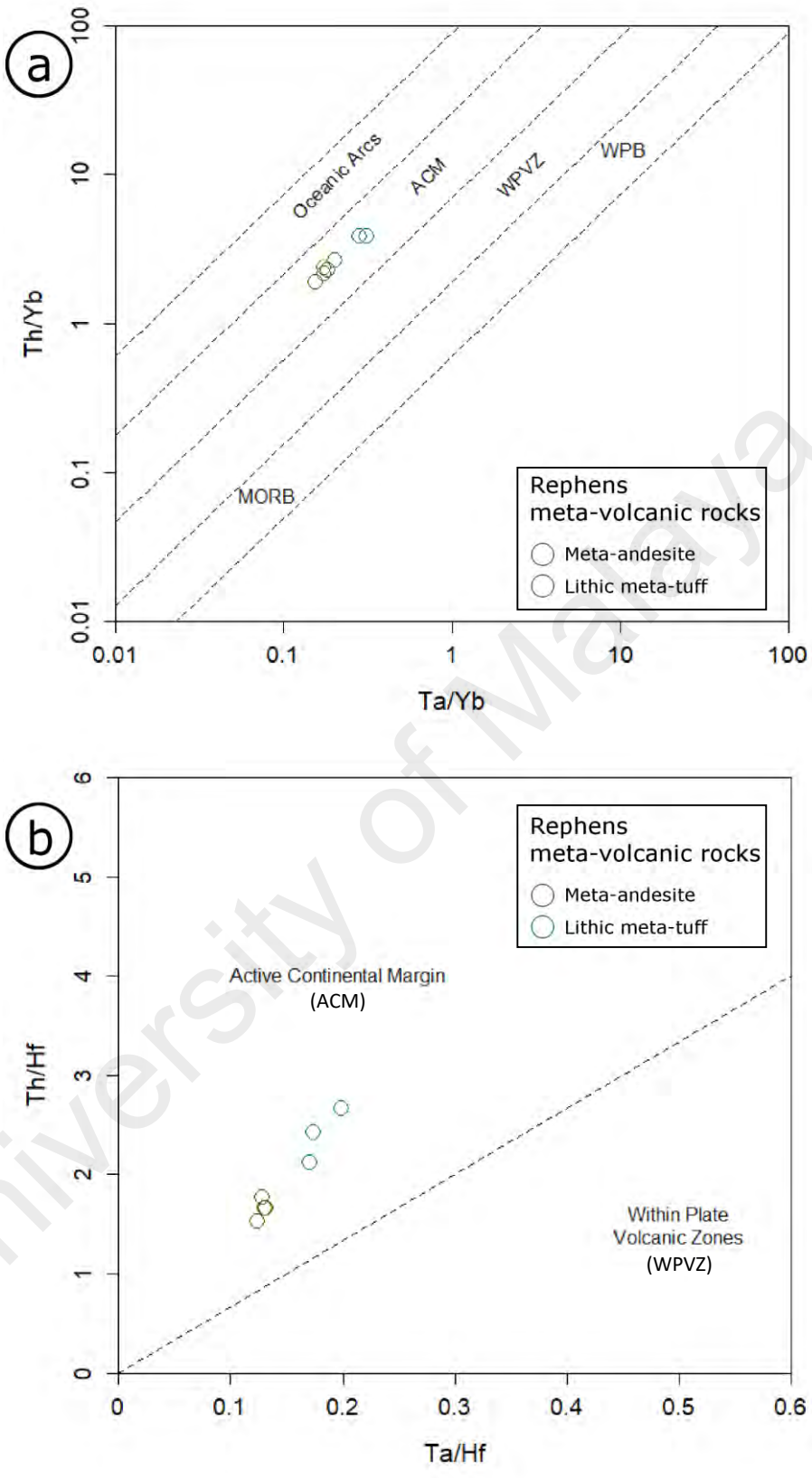

Figure 4.20: Geotectonic discrimination diagrams for silicic to intermediate volcanic rocks (Rephens meta-volcanic rocks). Both diagrams are after Schandl and Gorton (2002). (a) Ta/Hf vs. Th/Hf plot (b) Ta/Yb vs. Th/Yb plot.

4.3.3 Meta-dolerite intrusions

Twenty-three meta-dolerite samples were analyzed for whole-rock major and trace element compositions. The meta-dolerite SiO_2 values are mafic (45-52 wt. %) and vary between 44.59 wt. % to 50.76 wt. %. The meta-dolerite also had varying MgO content (4.67 to 8.25 wt. %). The L.O.I content for the meta-dolerite is low to moderate, varying from 0.50 % to 5.29 %. The SiO_2 vs. TFe_2O_3[2]/MgO volcanic rock series discrimination diagram (Miyashiro, 1975) (Figure 4.21a) indicates the meta-dolerite samples plot within the tholeiite series field. The immobile elements ternary diagram of TiO_2-Zr+Y-Cr after Davies et al. (1979) (Figure 4.21b) also demonstrate similar results; the meta-dolerite samples follow the tholeiitic trend. For rock classification, the meta-dolerite samples are plotted on the total alkali-silica (TAS) diagram (Middlemost, 1994) (Figure 4.22a). Due to its low SiO_2 content, the meta-dolerite samples consistently plot within the basalt field. The immobile elements classification diagram Nb/Y vs. Zr/Ti (Pearce 1996) (Figure 4.22b) show the meta-dolerite are certainly comparable to basalt and can be further divided into alkaline and sub-alkaline basalt types using the Nb/Y ratio.

The chondrite (Boynton, 1983) normalized REE variation diagram of the meta-dolerite samples are shown in Figure 4.23a. The alkaline meta-dolerite samples REE patterns (La_N/Yb_N: 8.0 - 9.2) exhibit a steeper slope compared to the sub-alkaline meta-dolerite samples (La_N/Yb_N: 1.3 - 2.8). Overall, both alkaline and sub-alkaline patterns do not show pronounced positive (>1) or negative (<1) Eu-anomalies (Eu/Eu*: 0.84-1.27). In comparison to the normal mid-ocean ridge basalt (N-MORB) REE pattern (Sun and Mcdonough, 1989), the meta-dolerite samples are slightly more enriched in light REE. The primitive mantle (Sun and Mcdonough, 1989) normalized trace element variation diagram is shown in Figure 4.23b. Overall, both alkaline and sub-alkaline show enrichment in Th, U, Nb, Ta, La and Ce in comparison to the N-MORB pattern (Sun and

[2] TFe_2O_3 = Total iron oxide. Total iron oxide may be expressed as $TFe_2O_3 = (1.11 \times FeO) + Fe_2O_3$

Mcdonough, 1989). Although comparison with Early Paleozoic Tibetan plateau ophiolites and N-MORB suggest the meta-dolerite samples differs from ridge settings, geochemical features that typically characterize subduction environment, such as Nb-Ta, Zr-Hf and Ti negative anomalies (C. Li et al., 2015) are also not observed in both alkaline and sub-alkaline meta-dolerite patterns.

On the Ti vs. Zr geotectonic discriminant plot (Figure 4.24a) after Pearce (1982), both alkaline and sub-alkaline meta-dolerite samples plot inside within-plate lavas field. However, there is an overlap into the MORB field. On the Th-Hf/3-Ta geotectonic ternary diagram (Figure 4.24b) after Wood (1980), almost all meta-dolerite samples plot inside the E-MORB and within-plate tholeiite (WPT) field. The alkaline meta-dolerite is observed to plot closer to the within-plate alkaline basalt field (WPA). Although binary and ternary trace element tectonic discrimination diagrams are widely used for basalt tectonic setting interpretation, not all of the important diagnostic features for basalts can be captured in a single plot. For a better idea of the tectonic environment, it is best to complement the interpretation with other types of geological information and normalized trace element spidergram (C. Li et al., 2015).

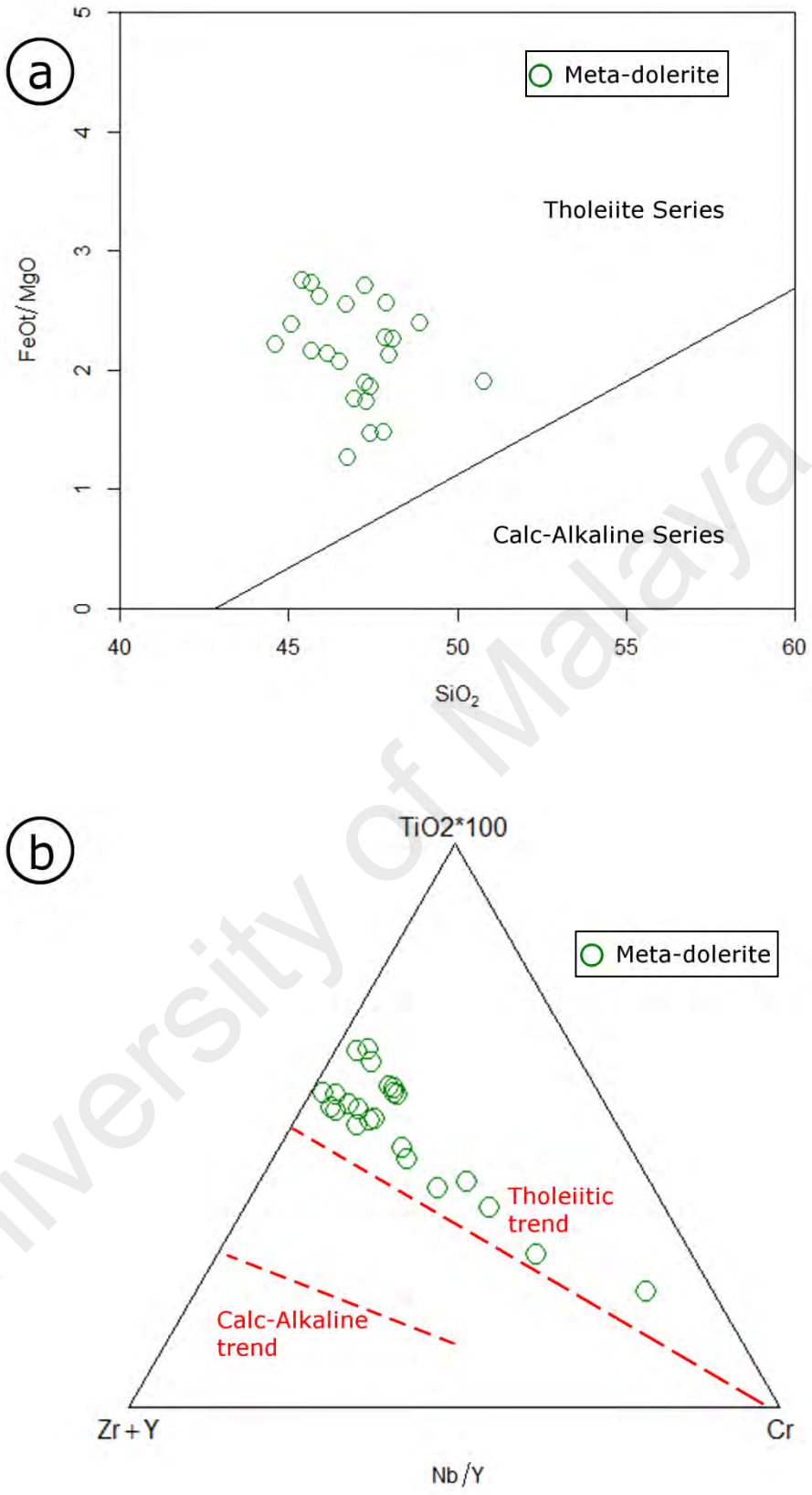

Figure 4.21: Classification plots for meta-dolerite (Tholeiite series vs. Calc-alkaline series). (a) FeOt/MgO vs. SiO_2 plot (Miyashiro, 1975). (b) (Zr + Y) - (TiO2 × 100) - Cr ternary diagram (Davies et al., 1979).

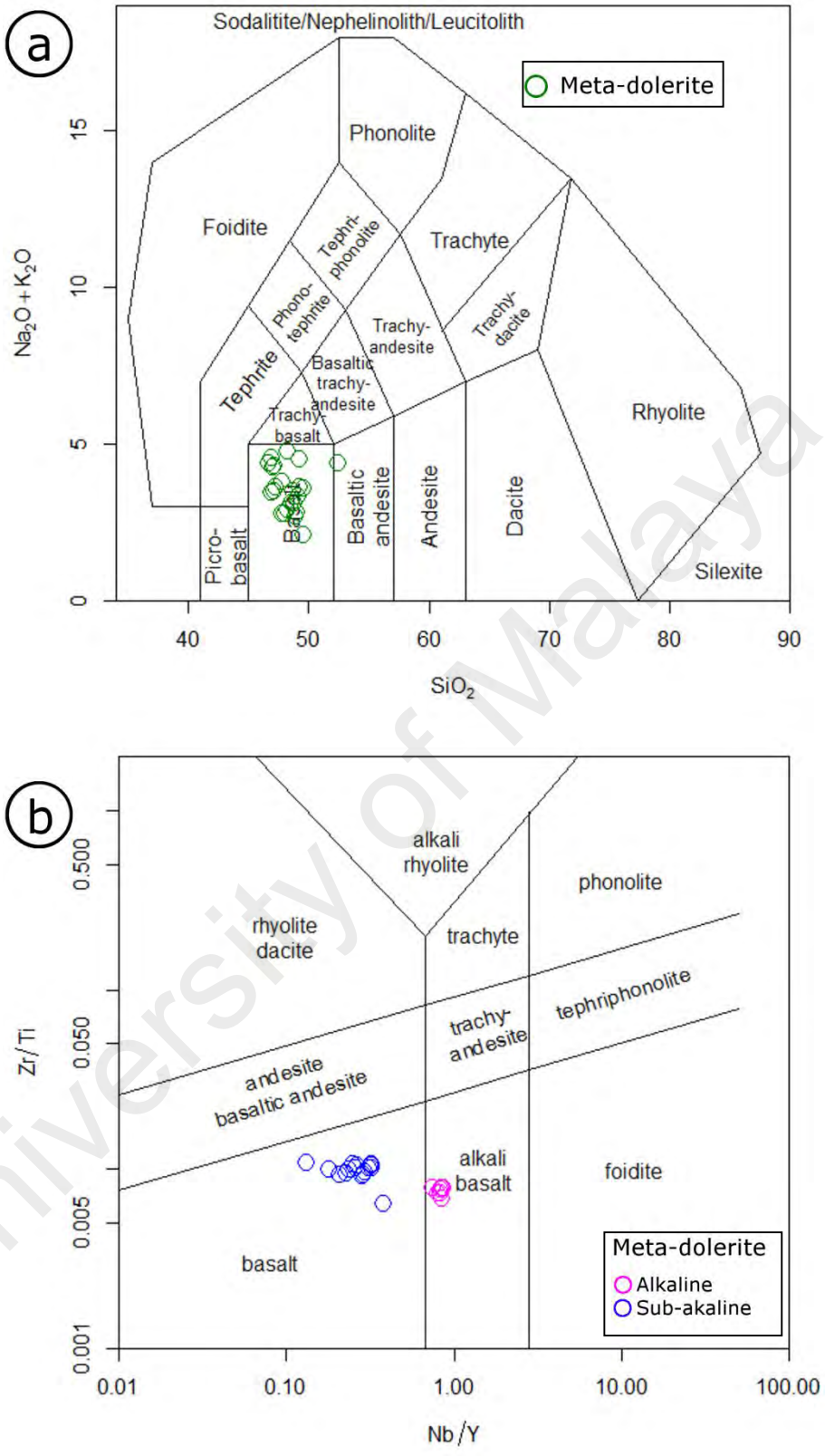

Figure 4.22: Classification plots for meta-dolerite. (a) Na_2O+K_2O vs. SiO_2 plot (Middlemost, 1994). (b) Zr/Ti vs. Nb/Y plot (Pearce, 1996).

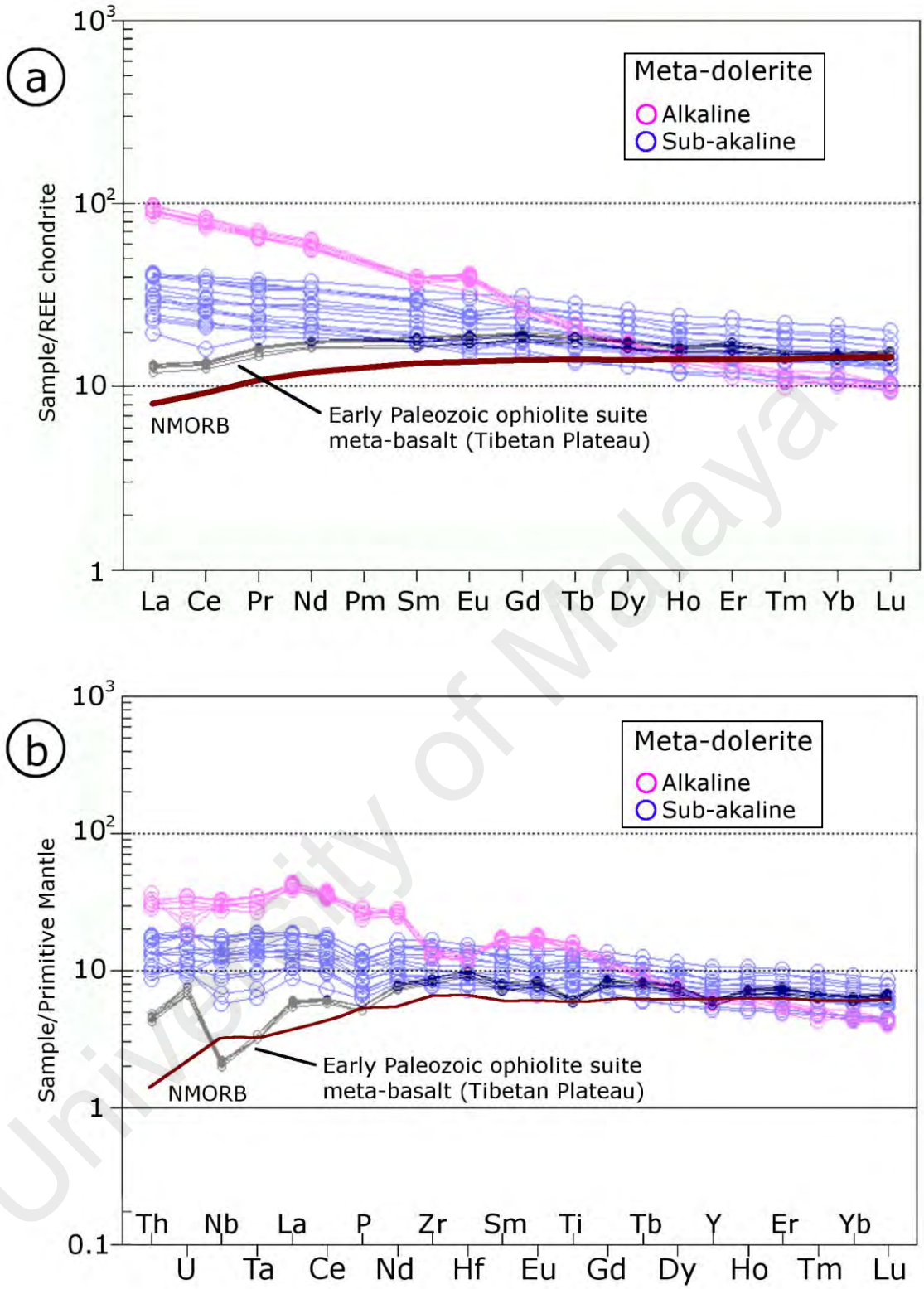

Figure 4.23: Trace element spider plots for meta-dolerite. (a) Chondrite-normalized REE spider plot. REE abundances for chondrites are from Boynton (1983). (b) Primitive mantle-normalized spider plot. Trace element abundances for primitive mantle are after Sun and McDonough (1989). Present-day N-MORB patterns (Sun and McDonough, 1989) and Early Paleozoic ophiolite suite meta-basalt of N-MORB characteristics from Tibetan Plateau (Zhai et al., 2015) were included in the diagram for comparison.

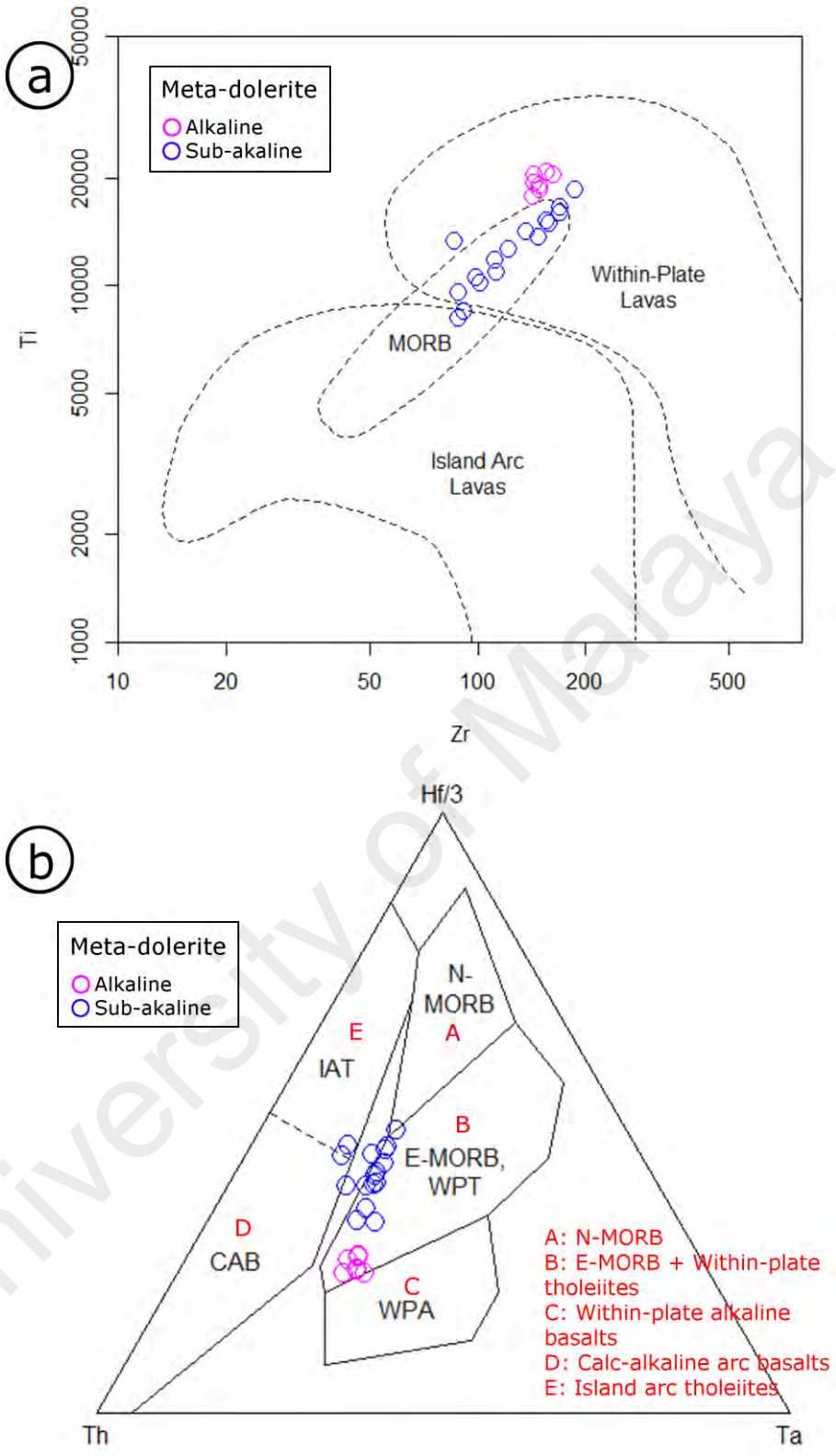

Figure 4.24: Geotectonic discriminant diagram for basic rocks. (a) Ti vs. Zr plot after Pearce (1982). (b) Th - (Hf/3) - Ta ternary diagram after Wood et al. (1979) and Wood (1980).

4.4 Zircon U-Pb isotope geochronology

Zircon grains were extracted from ten meta-volcanic samples. Zircons grains from eight Gerik-Dinding meta-volcanic rock samples are characteristically yellowish brown to colorless, transparent, euhedral and display long to short prismatic forms. On the other hand, zircon grains obtained from two Rephens meta-volcanic rock samples are normally colorless, transparent, euhedral and display long to short prismatic forms. The zircon crystals range in length from 100 μm to 250 μm. In cathodoluminescence (CL) images (Figure 4.25 to 4.27), most zircons show oscillatory zoning, which is indicative of magmatic growth (Corfu et al., 2003; Hoskin and Schaltegger, 2003). Zircons with rounded or oval shapes and complex internal textures are rare. The zircon U-Pb isotope geochronology data is listed in Appendix F and presented in terms of concordia diagrams and weighted mean diagrams. The weighted average $^{206}Pb/^{238}U$ ages were calculated using only concordant and consistent data, which are indicated by the ovals in each concordia plots. All the age errors are given at the 2σ level. The geochronology results can be summarized as follows:

a) Fifteen data spots from LAWIN-1 zircons were acquired for this study. After data correction and reduction, the obtained twelve consistent and concordant age data fall within 455-492 Ma and yielded a weighted mean $^{206}Pb/^{238}U$ age of 470.8 ± 4.6 Ma (2σ, MSWD = 1.6) (Figure 4.28). The zircons used for weighted mean age calculation have variable U (74-1734 ppm) and Th (55-1206 ppm) content and yield relatively high Th/U ratios (0.35-1.82). Three concordant Mesoproterozoic ages (1.1-1.7 Ga) are also found in LAWIN-1 zircons.

b) Twenty-eight data spots from JERAI-1 zircons were acquired for this study. After data correction and reduction, the obtained twenty-three consistent and concordant age data fall within 467-498 Ma and yielded a weighted mean $^{206}Pb/^{238}U$ age of 480.5 ± 4.2 Ma (2σ, MSWD = 3.0) (Figure 4.29). The zircons used for weighted

mean age calculation have variable U (83-1458 ppm) and Th (76-1237 ppm) content and yield relatively high Th/U ratios (0.47-1.13). Four concordant Late to Middle Cambrian ages (499-510 Ma) and one concordant Neoarchean age (2.7 Ga) are also found in JERAI-1 zircons.

c) Thirty-nine data spots from LEBEY-1 zircons were attained for this study. After data correction and reduction, the obtained thirty-four consistent and concordant age fall within 458-493 Ma and yielded a weighted mean $^{206}Pb/^{238}U$ age of 472.5 ± 3.1 Ma (2σ, MSWD = 2.7) (Figure 4.30). The zircons used for weighted mean age calculation have variable U (126-967 ppm) and Th (88-543 ppm) content and yield relatively high Th/U ratios (0.12-0.95). Three concordant Early Cambrian ages (494-498 Ma) and two concordant Mesoproterozoic ages (1.1-1.2 Ga) are also found in LEBEY-1 zircons.

d) Forty-two data spots from TEMNG-1 zircons were acquired for this study. After data correction and reduction, the obtained thirty-five consistent and concordant age fall within 459-489 Ma and yielded a weighted mean $^{206}Pb/^{238}U$ age of 474.2 ± 2.9 Ma (2σ, MSWD = 2.3) (Figure 4.31). The zircons used for weighted mean age calculation have variable U (140-771 ppm) and Th (47-609 ppm) content and yield relatively high Th/U ratios (0.17-1.48). Four concordant Late to Middle Cambrian ages (492-512 Ma), one concordant Neoproterozoic age (787 Ma), one concordant Mesoproterozoic age (1.4 Ga) and one concordant Paleoproterozoic age (1.8 Ga) are also found in TEMNG-1 zircons.

e) Twenty-six data spots from BERU-1 zircons were acquired for this study. After data correction and reduction, the obtained twenty-one consistent and concordant age fall within 444-471 Ma and yielded a weighted mean $^{206}Pb/^{238}U$ age of 460.0 ± 2.4 Ma (2σ, MSWD = 1.4) (Figure 4.32). The zircons used for weighted mean age calculation have variable U (128-656 ppm) and Th (49-394 ppm) content and yield

relatively high Th/U ratios (0.25-0.62). Four concordant Early Ordovician to Early Cambrian ages (484-546 Ma) and one concordant Paleoproterozoic age (1.8 Ga) are also found in BERU-1 zircons.

f) Thirty-five data spots from SIPUT-1 zircons were acquired for this study. After data correction and reduction, the obtained thirty-one consistent and concordant ages fall within 460-499 Ma and yielded a weighted mean $^{206}Pb/^{238}U$ age of 476.0 ± 3.7 Ma (2σ, MSWD = 2.9) (Figure 4.33). The zircons used for weighted mean age calculation have variable U (132-660 ppm) and Th (86-361 ppm) content and yield relatively high Th/U ratios (0.39-0.74). Two concordant Middle Cambrian ages (505-516 Ma), one concordant Neoproterozoic age (724 Ma) and one concordant Mesoproterozoic age (1.1 Ga) are also found in SIPUT-1 zircons.

g) Twenty-six data spots from SIPUT-2 zircons were acquired for this study. After data correction and reduction, the obtained twenty-four consistent and concordant age fall within 446-477 Ma and yielded a weighted mean $^{206}Pb/^{238}U$ age of 462.3 ± 3.6 Ma (2σ, MSWD = 2.4) (Figure 4.34). The zircons used for weighted mean age calculation have variable U (205-792 ppm) and Th (52-379 ppm) content and yield relatively high Th/U ratios (0.19-0.79). Two concordant Middle to Early Cambrian ages (506-529 Ma) are also found in SIPUT-2 zircons.

h) Forty-one data spots from DIND-1 zircons were acquired for this study. After data correction and reduction, the obtained thirty-one consistent and concordant ages fall within 459-501 Ma and yielded a weighted mean $^{206}Pb/^{238}U$ age of 479.1 ± 3.3 Ma (2σ, MSWD = 2.2) (Figure 4.35). The zircons used for weighted mean age calculation have variable U (115-601 ppm) and Th (73-219 ppm) content and yield relatively high Th/U ratios (0.18-0.83). One concordant Early Cambrian age (521 Ma), seven concordant Neoproterozoic ages (665-930 Ma) and two concordant Paleoproterozoic ages (1.6 Ga) are also found in DIND-1 zircons.

i) Forty-three data spots from REP-1 zircons were acquired for this study. After data correction and reduction, the obtained twenty-one consistent and concordant ages fall within 331-355 Ma and yielded a weighted mean $^{206}Pb/^{238}U$ age of 342.6 ± 3.1 Ma (2σ, MSWD = 2.9) (Figure 4.36). The zircons used for weighted mean age calculation have variable U (29-580 ppm) and Th (66-730 ppm) content and yield relatively high Th/U ratios (0.43-0.95 ppm). Eight concordant Devonian ages (359-418 Ma), five concordant Silurian ages (436-443 Ma), eight concordant Ordovician ages (445-470 Ma) and one Mesoproterozoic age (1.2 Ga) are also found among REP-1 zircons

j) Thirty-five data spots from GAB-1 zircons were acquired for this study. After data correction and reduction, the obtained twenty consistent and concordant ages fall within 342-364 Ma and yielded a weighted mean $^{206}Pb/^{238}U$ age of 354.2 ± 3.4 Ma (2σ, MSWD = 2.9) (Figure 4.37). The zircons used for weighted mean age calculation have variable U (74-891 ppm) and Th (185-3087 ppm) content and yield relatively high Th/U ratios (0.13-0.58). One concordant Early Devonian age (398 Ma), Three concordant Silurian ages (426-442 Ma), Eight concordant Ordovician ages (444-490 Ma), One concordant Cambrian age (692 Ma), One concordant Mesoproterozoic age (1.2 Ga) and One concordant Paleoproterozoic age (1.7 Ga) are also found among GAB-1 zircons

The analyzed spots' relatively high Th/U values (> 0.1) and the zircon magmatic zoning pattern in CL images, suggest that these analyzed zircons are characteristic of magmatic zircons (Compton et al., 1986; Schaltegger et al., 1999), and the acquired results should represent the time of crystallization for the protolith. The Middle Ordovician and Early Carboniferous zircon U-Pb ages acquired from Gerik-Dinding and Rephens meta-volcanic rocks represents the first ever geochronology evidence of the Early Paleozoic volcanism in Western Peninsular Malaysia

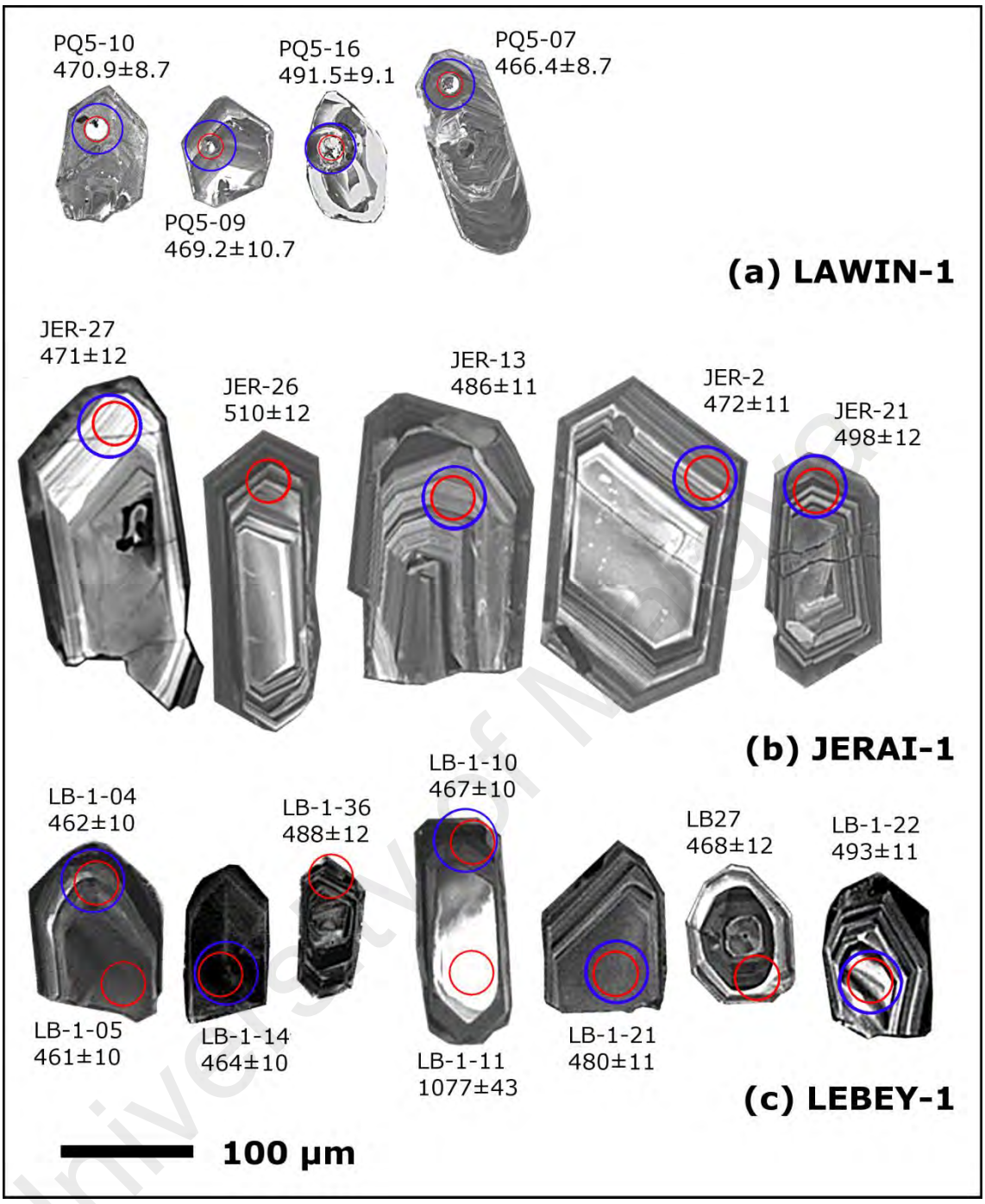

Figure 4.25: Cathodoluminescence (CL) images of representative zircon grains from Gerik-Dinding meta-volcanic rocks. (a) zircons from LAWIN-1 sample. (b) zircons from JERAI-1 sample. (c) zircons from LEBEY-1 sample. Red and blue circles show the locations of U-Pb dating and Hf analyses, respectively. The scale bar on the CL images is 100 µm. Areas that appear dark on zircon in CL images are relatively rich in U and Y while areas that appear bright on zircon are relatively poor in those trace elements (Rubatto and Gebauer, 2000). Zircon rims are useful for dating magmatic events if unaltered/undisturbed. They represent the final stage of zircon crystallization.

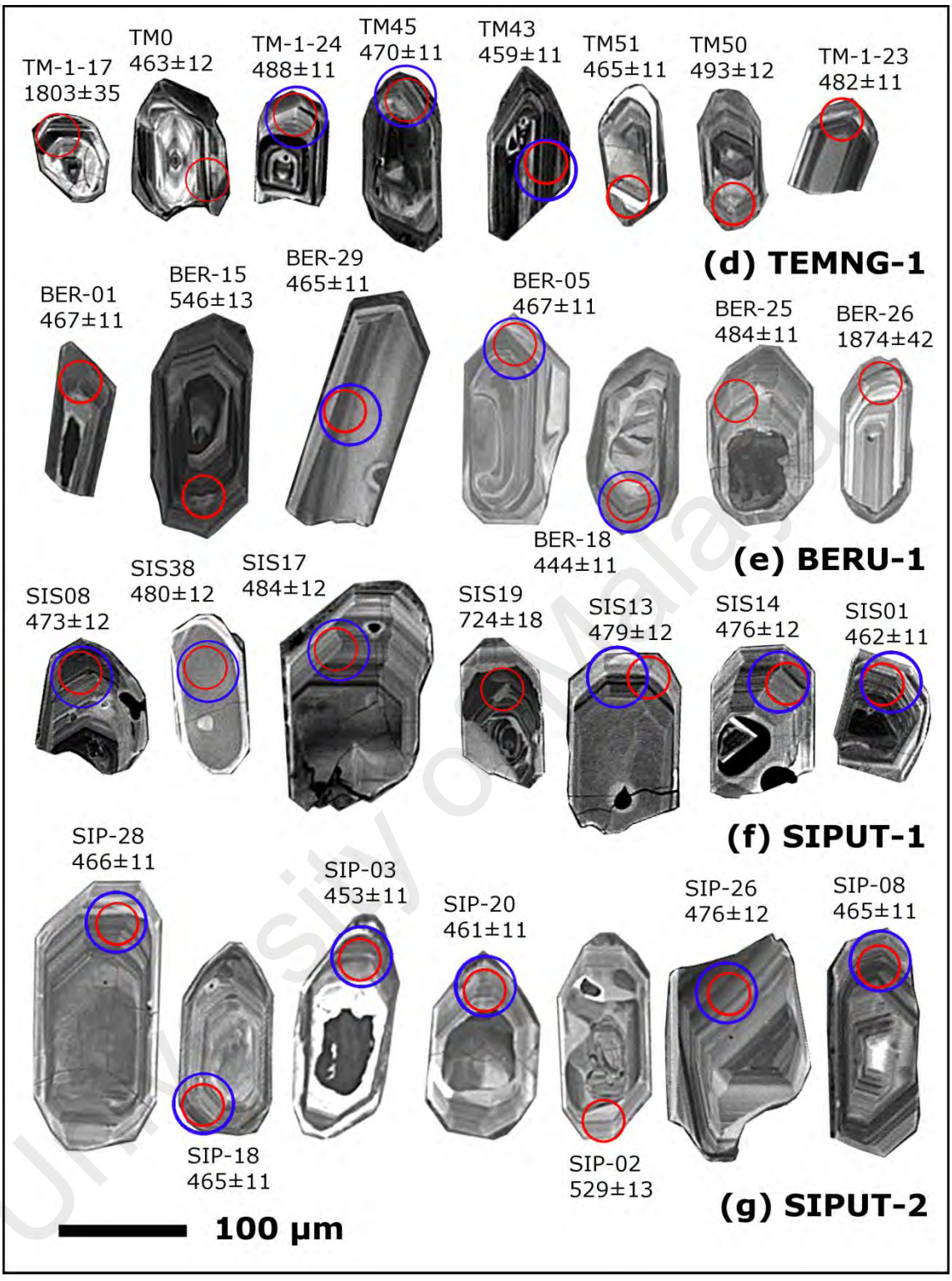

Figure 4.26: Cathodoluminescence (CL) images of representative zircon grains from Gerik-Dinding meta-volcanic rocks. (d) zircons from TEMNG-1 sample. (e) zircons from BERU-1 sample. (f) zircons from SIPUT-1 sample. (g) zircons from SIPUT-2 sample. Red and blue circles show the locations of U-Pb dating and Hf analyses, respectively. The scale bar on the CL images is 100 µm.

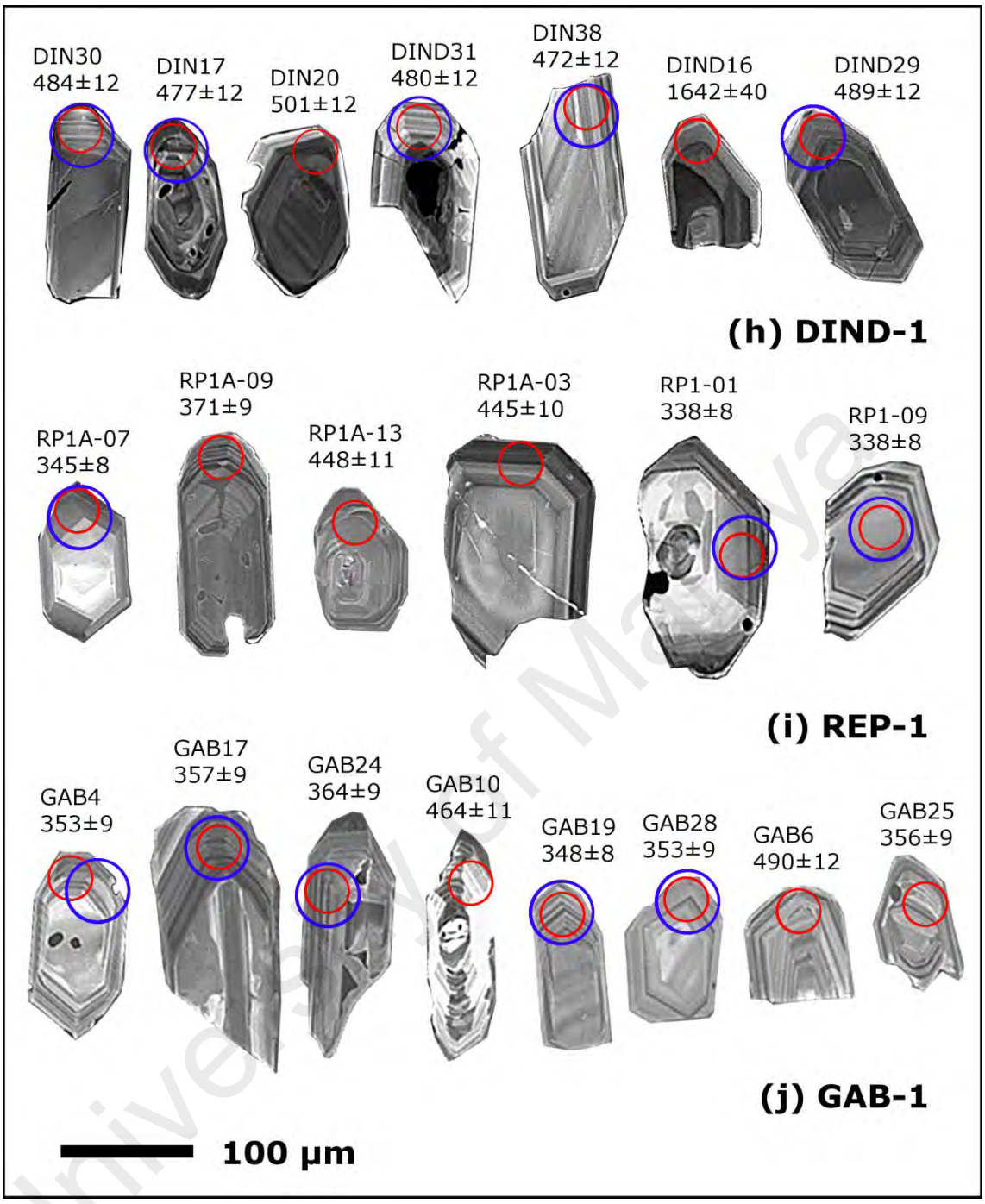

Figure 4.27: Cathodoluminescence (CL) images of representative zircon grains from Gerik-Dinding meta-volcanic rocks and Rephens meta-volcanic rocks (REP-1 and GAB-1). (h) zircons from DIND-1 sample. (i) zircons from REP-1 sample. (j) zircons from GAB-1 sample. Red and blue circles show the locations of U-Pb dating and Hf analyses, respectively. The scale bar on the CL images is 100 µm.

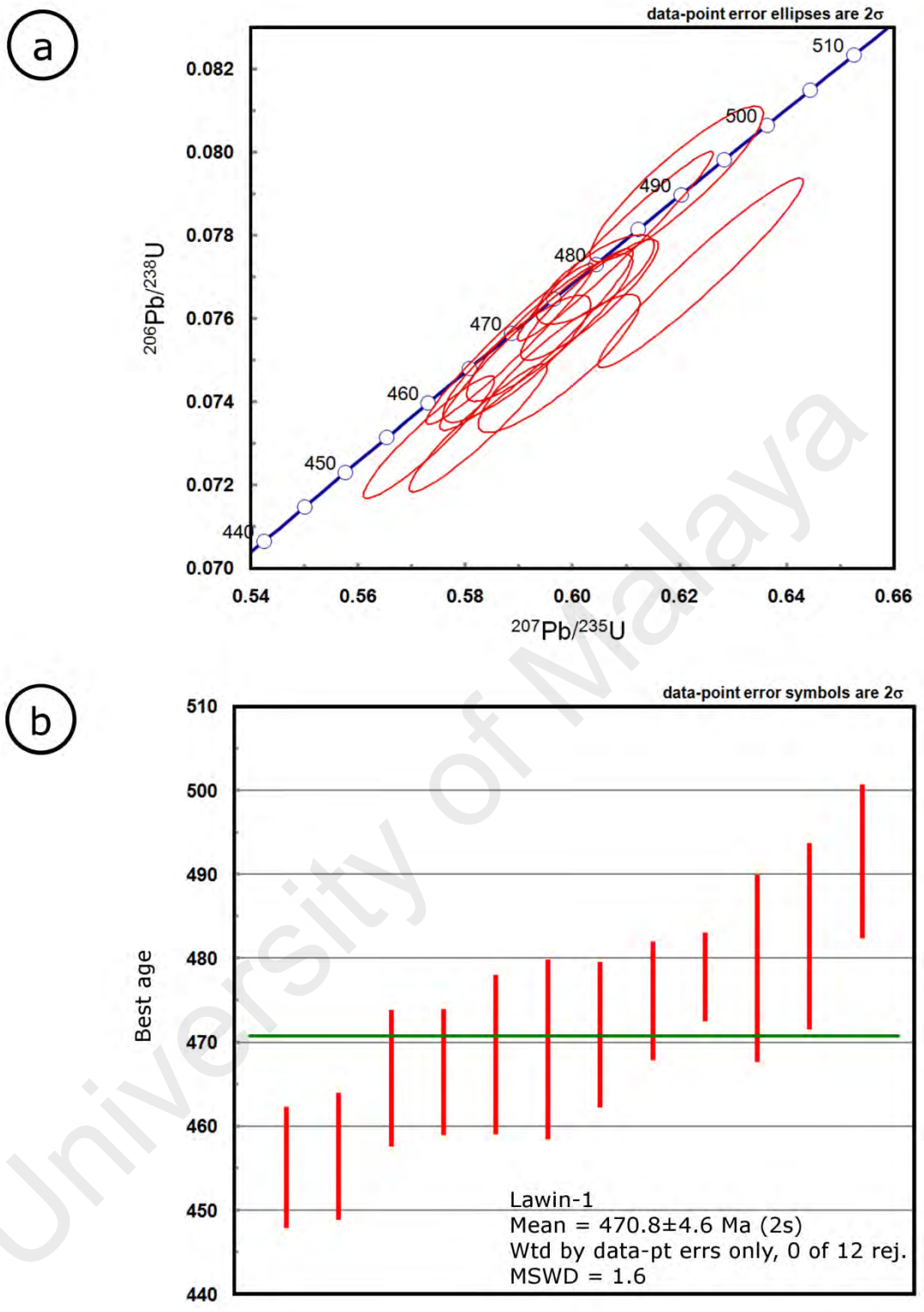

Figure 4.28: LAWIN-1 zircon U–Pb age concordia and weighted average plots. (a) The concordia plots for LAWIN-1. (b) The weighted average plot for LAWIN-1.

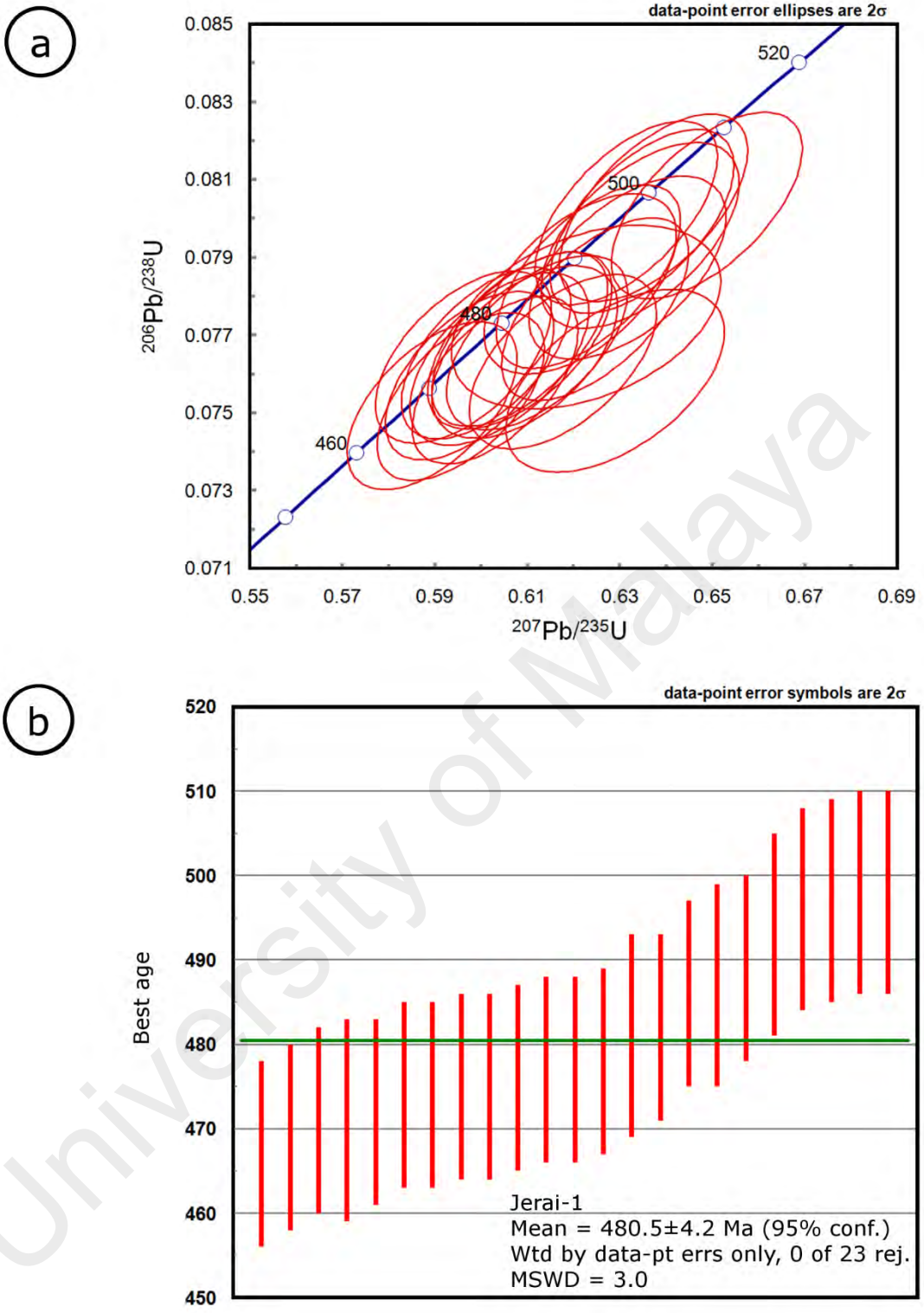

Figure 4.29: JERAI-1 zircon U–Pb age concordia and weighted average plots. (a) The concordia plots for JERAI-1. (b) The weighted average plot for JERAI-1.

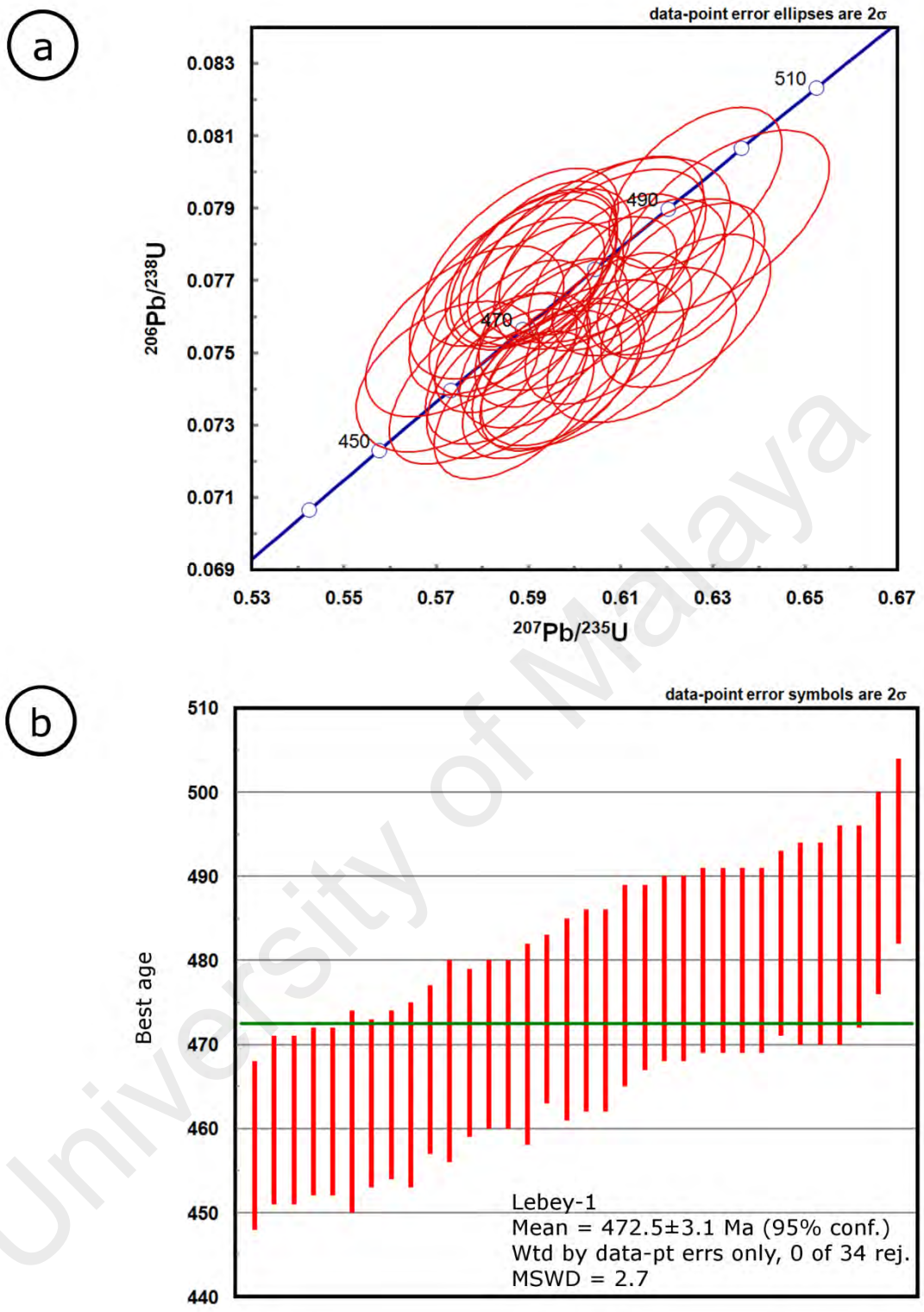

Figure 4.30: LEBEY-1 zircon U–Pb age concordia and weighted average plots. (a) The concordia plots for LEBEY-1. (b) The weighted average plot for LEBEY-1.

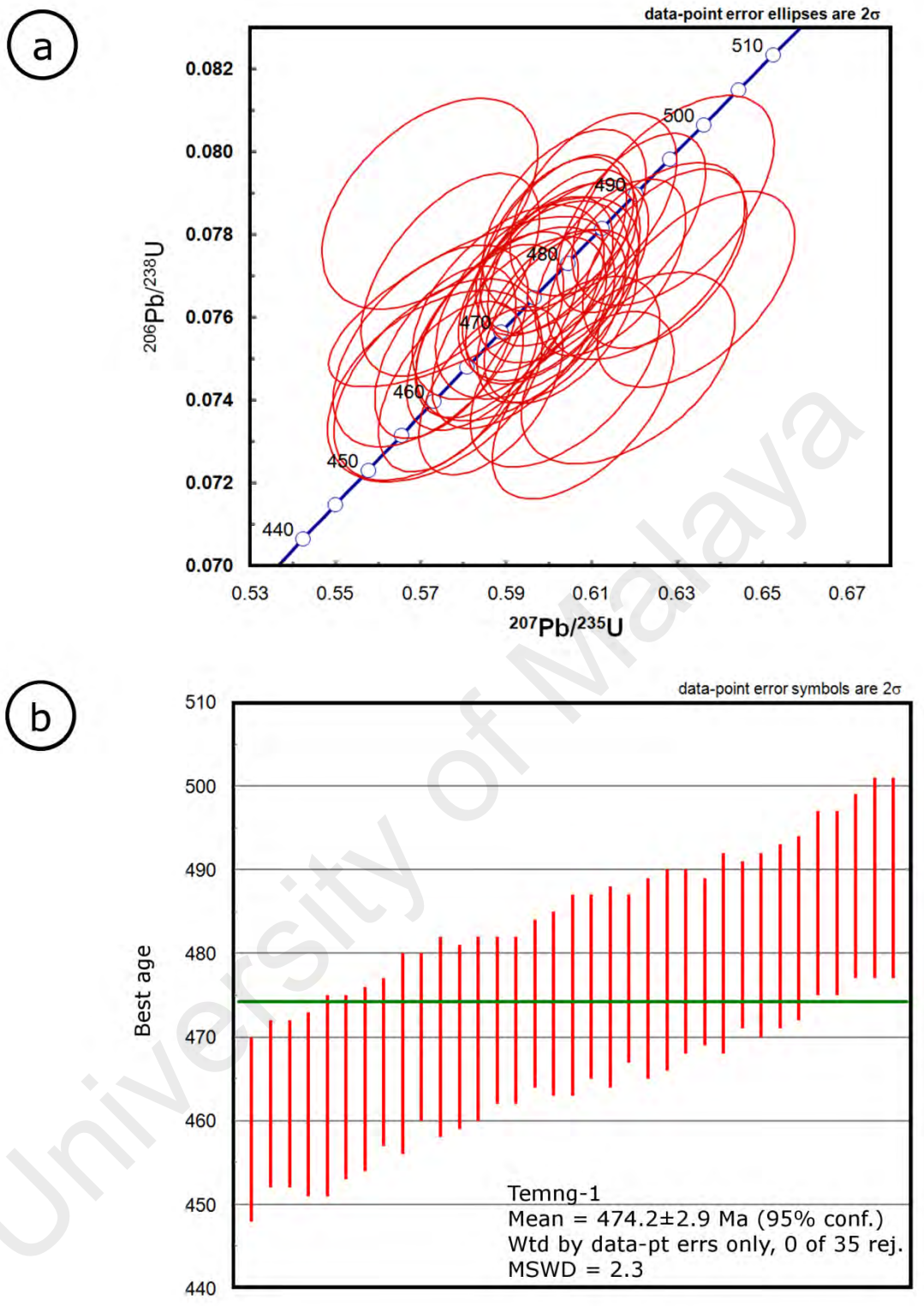

Figure 4.31: TEMNG-1 zircon U–Pb age concordia and weighted average plots. (a) The concordia plots for TEMNG-1. (b) The weighted average plot for TEMNG-1.

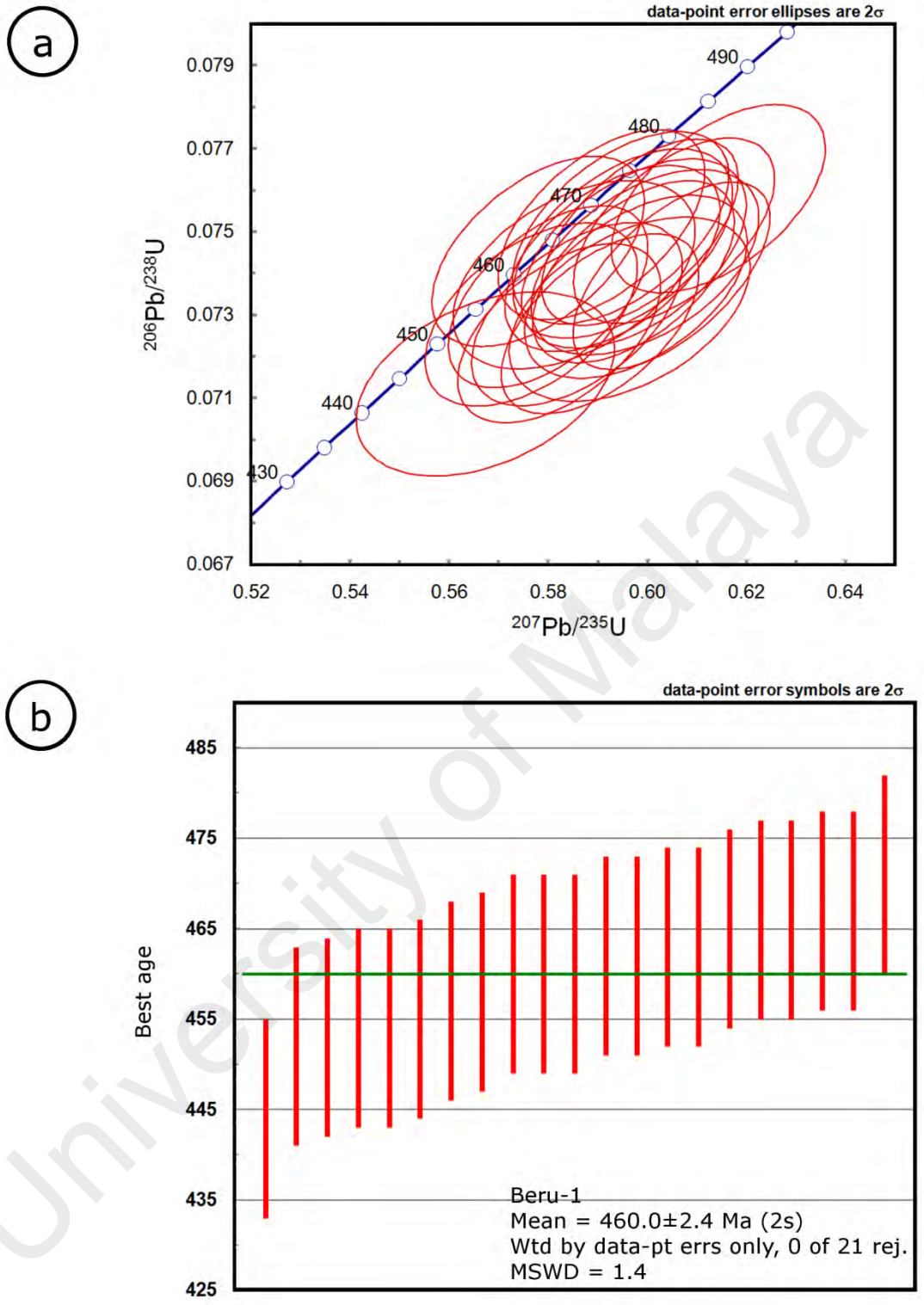

Figure 4.32: BERU-1 zircon U–Pb age concordia and weighted average plots. (a) The concordia plots for BERU-1. (b) The weighted average plot for BERU-1.

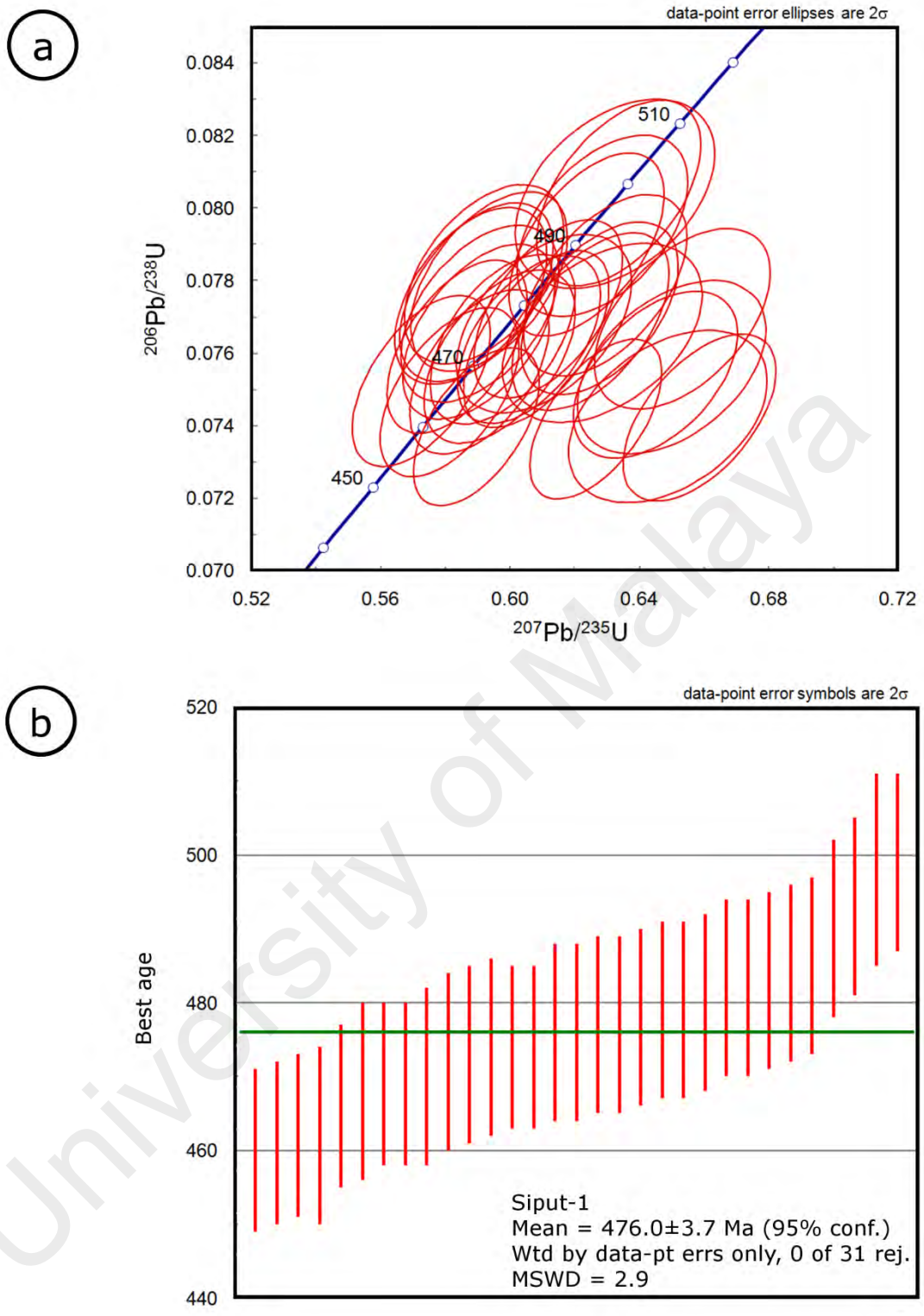

Figure 4.33: SIPUT-1 zircon U–Pb age concordia and weighted average plots. (a) The concordia plots for SIPUT-1. (b) The weighted average plot for SIPUT-1.

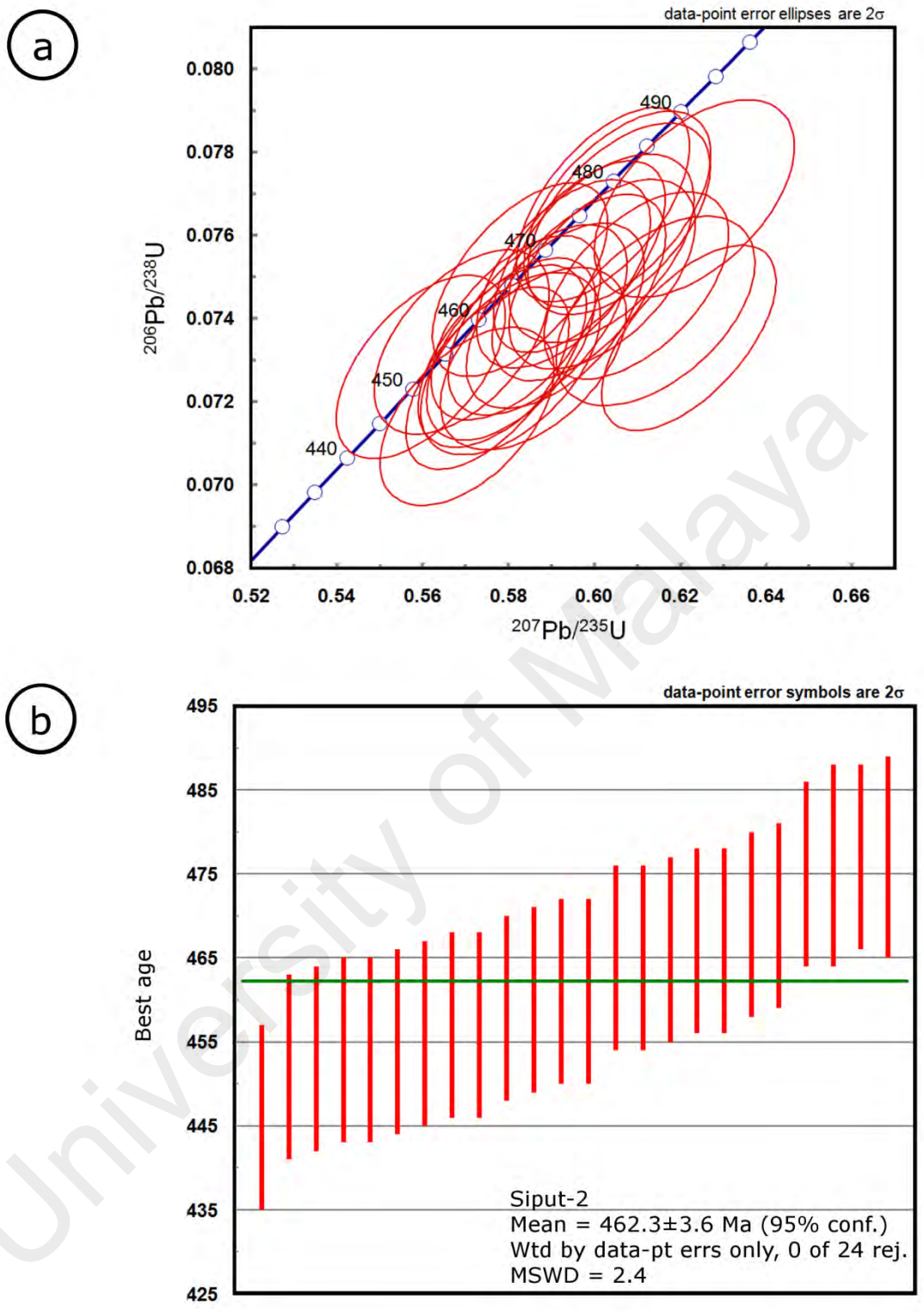

Figure 4.34: SIPUT-2 zircon U–Pb age concordia and weighted average plots. (a) The concordia plots for SIPUT-2. (b) The weighted average plot for SIPUT-2.

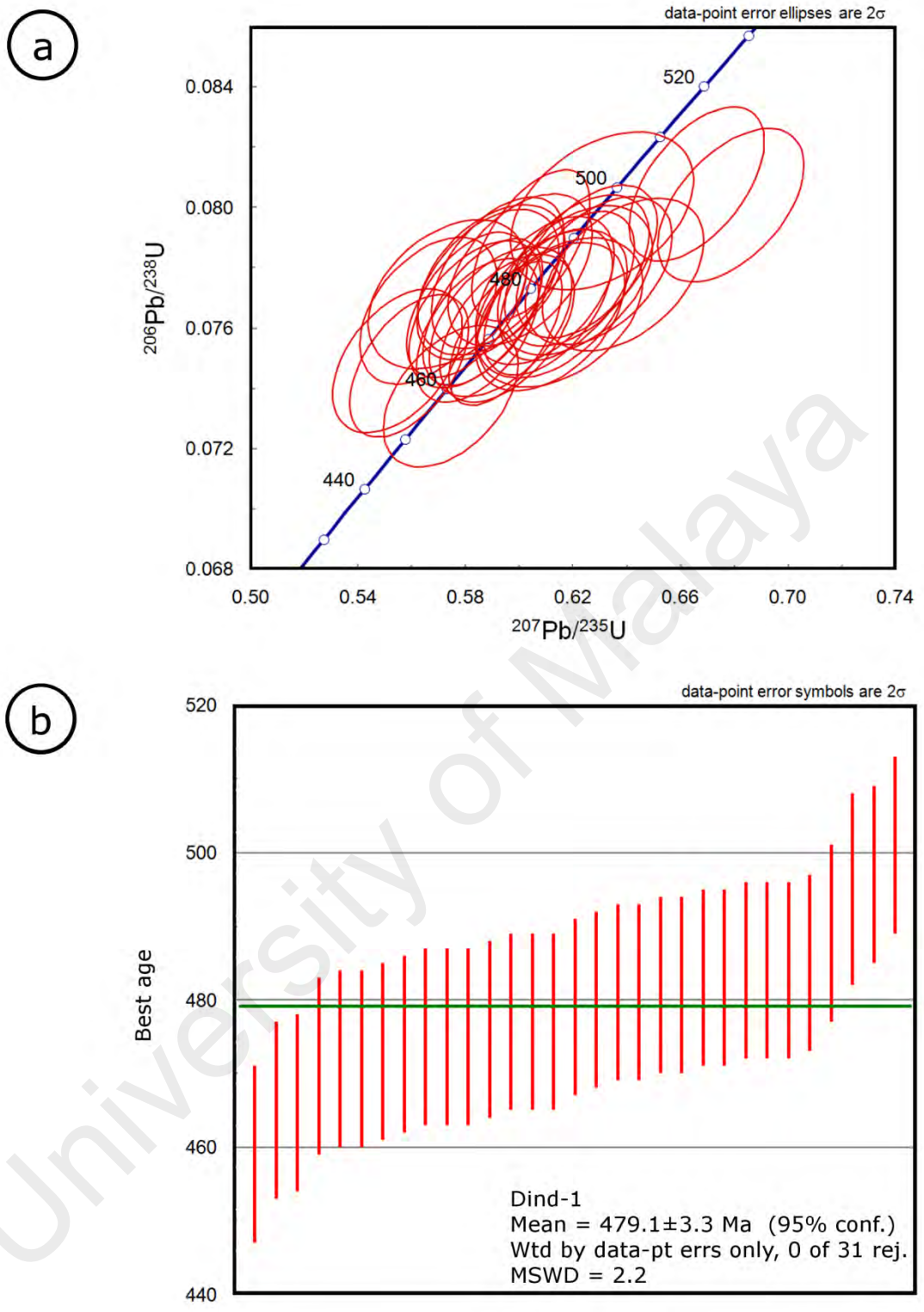

Figure 4.35: DIND-1 zircon U–Pb age concordia and weighted average plots. (a) The concordia plots for DIND-1. (b) The weighted average plot for DIND-1.

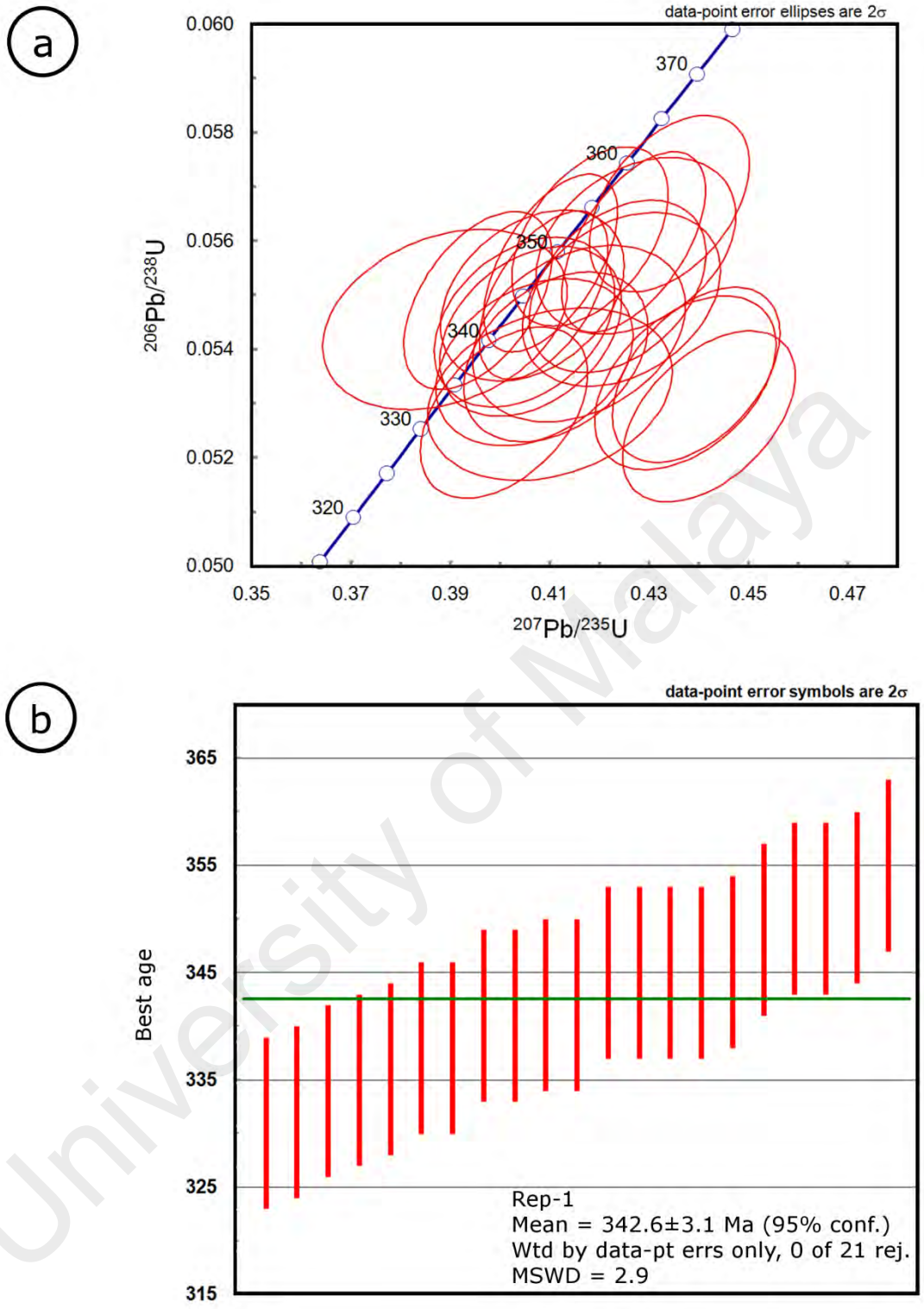

Figure 4.36: REP-1 zircon U–Pb age concordia and weighted average plots. (a) The concordia plots for REP-1. (b) The weighted average plot for REP-1.

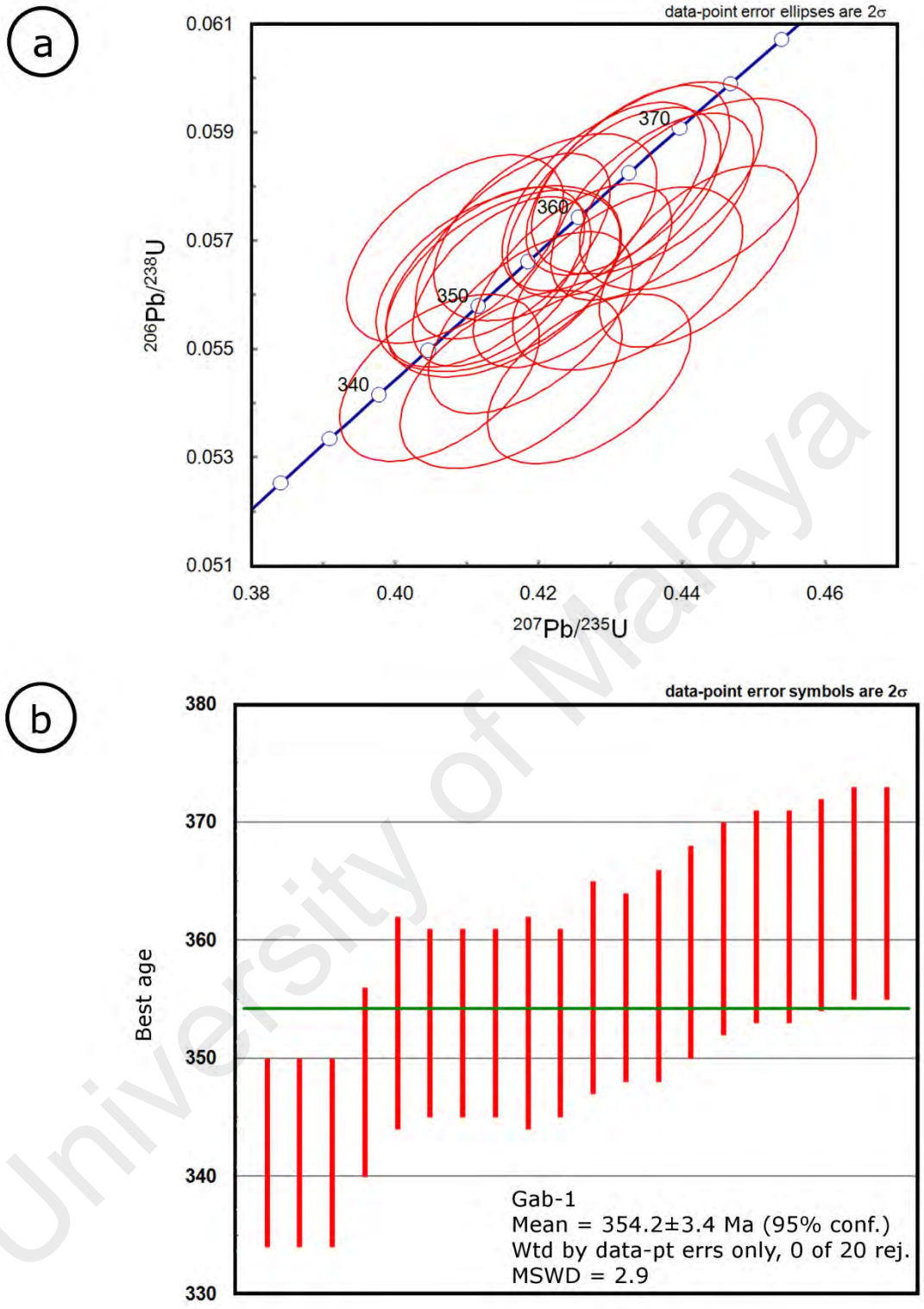

Figure 4.37: GAB-1 zircon U–Pb age concordia and weighted average plots. (a) The concordia plots for GAB-1. (b) The weighted average plot for GAB-1.

4.5 Zircon Lu-Hf isotope

In situ zircon Lu-Hf isotope analysis were carried out on the 143 dated zircons (112 Ordovician, 28 Carboniferous and 3 Mesoproterozoic zircons) from the ten meta-volcanic rocks samples. The Lu-Hf isotope measurements were guided by CL images and performed on the same spots or the same age domains used for U-Pb age determination. The zircon Lu-Hf isotope data are listed in Appendix G. The model Hf age of zircons, T_{DM2} is calculated using two-stage model relative to a depleted mantle source. Despite the fact that a single-stage model Hf age will suffice for whole-rock Lu-Hf isotope analyses, mineral Lu-Hf isotope studies such as zircons will require a two-stage model Hf age (Nebel et al., 2007).

The Ordovician magmatic zircons have modern $^{176}Hf/^{177}Hf$ isotope compositions in the range of 0.282060-0.282522. The $\varepsilon Hf_{(T)}$ values from these magmatic zircons vary between +0.85 and −15.7 with peaks at −2 to −5, which correspond to T_{DM2} model ages between 1.3 Ga and 2.4 Ga with peaks at 1.5 Ga to 1.6 Ga (Figure 4.38a). Such varied $\varepsilon Hf_{(T)}$ values indicate that these magmatic zircons were crystallized from a crustal-derived melt with possible minor mantle contribution. The three Mesoproterozoic inherited zircons from LAWIN-1 sample have $\varepsilon Hf_{(T)}$ values from +3.2 to +6.4, yielding T_{DM2} model ages of 1.54–2.17 Ga. Highly positive $\varepsilon Hf_{(T)}$ values suggest that these inherited zircons could be crystallized from partial melting of juvenile crust or mantle-derived melt. The Carboniferous magmatic zircons have modern $^{176}Hf/^{177}Hf$ isotope compositions in the range of 0.292177-0.282880. The magmatic zircons of the REP-1 sample have exclusively positive $\varepsilon Hf_{(T)}$ values ranging from +3.4 to +10.3, corresponding to two-stage depleted-mantle model ages (T_{DM2}) of between 648 Ma and 1083 Ma (Figure 4.38b). The $\varepsilon Hf_{(T)}$ values from these magmatic zircons of the GAB-1 sample fluctuate from -13.9 to 10.5, corresponding to two-stage depleted-mantle model ages (T_{DM2}) of between 662 Ma and 2164 Ma (Figure 4.38b).

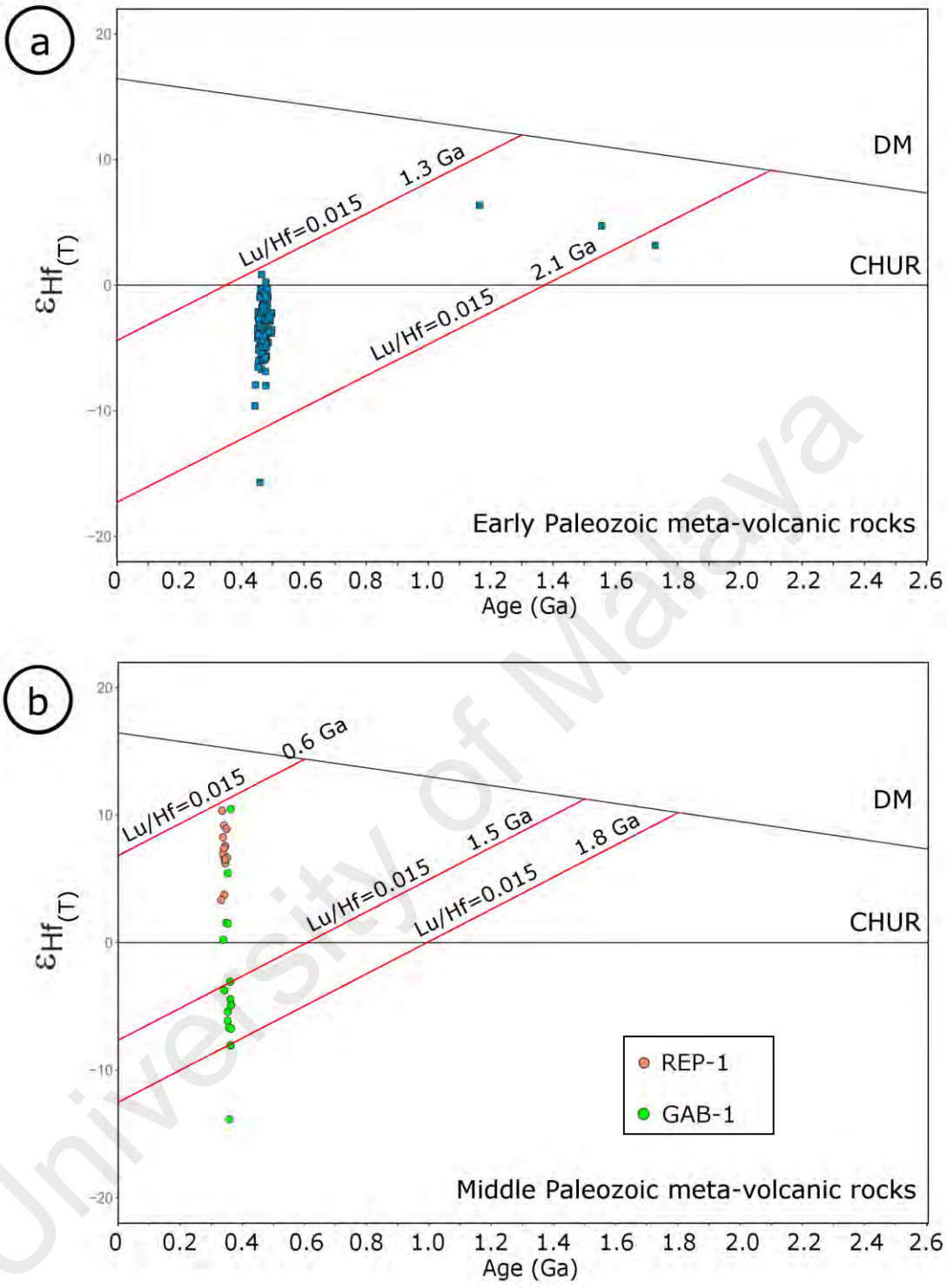

Figure 4.38: Plot of zircon $\varepsilon Hf_{(T)}$ values vs. U–Pb ages. (a) Early Paleozoic (~Middle Ordovician) Gerik-Dinding meta-volcanic rocks. (b) Middle Paleozoic (~Early Carboniferous) Rephens meta-volcanic rocks. The red lines represent the calculated T_{DM2}, the zircon Hf isotope "crustal" model age based on a depleted-mantle source and an assumption that the protolith of the zircon's host magma has the average continental crustal $^{176}Lu/^{177}Hf$ ratio of 0.015 (Griffin et al., 2002).

4.6 Chapter Summary

1. Gerik-Dinding meta-volcanic rocks can be separated into meta-lithic tuff, meta-crystal tuff and meta-rhyolite. The analyzed meta-crystal tuff and meta-rhyolite have variable SiO_2 content (60.68-82.56 wt. %) and classification using immobile element suggest that they are equivalent to rhyolite. They are also mainly enriched in LREE. The meta-volcanic rocks primitive mantle normalized spider plot show depletion in Nb, Ta, Ti, and P, which are typically observed in arc-related rocks.
2. Rephens meta-volcanic rocks can be divided into meta-lithic tuff (SiO_2: 67.17-71.48 wt. %) and meta-andesite (SiO_2: 56.95-62.41 wt. %). Classification using immobile elements suggest that the meta-lithic tuff is similar to rhyolite/dacite while the meta-andesite is comparable to andesite. They are generally enriched in LREE. The meta-volcanic rocks primitive mantle normalized spider plot display depletion in Nb, Ta, Ti, and P, which are characteristically perceived in arc-related rocks.
3. The meta-dolerite is geochemically similar to basaltic rock (SiO_2: 44.11 to 51.03 wt. %) and can be divided into alkaline to sub-alkaline groups using immobile element ratio Nb/Y. They also show elevated LREE content. The absence of Nb-Ta, Zr-Hf and Ti negative anomalies with the results from the discrimination diagrams shows within-plate and non-subduction settings for the meta-dolerite.
4. Zircons from eight Gerik-Dinding meta-volcanic rock samples yielded Early to Middle Ordovician weighted mean $^{206}Pb/^{238}U$ ages between 460 and 480 Ma. Zircons from two Rephens meta-volcanic rock samples yielded two Early Carboniferous weighted mean $^{206}Pb/^{238}U$ ages, 342.6 ± 3.1 Ma and 354.2 ± 3.4 Ma.
5. The Gerik-Dinding meta-volcanic rock zircon $\varepsilon Hf_{(T)}$ values vary from +6 to −15, while the zircon Hf two-stage model ages (T_{DM2}) range from 1.3 to 2.3 Ga. The Rephens meta-volcanic rock zircon $\varepsilon Hf_{(T)}$ values vary from +10 to −14, while the zircon Hf two-stage model ages (T_{DM2}) range from 0.6 to 2.1 Ga.

CHAPTER 5: DISCUSSION AND CONCLUSION

5.1 Introduction

In this chapter, the observations and data presented (whole-rock geochemistry analyses and zircon U-Pb and Lu-Hf analyses) in the previous results chapter will be discussed to provide a more thorough interpretation of the petrogenesis and tectonic setting of the Early to Middle Paleozoic meta-volcanic rocks in Western Peninsular Malaysia. Comparisons of relevant geochemical information and data from other researchers will also be carried out to support the discussion. The data from the Early Paleozoic Gerik-Dinding meta-volcanic rocks will be discussed first, followed by the data from the meta-dolerite, and, finally the data from the Middle Paleozoic Rephens meta-volcanic rocks. The discussion for both of the meta-volcanic rocks sections will include the nature of the magma source region and the tectonic setting, while the meta-dolerite section will only comprise the possible tectonic setting.

The nature of the magma source region will be discussed using the zircon Lu-Hf isotopic data. Zircon Lu-Hf isotopic analysis has long been broadly utilized as a powerful geochemical tracer tool in investigating and discriminating source between depleted mantle, chondrite and crustal reservoirs (Geng et al., 2012; Kröner et al., 2012). Low $^{176}Hf/^{177}Hf$ ratios and $\varepsilon Hf_{(T)}$ values in zircons indicate derivation from crust or contamination by the crust, while high $^{176}Hf/^{177}Hf$ ratios and $\varepsilon Hf_{(T)}$ values in zircons represent derivation from the mantle or juvenile crustal material derived by the differentiation of mantle material (Kinny and Maas, 2003). The zircon Lu-Hf isotopic system has a high closure temperature (Patchett, 1983; Cherniak et al., 1997; Cherniak and Watson, 2003) and the isotope ratio will not change as partial melting or fractional crystallization progresses. Hence, heterogeneity in the zircon Lu-Hf isotopic system may indicate mixing of mantle and crust (Bolhar et al., 2008).

5.2 Early Paleozoic Gerik-Dinding meta-volcanic rocks

5.2.1 Nature of the magma source region

Silicic volcanic rocks such as the Gerik-Dinding meta-volcanic rocks could have been generated by extensive fractional crystallization of basaltic magmas, or produced by partial melting of crustal material induced through underplating of mantle-derived basaltic magma (Clemens, 2003; Kemp et al., 2006, 2007). However, in the case of extensive fractional crystallization of basaltic magma, the isotopic composition of the mantle-derived magmas (depleted mantle or enriched mantle) would not have been altered during the process of closed-system fractional crystallization (Hu et al., 2013). On the other hand, in the scenario of partial melting of crustal material, the underplated mantle-derived basaltic magma would not only have heated the overlying crust, but also interacted with the crustal-derived rhyolitic magmas, consequently changing their isotopic compositions (Hu et al., 2013). Most Early Paleozoic felsic igneous rocks recognized in the series of terranes along the East Gondwana Proto-Tethys margin are interpreted to have been produced by this type of process (Liu et al., 2009; X. X. Wang et al., 2011; Y. Wang et al., 2013; Zhu et al., 2012; Hu et al., 2013).

The Gerik-Dinding meta-volcanic rocks Early to Middle Ordovician magmatic zircons show varied zircon $\varepsilon Hf_{(T)}$ values from +0.85 to −15.7 with peaks at −2 to −5 (Figure 5.1a), suggesting the volcanic rock magma could either be derived from fractional crystallization of mafic magma from enriched mantle source that has been metasomatized by sediments or fluids or partial melting of ancient crustal material. However, it is unlikely that the Gerik-Dinding meta-volcanic rocks were generated by extensive fractional crystallization of such mafic magmas, as no coeval basaltic volcanic rocks of such geochemical signature were encountered during field investigation. Furthermore, the process of fractional crystallization to generate rhyolitic magmas always requires voluminous mafic magmas. Partial melting of ancient crustal material is the most likely

origin of the Gerik-Dinding meta-volcanic rocks as meta-volcanic rocks' dominantly negative zircon $\varepsilon Hf_{(T)}$ values, combined with zircon Lu-Hf model ages (T_{DM2} = 1.34 to 2.35 Ga) point out that Mid-Mesoproterozoic to Mid-Paleoproterozoic crustal material is their major source component. A few inherited zircon ages (1.3 to 1.9 Ga, n = 7) found during the dating process support this assertion. Judging from the meta-volcanic rocks chondrite-normalized REE patterns and primitive mantle normalized trace element patterns (e.g., Th (>10 ppm) and U (>2.0 ppm) contents and low Eu/Eu* ratios (<1.0)), the upper continental crust (Rudnick and Fountain, 1995) was most expected involved in the magma generation of the meta-volcanic rocks.

It is also worth mentioning that the Gerik-Dinding meta-volcanic rocks zircon Lu-Hf model ages are comparable to the zircon Lu-Hf model age (Mesoproterozoic to Paleoproterozoic) of Late Triassic magmatic ($\varepsilon Hf_{(T)}$ = −5 to −15) (Quek et al., 2017) and detrital zircons ($\varepsilon Hf_{(T)}$ = −8 to −29) (Sevastjanova et al., 2012) from Western Peninsular Malaysia (Figure 5.1a). The finding of Mid-Mesoproterozoic to Mid-Paleoproterozoic crustal material in the basement rocks of Western Peninsular Malaysia reinforce Liew and Mcculloch (1985) and Liew and Page (1985) claim that the Western Peninsular Malaysia has a Late Mesoproterozoic crystalline basement. It also supports Lin et al. (2013) proposal that the Mesoproterozoic to Paleoproterozoic crustal component is distributed along the East Gondwana Proto-Tethys margin, extending from Turkey, Iran, NW Himalaya, Namcha Barwa, Central Lhasa, Baoshan to Peninsular Thailand and Malaysia (Central and North Sibumasu Terrane) (Miller et al., 2001; Ramezani and Tucker, 2003; Cawood et al., 2007; Liu et al., 2009; Ustaömer et al., 2009; Saki, 2010; Zhang et al., 2012; Zhu et al., 2012).

The Gerik-Dinding meta-volcanic rocks negative to positive zircon $\varepsilon Hf_{(T)}$ value range is divergent from the negative zircon $\varepsilon Hf_{(T)}$ values of the strongly crustal Baoshan granitoids (ca. 500 Ma) from Western Yunnan Province (Liu et al., 2009), and are more

comparable with the zircon $\varepsilon Hf_{(T)}$ value range of other Early Paleozoic metamorphosed magmatic rocks of East Gondwana Proto-Tethys margin such as the Lhasa Terrane Zhaqian and Zhakang meta-rhyolite (ca. 510 & ca. 544 Ma) (Hu et al., 2013) and Peninsular Thailand Khao Tao orthogneiss (ca. 502 Ma) (Lin et al., 2013) (Figure 5.1a), which are interpreted to contain minor mantle-derived magma contributions. This suggests an underplated mantle-derived basaltic magma may have interacted with the Gerik-Dinding meta-volcanic rocks parent magma. In summary, the parent melts of the Gerik-Dinding meta-volcanic rocks were generated by partial melting of Mid-Mesoproterozoic to Mid-Paleoproterozoic upper crustal material with minor mantle-derived magma contributions from underplated mantle-derived basaltic magma.

5.2.2 Tectonic setting and implication

An Andean-type orogeny in response to the Early Paleozoic subduction of Proto-Tethys Ocean and collision with Asian micro-continental fragments (AMF) is preferred here for the Early Paleozoic magmatism on the terranes located along East Gondwana Proto-Tethys margin compared to a post-collision extensional setting in response to the final assembly of Gondwana, for several reasons: (1) the presence of Cambrian (525-510 Ma) arc-related magmatic rocks in Lhasa Terrane (Hu et al., 2013; Ding et al., 2014); (2) the emplacement age of the majority of Early Paleozoic magmatic rocks (540-460 Ma) far lagged the final assembly of Gondwana (570-520 Ma) (Cawood and Buchan, 2007; Cawood et al., 2007), and; (3) the structural evidence of Cambrian-Ordovician deformation and high-pressure metamorphism in the several terranes that are related to the orogeny (Gehrels et al., 2003, 2006b; Zhang et al., 2014). Based on Zhu et al. (2012), Hu et al. (2015) and Li et al. (2016) tectonic models, an Andean-type magmatism was almost certainly present along the East Gondwana proto-Tethyan margin by ca. 530 Ma (Figure 5.3a) and ended after the collision with Asian micro-continental fragments at ca.

510 Ma. After the collision, slab-breakoff is suggested to have taken place at 500-490 Ma and was followed by lithospheric thickening at ca. 490-475 Ma (Hu et al., 2015; Li et al., 2016). The subsequent lithospheric delamination at ca. 475-460 Ma triggered an extensive magmatism which finally vanished at ca. 450 Ma (Li et al., 2016).

The Gerik-Dinding meta-volcanic rocks' primitive mantle normalized trace element patterns exhibit strong negative Nb-Ti-P anomalies, which are typically observed in subduction-related rocks (Green, 1995). The meta-volcanic rocks also plot within the active continental margin (ACM) field on the Th/Hf vs. Ta/Hf and Th/Yb vs. Ta/Yb tectonic discrimination diagrams, which are based on immobile elements and are effective for the investigation of altered felsic volcanic rocks (Schandl and Gorton, 2002). When compared with other Early Paleozoic (Cambrian to Ordovician) subduction-related felsic magmatic rocks (Zhu et al., 2012; Hu et al., 2013) along the East Gondwana proto-Tethyan margin (Figure 5.1b), the Gerik-Dinding meta-volcanic rocks trace element patterns strongly resemble their patterns. Although this could be conceived as evidence of a subduction component, the extensive involvement of continental crust component suggests the subduction signature may be a sign of the nature of the source material rather than the tectonic processes acting upon them (Roberts and Clemens, 1993). Zircon U-Pb age results obtained from this work indicate that the Gerik-Dinding meta-volcanic rocks were formed between 460 to 480 Ma. The oldest age of 480 Ma from the meta-volcanic rock sample ostensibly represents the initial emplacement of this episode of magmatism. A suitable explanation for Gerik-Dinding meta-volcanic rocks tectonic setting, however, should be supported by the evidence from regional geology.

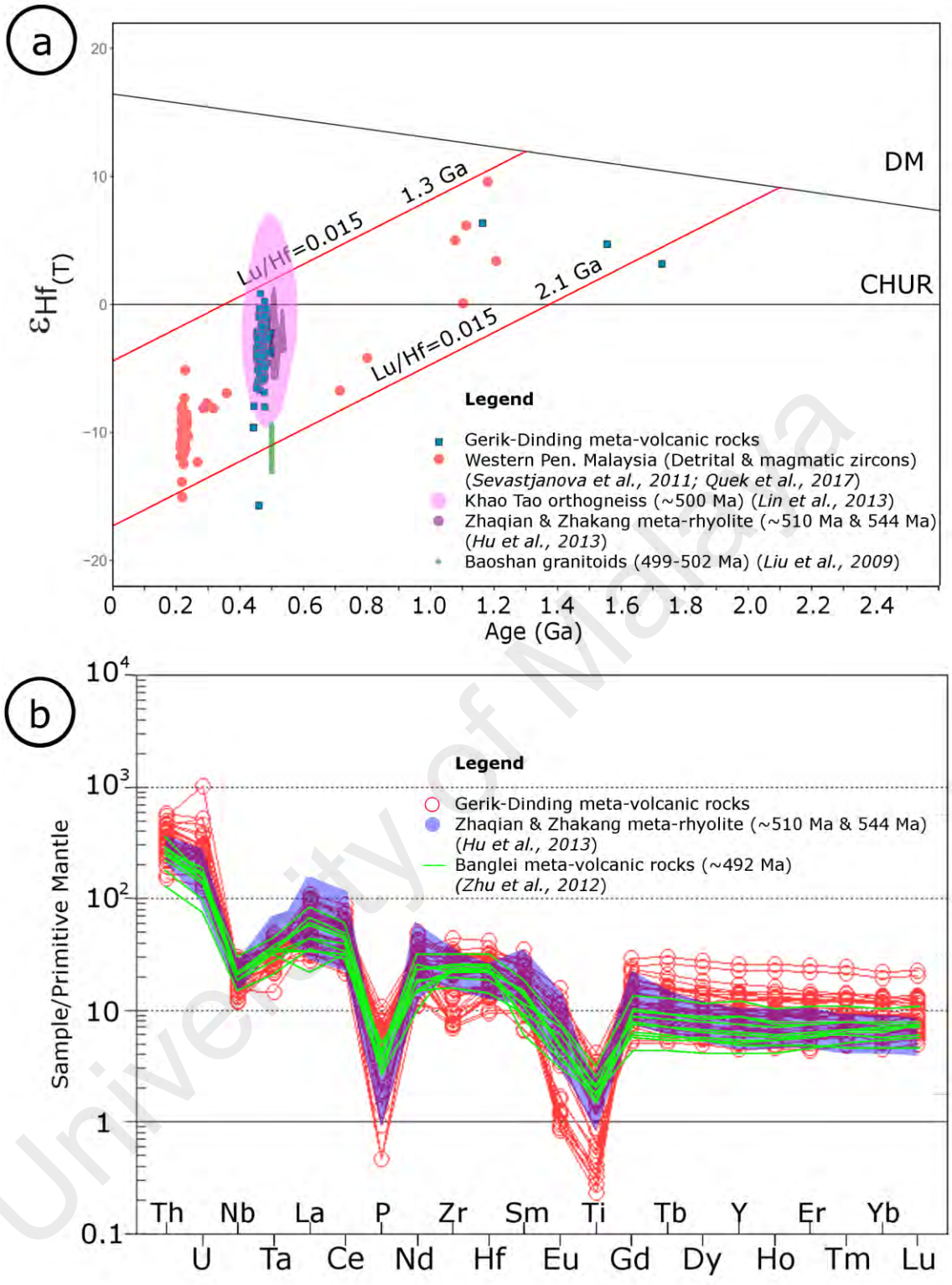

Figure 5.1: Comparison of Gerik-Dinding meta-volcanic rocks geochemical data with available Cambrian-Ordovician magmatic rocks geochemical data from other terranes. (a) Plot of zircon $\varepsilon Hf_{(T)}$ values vs. U–Pb ages. (b) Primitive mantle normalized trace element spider plots.

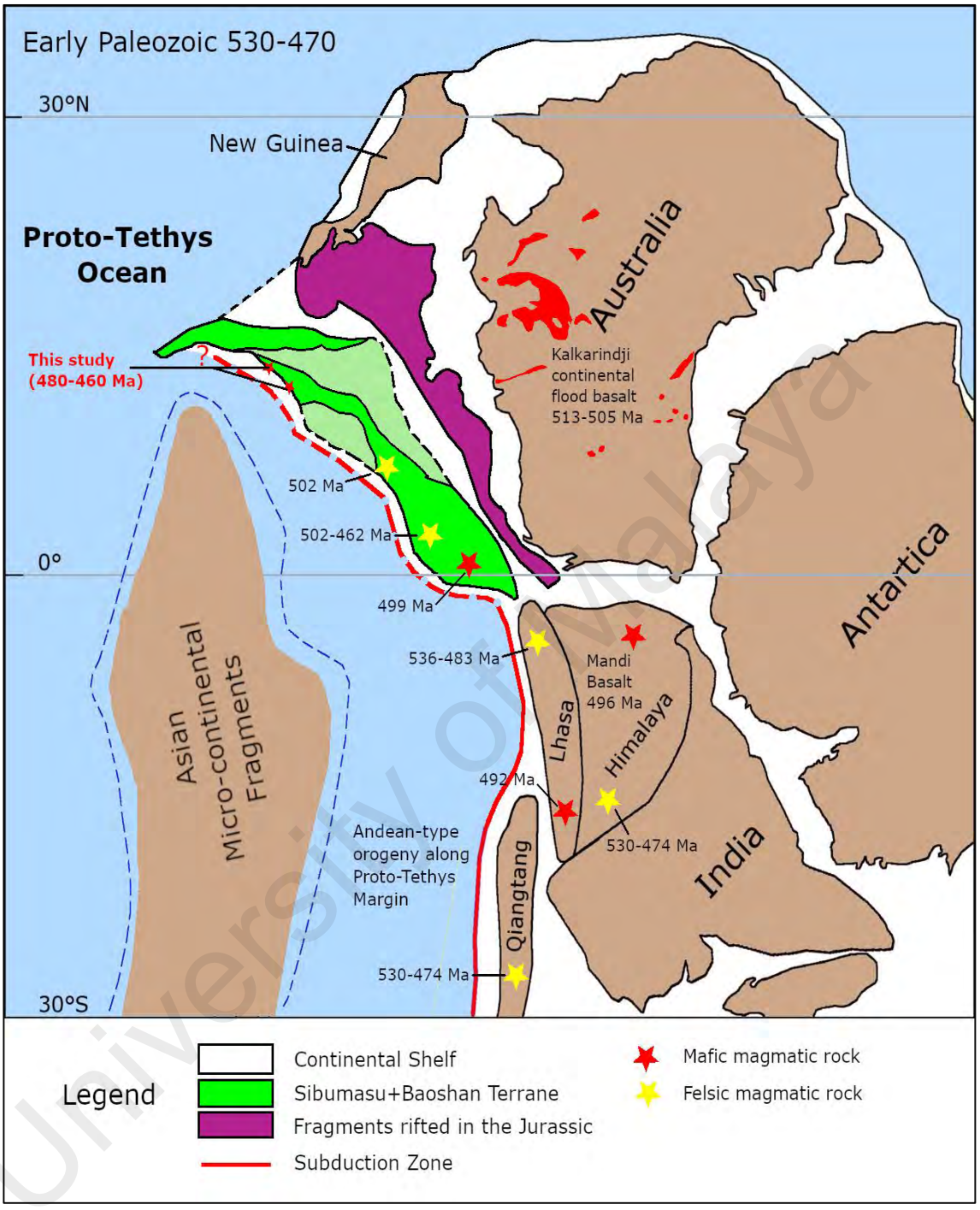

Figure 5.2: The Early Paleozoic (530-470 Ma) reconstruction of East Gondwana margin showing the locations of Gerik-Dinding meta-volcanic rocks. This diagram is modified after Hu et al. (2015) and G. Li et al. (2015).

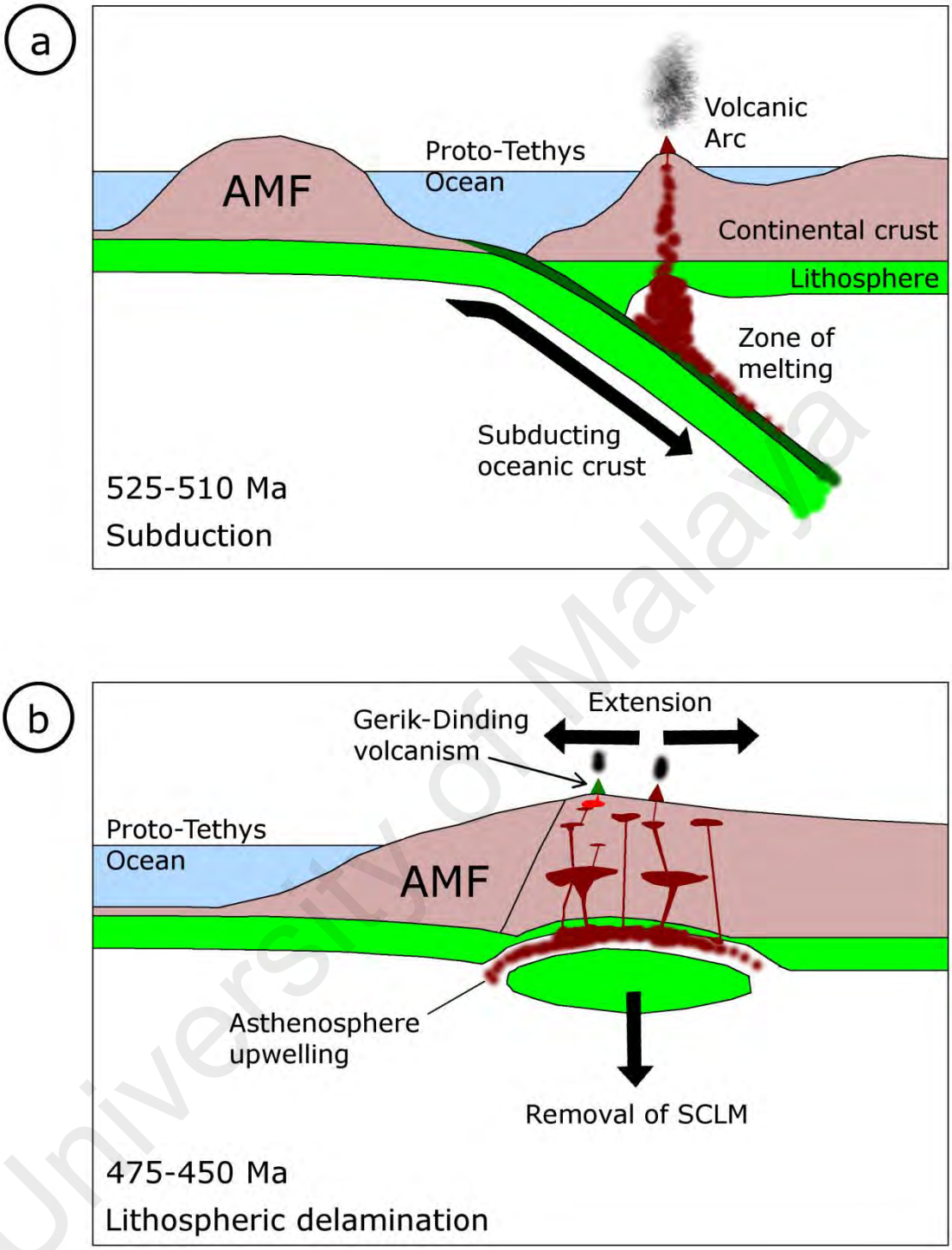

Figure 5.3: Diagrams illustrating the tectonic evolution of the East Gondwana Proto-Tethys margin (Western Peninsular Malaysia) in the Early Paleozoic. (a) Subduction during Cambrian. (b) Lithospheric delamination during Middle Ordovician. AMF = Asian Micro-continental fragments.

According to Zhu et al. (2012), Hu et al. (2015) and Li et al. (2016) Early Paleozoic paleogeographic reconstruction (Figure 5.2), the Gerik-Dinding meta-volcanic rocks are situated at the north of the Sibumasu Terrane. Although Cambrian arc-related volcanic rocks of Proto-Tethys Ocean subduction are not well exposed in this part of Sibumasu Terrane, the discovery of Cambrian Khao Tao orthogneiss in Peninsular Thailand (Lin et al., 2013) suggest that the Early Paleozoic Andean-type subduction and the associated orogenic events of the East Gondwana Proto-Tethys margin is likely to be extended to this area (Figure 5.2). The formation age of the Gerik-Dinding meta-volcanic rocks (480-460 Ma) coincides with the post-collision stage from the final amalgamation of AMF onto the East Gondwana Proto-Tethys margin. Lithospheric delamination during the post-collision period would have induced the hot asthenosphere to underplate continental crust and trigger crustal anatexis (Figure 5.3b). Seeing that the Proto-Tethys Ocean subduction underneath the East Gondwana Proto-Tethys margin is suggested to have ended at ca. 510 Ma (Li et al., 2016), the subduction component signatures in the Gerik-Dinding meta-volcanic rocks are most likely inherited from the protolith related to the previous subduction activity. Such a scenario is consistent with the nature of the Gerik-Dinding meta-volcanic rocks magma source.

5.3 Meta-dolerite

5.3.1 Possible tectonic setting for the meta-dolerite

The Western Peninsular Malaysia meta-dolerite intrusion age could be constrained to Late Cambrian until Early Silurian, (500-430 Ma) as these intrusions are penecontemporaneous with Early Paleozoic meta-sedimentary rocks. According to the tectonic models of Zhu et al. (2012) and Hu et al. (2015), at 500-490 Ma, a slab break-off introduced bimodal volcanism in the East Gondwana Proto-Tethys margin (Figure 5.4a). The resulting mafic magmatism is comparable to Andean arc basalts. However, the meta-

dolerite rather weak to absent Nb-Ta negative anomalies on the primitive mantle normalized variation diagram, the low La/Nb (<2, 0.90-1.58), the low Th/Ce and the low Th/La (González-Menéndez et al. 2013), reveal a weak to absent subduction signature. Furthermore, comparison of the meta-dolerite trace element patterns with the trace element patterns other East Gondwana Proto-Tethys margin subduction-related basalts such as the Late Cambrian Kalkarindji basalt (back-arc extension) (Glass et al., 2006) and the Late Cambrian Central Lhasa basalt (slab break-off) (Zhu et al., 2012) (Figure 5.5a and 5.5b) also reveal the lack of affinity with a subduction setting.

The meta-dolerite trace element geochemical data patterns, supported by tectonic discrimination plot Ti vs. Zr plot after Pearce (1982) and Th-Zr-Nb ternary diagram after Wood (1980), indicate that the parent magma of the meta-dolerite was most likely emplaced in an active continental rift or a within-plate setting. Besides that, the meta-dolerite trace element patterns similarities to the Early Paleozoic (Mid to Late Ordovician) within-plate basalt example (Argentina Sierra del Tigre basalts) (González-Menéndez et al. 2013) (Figure 5.6a and 5.6b) also supports a within-plate setting for the meta-dolerite. We propose that the lithospheric delamination event (475-460 Ma) following the continental collision with AMF and lithospheric thickening (Figure 5.4b) may have caused an extensional regime at the East Gondwana Proto-Tethys margin, which permitted the meta-dolerite parent magma to intrude into the thinned continental crust. Therefore, the subcontinental mantle which generated the meta-dolerite magma was not modified by subduction fluids. As alkaline basalts originated in the mantle at deeper depths compared to sub-alkaline basalts (Webber, 1966), we suggest the alkaline meta-dolerite may have intruded slightly earlier than the sub-alkaline meta-dolerite.

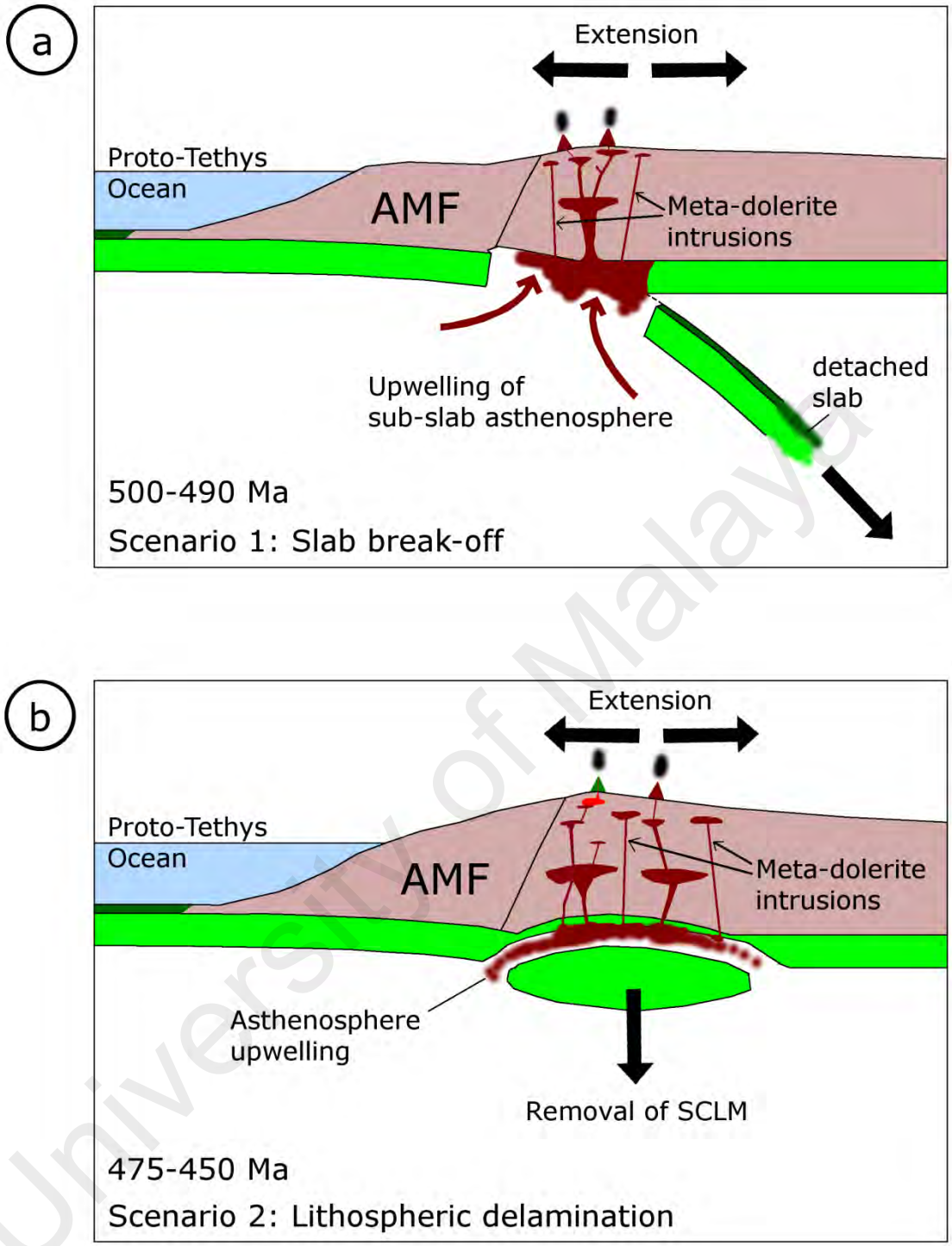

Figure 5.4: Diagrams showing the probable tectonic scenario for the meta-dolerite at Western Peninsular Malaysia. (a) Slab break-off during Late Cambrian (500-490 Ma). (b) Lithospheric delamination during Middle Ordovician (475-450 Ma). AMF = Asian Micro-continental fragments.

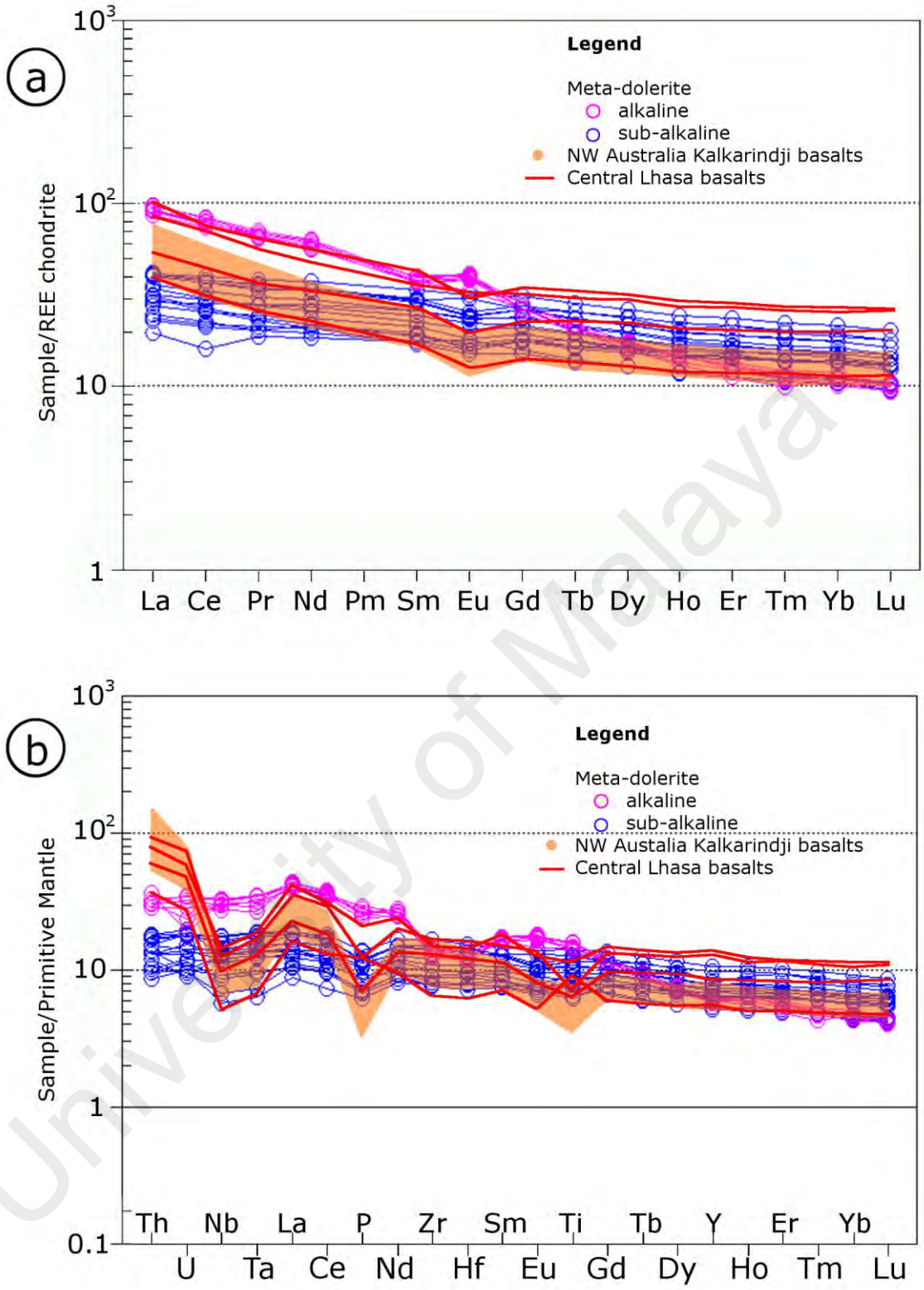

Figure 5.5: Comparison of meta-dolerite trace element patterns with NW Australia Early Paleozoic Kalkarindji basalt and Central Lhasa basalt. Kalkarindji basalt data are from Glass et al. (2006) while Central Lhasa basalt data are from Zhu et al. (2012). (a) Chondrite-normalized REE spider plot. (b) Primitive mantle normalized trace element spider plots.

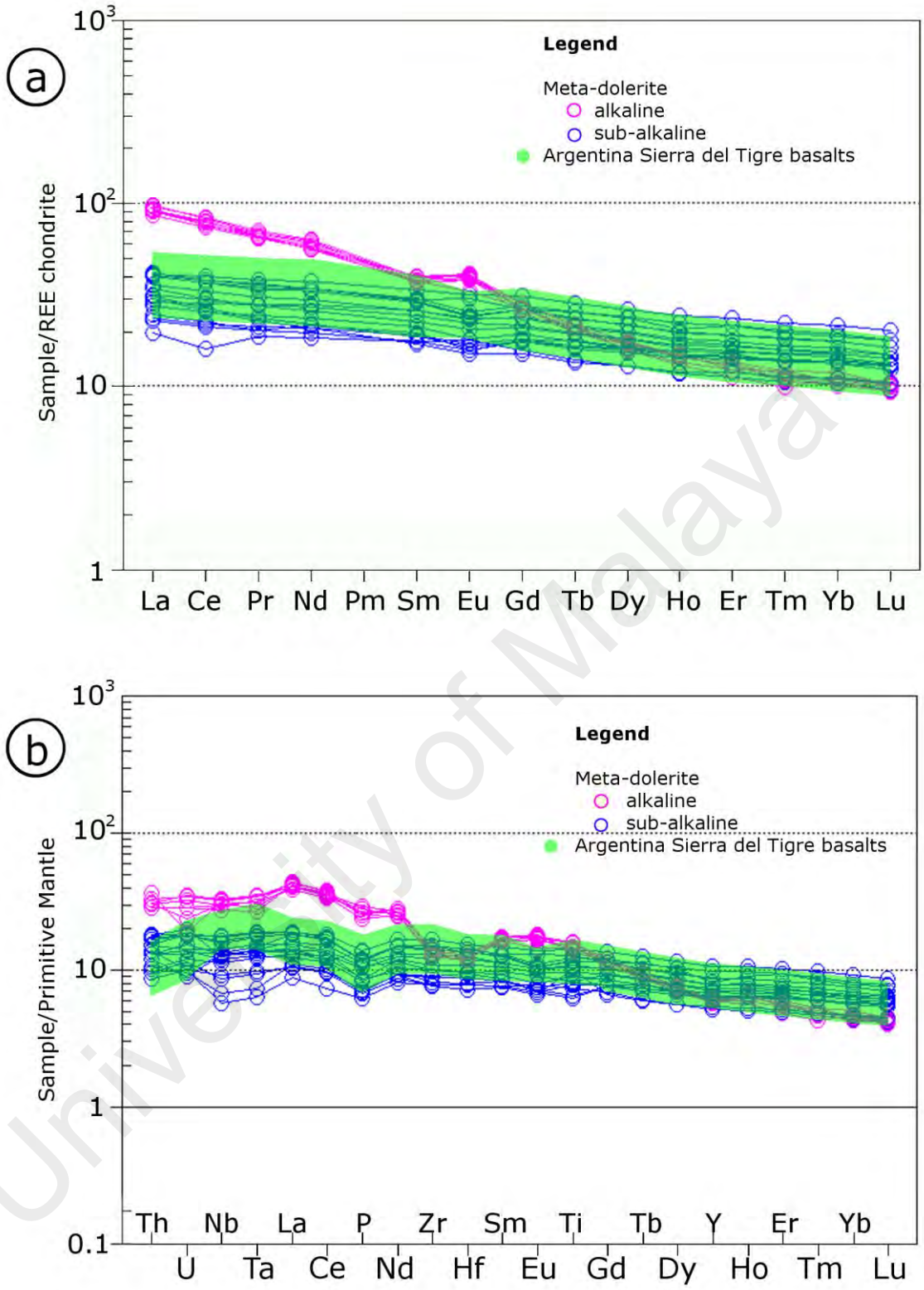

Figure 5.6: Comparison of meta-dolerite trace element patterns with Early Paleozoic Argentina Sierra del Tigre basalt. Sierra del Tigre basalt data are from González-Menéndez et al. (2013). (a) Chondrite-normalized REE spider plot. (b) Primitive mantle normalized trace element spider plots.

5.4 Middle Paleozoic Rephens meta-volcanic rocks

5.4.1 Nature of the magma source region

The meta-andesite with SiO_2 content (56.95 to 62.41 wt. %) exhibit metaluminous character while the meta-lithic tuff with SiO_2 content (67.17 to 71.48 wt. %) exhibits peraluminous character. Even though the chemical compositions and emplacement locations of the meta-andesite and meta-lithic tuff were distinct, their zircon U-Pb age (~342 Ma and ~354 Ma) suggest that these two meta-volcanic rocks were emplaced around the same period. Two viable processes have been suggested for the origin of the intermediate to felsic Rephens meta-volcanic rocks: (1) fractional crystallization from a mantle-derived basaltic magma; and (2) crustal anataxis due to underplating by mantle-derived mafic magma with distinct isotopic compositions (Shellnutt and Zhou, 2007; Zhu et al., 2007; Jones et al., 2011; Jiang et al., 2015). However, fractional crystallization of a mantle-derived basaltic magma to generate felsic magma is unlikely, as no coeval basaltic rocks were encountered during field investigation.

The meta-andesite (REP-1) T_{DM2} age (648 Ma and 1083 Ma) and variable positive zircon $\varepsilon Hf_{(T)}$ values (3.4 to 10.3) suggest zircon Lu-Hf isotopic heterogeneity and may indicate mixing of middle to lower crust with a mantle component. The meta-andesite chondrite-normalized REE patterns and primitive mantle normalized trace element patterns suggest that the middle continental crust (Rudnick and Fountain, 1995) was involved in the generation of the meta-andesite. We suggest the meta-andesite parent magma was generated by the partial melting of juvenile Neoproterozoic middle continental crust from a series of underplated mantle-derived basaltic magmas. On the other hand, the meta-lithic tuff (GAB-1) T_{DM2} age (662-2164 Ma) and spread of zircon $\varepsilon Hf_{(T)}$ values (-13.9 to 10.5) also suggest zircon Hf isotopic heterogeneity. According to the meta-lithic tuff chondrite-normalized REE patterns and primitive mantle normalized trace element patterns, the upper continental crust (Rudnick and Fountain, 1995) was

most likely involved in the magma generation of the meta-lithic tuff. We propose that the parent magma of the meta-lithic tuff could be generated from partial melting of an inhomogeneous basement such as a mixing source of Neoproterozoic juvenile middle crust with Paleoproterozoic upper continental crust. It is also worth noting that the meta-lithic tuff zircon $\varepsilon Hf_{(T)}$ values are quite similar to zircon $\varepsilon Hf_{(T)}$ values of Late Devonian to Early Carboniferous magmatic rocks data from South Lhasa Terrane that are resulted from partial melting of Paleoproterozoic crustal materials (Guo et al., 2016) (Figure 5.7a).

5.4.2 Tectonic setting and implication

The zircon U-Pb age of the Rephens meta-volcanic rocks (~342 Ma and ~354 Ma) implies the presence of previously unidentified Early Carboniferous volcanism in Western Peninsular Malaysia. Due to the lack of exposure from intense weathering and dense vegetation, and the strong overprinting of the dominant crustal forming orogeny from Late Triassic Sibumasu Terrane and Indochina-East Malaya Block collision, the evidence of Early Carboniferous magmatism was not discovered during the previous zircon provenance study in Western Peninsular Malaysia (Sevastjanova et al., 2011), although Devonian detrital zircons are reported within the continental Mesozoic sequences at Eastern Peninsular Malaysia (Sevastjanova et al., 2011; Basori et al., 2018). After the Early Paleozoic Andean-type active continental margin concluded at the East Gondwana Proto-Tethys margin, the East Gondwana margin was characterized as a passive margin until Early Devonian (Cawood et al., 2007). Also around the Early Devonian, the Paleo-Tethys Ocean began to open. During Middle Devonian, the Paleo-Tethys Ocean was already a wide ocean around the equator (Metcalfe, 2011, 2013) (Figure 5.8). At the same time, the Paleo-Tethys Ocean was being consumed at a north-dipping subduction beneath the Hun superterrane (Stampfli and Borel, 2002), Kazakhstan (Metcalfe, 2011), and North China (Pan et al., 2004).

Zhu et al. (2013) suggested the calc-alkaline and metaluminous Late Devonian granitoids (367–364 Ma) revealed in the Western Qiangtang and Southern Lhasa subterranes (Mu et al., 2005; Dong et al., 2010, 2014; Pullen et al., 2011) indicate that a subduction zone could have existed along the southern rim of the Paleo-Tethys Ocean. This theory is further supported by Guo et al. (2016) arc-related detrital zircons (390-365 Ma). The ensuing Late Devonian-Early Carboniferous magmatism (ca. 350 Ma) (Li et al., 2006) and detrital zircons (365-330 Ma) (Guo et al., 2016) with geochemical features resulting from varying degrees of mixing between melts derived from the anatexis of mature continental crustal materials and juvenile mantle materials may represent an extensional magmatic event (from slab roll back), which eventually resulted in the opening of a back-arc oceanic basin (Sumdo/Songdo Paleo-Tethys Ocean) (Yang et al., 2009; Zeng et al., 2009; Cheng et al, 2012; Guo et al., 2016).

The Rephens meta-volcanic rocks primitive mantle normalized trace element patterns exhibit strong negative Nb-Ti-P anomalies, which are typically observed in subduction-related rocks (Green, 1995; Rudnick and Fountain, 1995; Rudnick and Gao, 2003). Furthermore, the meta-volcanic rocks plot within the active continental margin (ACM) field on the Th/Hf vs. Ta/Hf and Th/Yb vs. Ta/Yb tectonic discrimination diagrams (Schandl and Gorton, 2002). The Rephens meta-volcanic rocks trace element patterns also bear a resemblance to the Late Devonian to Early Carboniferous metamorphosed magmatic rocks with continental arc signature from South Lhasa Terrane (Dong et al., 2014) (Figure 5.7b). Although this could be considered as an indication of subduction-related activity, the extensive involvement of crust component in the source suggests the subduction signature may be a sign of the nature of the source material rather than the tectonic processes acting upon them (Roberts and Clemens, 1993). An appropriate explanation for Rephens meta-volcanic rocks tectonic setting, however, should be supported by the evidence from regional geology.

The Rephens meta-volcanic rocks are located at the north of the Sibumasu Terrane. Although evidence in the region is limited, the discovery of the Rephens meta-volcanic rocks suggests it is possible that the south Paleo-Tethys Ocean subduction zone found in the Lhasa Terrane could be extended to the Sibumasu Terrane. Our zircon U-Pb age results (~342 Ma and ~354 Ma) indicate that the Rephens meta-volcanic rocks age coincides with an extension magmatic event (365-330 Ma) associated with the prolonged southern Paleo-Tethys Ocean subduction. The roll-back of the oceanic slab may have caused the upwelling of asthenosphere (Guo et al., 2016), which resulted in the melting of the continental crust. Such a tectonic setting is consistent with the geochemical affinities of the Rephens meta-volcanic rocks and nature of its magma source.

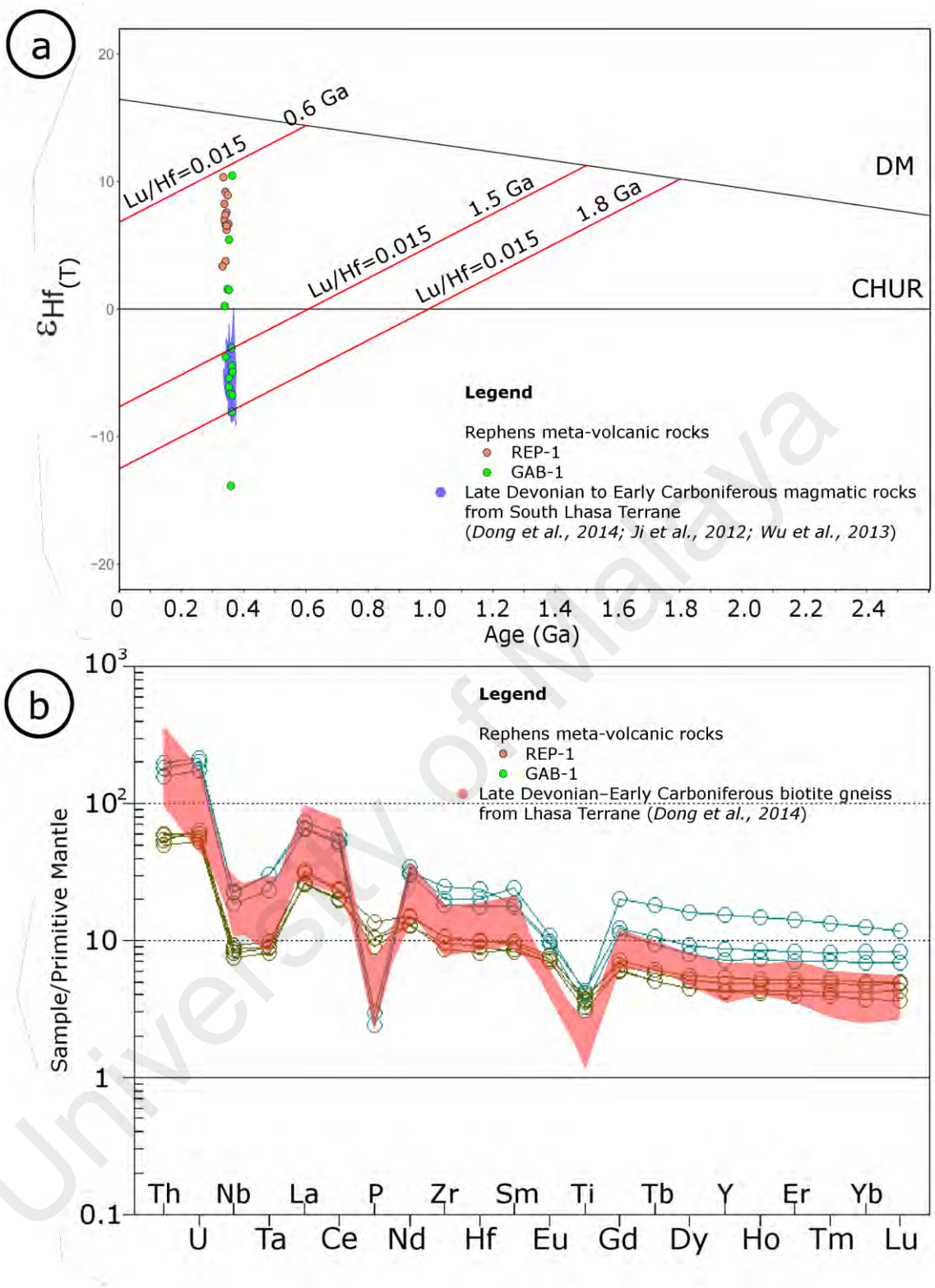

Figure 5.7: Comparison of Rephens meta-volcanic rocks geochemical data with available Late Devonian to Early Carboniferous magmatic rocks geochemical data from South Lhasa Terrane. (a) Plot of zircon εHf(T) values vs. U–Pb ages. (b) Primitive mantle normalized trace element spider plots.

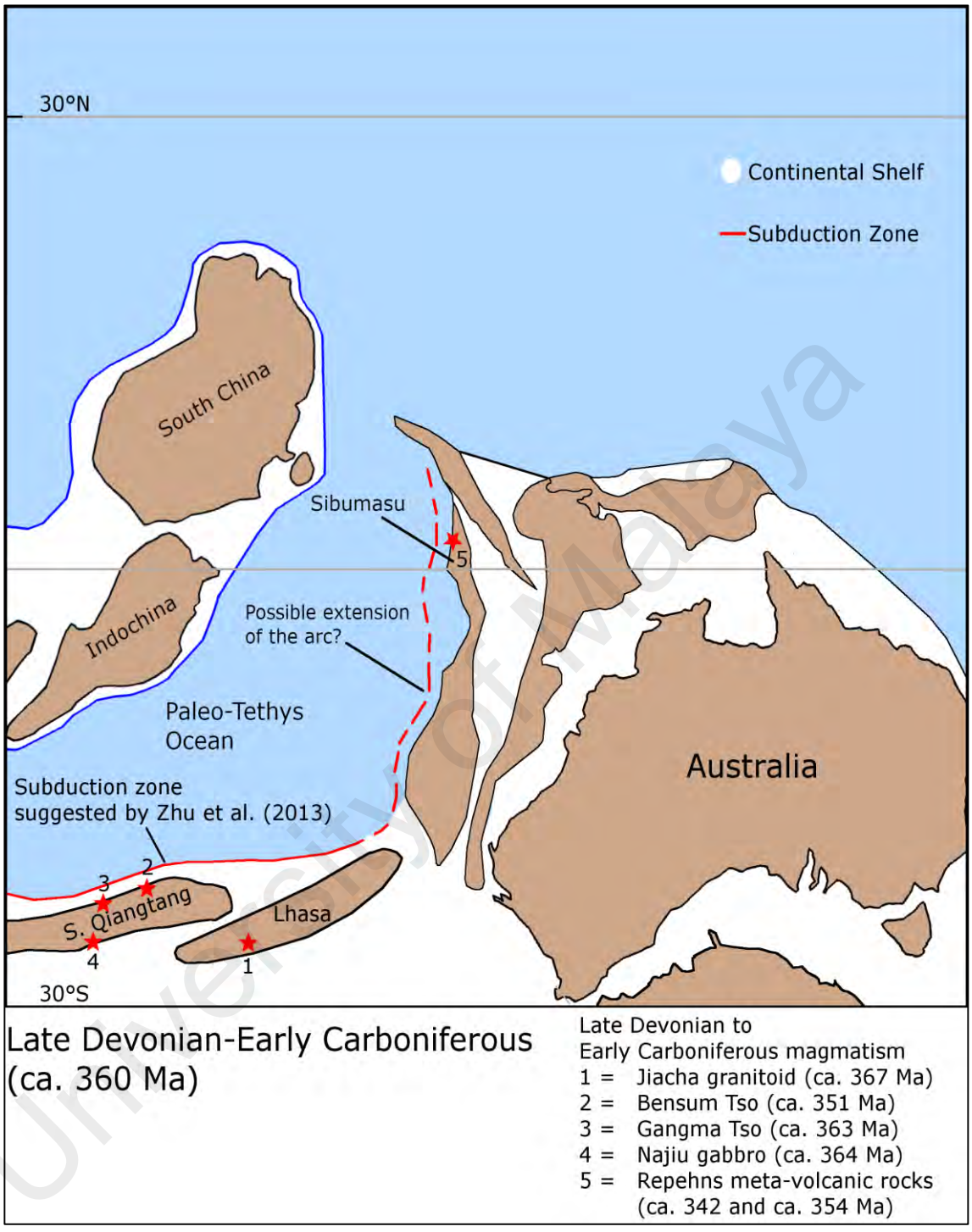

Figure 5.8: Late Devonian to Early Carboniferous reconstruction of East Gondwana margin. The location of other Late Devonian to Early Carboniferous magmatism and the Rephens meta-volcanic rocks are shown on the map. This diagram is modified after Zhu et al. (2013).

5.5 Conclusion

1. Whole-rock major and trace element geochemical analyses indicate that the Gerik-Dinding meta-volcanic rocks (SiO_2 content: 60.68 to 82.56 wt. %) are analogous to high-K calc-alkaline, metaluminous to peraluminous rhyolite. The magma was generated by partial melting of Mesoproterozoic to Paleoproterozoic crustal material with minor mantle-derived magma contributions. These meta-volcanic rocks have trace element signatures suggesting a subduction-related origin (depletion in Nb, Ti, and P) and the zircon U–Pb dated in the Early Paleozoic (480-460 Ma). The formation age of the meta-volcanic rocks coincides with the post-collision stage from the final amalgamation of Asia micro-continental fragments (AMF) onto the East Gondwana Proto-Tethys margin. Lithospheric delamination during the post-collision period would have induced the hot asthenosphere to underplate continental crust and trigger crustal anataxis. The subduction signature in the meta-volcanic rocks was most likely inherited from the protolith associated with the preceding Proto-Tethyan subduction.
2. The Western Peninsular Malaysia meta-dolerite is geochemically similar to basaltic rock (SiO_2: 44.11 to 51.03 wt. %) and can be divided into alkaline to sub-alkaline groups using immobile element ratio Nb/Y. The age of the meta-dolerite intrusion can be constrained to the Late Cambrian until the Early Silurian, (500-430 Ma) as these intrusions are penecontemporaneous with Early Paleozoic meta-sedimentary rocks. Nb-Ta negative anomalies are weak to absent, and the low La/Nb (<2), the low Th/Ce and the low Th/La ratio reveal the lack of a subduction signature. Their trace element geochemical data patterns, supported by tectonic discrimination plot, indicate that the magma was likely emplaced in an active continental rift or a within-plate setting. The lithospheric delamination event (475-460 Ma) following the continental collision with AMF and lithospheric thickening may have caused an extensional regime at the East

Gondwana Proto-Tethys margin, which permitted the meta-dolerite magma to intrude into the thinned continental crust.

3. Two types of Rephens meta-volcanic rocks has been found: (1) the meta-andesite with SiO_2 content (56.95 to 62.41 wt. %) is comparable andesite and (2) the meta-lithic tuff with SiO_2 content (67.17 to 71.48 wt. %) is comparable with rhyolite/dacite. The meta-andesite magma was probably generated by partial melting of juvenile Neoproterozoic middle continental crust from a series of underplated mantle-derived basaltic magmas. On the other hand, the meta-lithic tuff parent magma was probably generated partial melting of an inhomogeneous basement (Neoproterozoic juvenile middle crust with Paleoproterozoic upper continental crust). Both meta-volcanic rocks have trace element geochemical features suggesting a subduction-related origin (depletion in Nb, Ti, and P) and their zircon U–Pb dating of the meta-volcanic rocks suggests they formed in the Early Carboniferous (~342 Ma and ~354 Ma). The formation age of the meta-volcanic rocks coincides with extension magmatic event (365-330 Ma) from the prolonged southern Paleo-Tethys Ocean subduction. The roll-back of the oceanic slab may have caused the upwelling of asthenosphere which resulted in the melting of the continental crust
4. Early to Middle Paleozoic volcanism in Western Peninsular Malaysia is a relatively new topic and we recognize that there were a number of gaps in our knowledge that would benefit from further research. Future studies might, for example, research on Early to Middle Paleozoic plutonism in Western Peninsular Malaysia.

REFERENCES

Ali, J. R., & Aitchison, J. C. (2012). Comment on "Restoration of Cenozoic deformation in Asia and the size of Greater India" by DJJ van Hinsbergen et al. *Tectonics, 31*, 1-3.

Ali, J. R., Cheung, H. M., Aitchison, J. C., and Sun, Y. (2013). Palaeomagnetic re-investigation of Early Permian rift basalts from the Baoshan Block, SW China: constraints on the site-of-origin of the Gondwana-derived eastern Cimmerian terranes. *Geophysical Journal International, 193*, 650-663.

Andersen, T. (2002). Correction of common lead in U-Pb analyses that do not report 204Pb. *Chemical Geology, 192*, 59-79.

Basori, M. B. I., Leman, M. S., Zaw, K., Meffre, S., Large, R. R., Mohamed, K. R., Makoundi C. and Mohd Zin, M. (2018). Implications of U–Pb detrital zircon geochronology analysis for the depositional age, provenance, and tectonic setting of continental Mesozoic formations in the East Malaya Terrane, Peninsular Malaysia. *Geological Journal*, 1-10.

Blichert-Toft, J., and Albarède, F. (1997). The Lu-Hf isotope geochemistry of chondrites and the evolution of the mantle-crust system. *Earth and Planetary Science Letters, 148*, 243-258.

Bolhar, R., Weaver, S. D., Whitehouse, M. J., Palin, J. M., Woodhead, J. D., and Cole, J. W. (2008). Sources and evolution of arc magmas inferred from coupled O and Hf isotope systematics of plutonic zircons from the Cretaceous Separation Point Suite (New Zealand). *Earth and Planetary Science Letters, 268*, 312-324.

Boynton, W. V. (1983). Cosmochemistry of the rare earth elements: meteorite studies. In: Henderson, P. (Ed.), *Rare Earth Element Geochemistry* (pp. 63-114). Amsterdam: Elsevier.

Buddington, A. F., and Lindsley, D. H. (1964). Iron-titanium oxide minerals and synthetic equivalents. *Journal of Petrology, 5*, 310-357.

Burrett, C. and Stait, B. (1986). Southeast Asia as a part of an early Paleozoic Australian Gondwanaland. *Bulletin of the Geological Society of Malaysia, 19*, 103-107.

Cawood, P.A. and Buchan, C. (2007). Linking accretionary orogenesis with supercontinent assembly. *Earth-Science Reviews, 82*, 217-256.

Cawood, P.A., Johnson, M.R. and Nemchin, A.A. (2007). Early Palaeozoic orogenesis along the Indian margin of Gondwana: Tectonic response to Gondwana assembly. *Earth and Planetary Science Letters, 255*, 70-84.

Chen, F., Li, X. H., Wang, X. L., Li, Q. L., and Siebel, W. (2007). Zircon age and Nd–Hf isotopic composition of the Yunnan Tethyan belt, southwestern China. *International Journal of Earth Sciences, 96*, 1179-1194.

Chen, G.D., Peng, S.L., Dai, T.G., Yang, X.Y., Wu, Y.Z., Lai, J.Q., Liu, J.S., Liu, Y.N., Wang, L., Yang, M., Hu, B. and Dong, J. (2004). *Copper-polymetallic Crustbody Geotectonics Metallogeny of Yunnan Province*. Changsha: Central South University Publishing House.

Cheng, H., Zhang, C., Vervoort, J. D., Lu, H., Wang, C., and Cao, D. (2012). Zircon U–Pb and garnet Lu–Hf geochronology of eclogites from the Lhasa Block, Tibet. *Lithos, 155*, 341-359.

Cherniak, D. J., and Watson, E. B. (2003). Diffusion in zircon. *Reviews in Mineralogy and Geochemistry, 53*, 113-143.

Cherniak, D. J., Hanchar, J. M., and Watson, E. B. (1997). Diffusion of tetravalent cations in zircon. *Contributions to Mineralogy and Petrology, 127*, 383-390.

Chiu, H.Y., Chung, S.L., Zarrinkoub, M.H., Mohammadi, S.S., Khatib, M.M. and Iizuka, Y. (2013). Zircon U-Pb age constraints from Iran on the magmatic evolution related to Neotethyan subduction and Zagros orogeny. *Lithos, 162*, 70-87.

Clemens, J. D. (2003). S-type granitic magmas—petrogenetic issues, models and evidence. *Earth-Science Reviews, 61*, 1-18.

Compston, W., Williams, I.S., Campbell, I.H. and Gresham, J.J. (1986). Zircon xenocrysts from the Kambalda volcanics: age constraints and direct evidence for older continental crust below the Kambalda-Norseman greenstones. *Earth and Planetary Science Letters, 76*, 299-311.

Condie, K. C. (1997). Contrasting sources for upper and lower continental crust: the greenstone connection. *The Journal of Geology, 105*, 729-736.

Corfu, F., Hanchar, J.M., Hoskin, P.W. and Kinny, P. (2003). Atlas of zircon textures. *Reviews in Mineralogy and Geochemistry, 53*, 469-500.

Davies, J. F., Grant, R. W. E., and Whitehead, R. E. S. (1979). Immobile trace elements and Archean volcanic stratigraphy in the Timmins mining area, Ontario. *Canadian Journal of Earth Sciences, 16*, 305-311.

Ding, H., Zhang, Z., Dong, X., Yan, R., Lin, Y. and Jiang, H. (2015). Cambrian ultrapotassic rhyolites from the Lhasa terrane, south Tibet: evidence for Andean-type magmatism along the northern active margin of Gondwana. *Gondwana Research, 27*, 1616-1629.

Dong, M., Dong, G., Mo, X., Santosh, M., Zhu, D., Yu, J., Nie, F. and Hu, Z. (2013). Geochemistry, zircon U–Pb geochronology and Hf isotopes of granites in the Baoshan Block, Western Yunnan: Implications for Early Paleozoic evolution along the Gondwana margin. *Lithos, 179*, 36-47.

Dong, X., Zhang, Z.M., Geng, G.S., Liu, F., Wang, W. and Yu, F. (2010). Devonian magmatism from the southern Lhasa terrane, Tibetan Plateau. *Acta Petrologica Sinica, 26*, 2226–2232.

Dong, X., Zhang, Z., Liu, F., He, Z., and Lin, Y. (2014). Late Paleozoic intrusive rocks from the southeastern Lhasa terrane, Tibetan Plateau, and their Late Mesozoic metamorphism and tectonic implications. *Lithos, 198*, 249-262.

Dusel-Bacon, C., Bressler, J.R., Takaoka, H., Mortensen, J.K., Oliver, D.H., Leventhal, J.S., Newberry, R.J. and Bundtzen, T.K. (1998). *Stratiform zinc-lead mineralization in Nasina assemblage rocks of the Yukon-Tanana Upland in east-central Alaska*. Reston: U.S. Geological Survey.

Evins, L. Z., Jourdan, F., and Phillips, D. (2009). The Cambrian Kalkarindji Large Igneous Province: extent and characteristics based on new 40 Ar/39 Ar and geochemical data. *Lithos, 110*, 294-304.

Gehrels, G.E., DeCelles, P.G., Martin, A., Ojha, T.P., Pinhassi, G. and Upreti, B.N. (2003). Initiation of the Himalayan orogen as an early Paleozoic thin-skinned thrust belt. *GSA Today, 13*, 4-9.

Gehrels, G.E., DeCelles, P.G., Ojha, T.P., Upreti, B.N. (2006a). Geological and U–Pb geochronologic evidence for early Paleozoic tectonism in the Dadeldhura thrust sheet, far-west Nepal Himalaya. *Journal of Asian Earth Sciences, 28*, 385-408.

Gehrels, G.E., DeCelles, P.G., Ojha, T.P. and Upreti, B.N. (2006b). Geologic and U-Th-Pb geochronologic evidence for early Paleozoic tectonism in the Kathmandu thrust sheet, central Nepal Himalaya. *Geological Society of America Bulletin, 118*, 185-198.

Gehrels, G.E., Valencia, V.A. and Ruiz, J. (2008). Enhanced precision, accuracy, efficiency, and spatial resolution of U-Pb ages by laser ablation–multicollector–inductively coupled plasma–mass spectrometry. *Geochemistry, Geophysics, Geosystems, 9*, 1525-2027.

Gehrels, G.E., Kapp, P., DeCelles, P.G., Pullen, A., Blakey, R., Weislogel, A., Ding, L., Guynn, J., Martin, A., McQuarrie, N., Yin, A. (2011). Detrital zircon geochronology of pre-Tertiary strata in the Tibetan–Himalayan orogen. *Tectonics, 30*, 1-27.

Gehrels, G.E. and Pecha, M. (2014). Detrital zircon U-Pb geochronology and Hf isotope geochemistry of Paleozoic and Triassic passive margin strata of western North America. *Geosphere, 10*, 49-65.

Geng, Y., Du, L. and Ren, L. (2012). Growth and reworking of the early Precambrian continental crust in the North China Craton: constraints from zircon Hf isotopes. *Gondwana Research, 21*, 517-529.

Ghani, A.A., Searle, M., Robb, L., and Chung, S. L. (2013). Transitional IS type characteristic in the Main Range Granite, Peninsular Malaysia. *Journal of Asian Earth Sciences*, *76*, 225-240.

Ghani, A.A. and Singh, N. (2005). Petrology and geochemistry of the Sempah volcanic complex: Peninsular Malaysia. *Geological Society of Malaysia Bulletin, 51*, 103-121.

Ghani, A.A. (2009). Plutonism. In Hutchison, C.S. and Tan, D.N.K. (Eds.), *Geology of Peninsular Malaysia* (pp. 211-231). Kuala Lumpur: The University of Malaya and The Geological Society of Malaysia.

Glass, L. M., and Phillips, D. (2006). The Kalkarindji continental flood basalt province: A new Cambrian large igneous province in Australia with possible links to faunal extinctions. *Geology, 34*, 461-464.

Godin, L., Parrish, R.R., Brown, R.L., Hodges, K.V. (2001). Crustal thickening leading to exhumation of the Himalayan Metamorphic core of central Nepal: insight from U–Pb geochronology and 40Ar/39Ar thermochronology. *Tectonics, 20*, 729-747.

González-Menéndez, L., Gallastegui, G., Cuesta, A., Heredia, N., and Rubio-Ordóñez, A. (2013). Petrogenesis of Early Paleozoic basalts and gabbros in the western Cuyania terrane: Constraints on the tectonic setting of the southwestern Gondwana margin (Sierra del Tigre, Andean Argentine Precordillera). *Gondwana Research, 24*, 359-376.

Gorton, M. P., and Schandl, E. S. (2000). From continents to island arcs: a geochemical index of tectonic setting for arc-related and within-plate felsic to intermediate volcanic rocks. *The Canadian Mineralogist, 38*, 1065-1073.

Green, T. H. (1995). Significance of Nb/Ta as an indicator of geochemical processes in the crust-mantle system. *Chemical Geology, 120*, 347-359.

Griffin, W.L., Pearson, N.J., Belousova, E., Jackson, S.E., Van Achterbergh, E., O'Reilly, S.Y. and Shee, S.R. (2000). The Hf isotope composition of cratonic mantle: LAM-MC-ICPMS analysis of zircon megacrysts in kimberlites. *Geochimica et Cosmochimica Acta, 64*, 133-147.

Griffin, W. L., Wang, X., Jackson, S. E., Pearson, N. J., O'Reilly, S. Y., Xu, X., and Zhou, X. (2002). Zircon chemistry and magma mixing, SE China: in-situ analysis of Hf isotopes, Tonglu and Pingtan igneous complexes. *Lithos, 61*, 237-269.

Griffin, W.L., Belousova, E.A., Shee, S.R., Pearson, N.J. and O'Reilly, S.Y. (2004). Archean crustal evolution in the northern Yilgarn Craton: U–Pb and Hf-isotope evidence from detrital zircons. *Precambrian Research, 131*, 231-282.

Guo, L., Zhang, H. F., Harris, N., Xu, W. C., and Pan, F. B. (2016). Late Devonian-Early Carboniferous magmatism in the Lhasa terrane and its tectonic implications: Evidences from detrital zircons in the Nyingchi Complex. *Lithos, 245*, 47-59.

Hall, R. (2012). Late Jurassic–Cenozoic reconstructions of the Indonesian region and the Indian Ocean. *Tectonophysics, 570*, 1-41.

Hastie, A.R., Kerr, A.C., Pearce, J.A. and Mitchell, S.F. (2007). Classification of altered volcanic island arc rocks using immobile trace elements: development of the Th-Co discrimination diagram. *Journal of Petrology, 48*, 2341-2357.

Horstwood, M. S., Košler, J., Gehrels, G., Jackson, S. E., McLean, N. M., Paton, C., Pearson, N.J., Sircombe, K., Sylvester, P., Vermeesch, P., Bowring, J.F., Condon, D.J. and Schoene, B. (2016). Community-Derived Standards for LA-ICP-MS U-(Th-) Pb Geochronology–Uncertainty Propagation, Age Interpretation and Data Reporting. *Geostandards and Geoanalytical Research, 40*, 311-332.

Hoskin, P.W. and Schaltegger, U. (2003). The composition of zircon and igneous and metamorphic petrogenesis. *Reviews in mineralogy and geochemistry, 53*, 27-62.

Hu, P.Y., Li, C., Su, L., Li, C.B. and Yu, H. (2010). Zircon U-Pb dating of granitic gneiss in Wugong mountain area, central Qiangtang, Qinghai-Tibet Plateau: Age records of Pan-African movement and Indo-China movement. *Geology in China, 37*, 1050-1061.

Hu, P.Y., Li, C., Wang, M., Xie, C. and Wu, Y. (2013). Cambrian volcanism in the Lhasa terrane, southern Tibet: Record of an early Paleozoic Andean-type magmatic arc along the Gondwana proto-Tethyan margin. *Journal of Asian Earth Sciences, 77*, 91-107.

Hu, P.Y., Zhai, Q.G., Jahn, B.M., Wang, J., Li, C., Lee, H.Y. and Tang, S.H. (2015). Early Ordovician granites from the South Qiangtang terrane, northern Tibet: Implications for the early Paleozoic tectonic evolution along the Gondwanan proto-Tethyan margin. *Lithos, 220*, 318-338.

Hutchison, C.S. (1973a). Volcanic Activity. In: Gobbett, D. J. and Hutchison, C. S. (Eds.), *Geology of Malay Peninsula* (pp. 177-214). New York: Wiley-Interscience.

Hutchison, C.S. (1973b). Plutonic Activity. In: Gobbett, D. J. and Hutchison, C. S. (Eds.), *Geology of Malay Peninsula* (pp. 215-252). New York: Wiley-Interscience.

Hutchison, C.S. (1975). Ophiolite in southeast Asia. *Geological Society of America Bulletin, 86*, 797-806.

Jamil, A., Ghani, A. A., Zaw, K., Othman, S., and Quek, L. X. (2016). Origin and tectonic implications of the ~200 Ma, collision-related Jerai pluton of the Western Granite Belt, Peninsular Malaysia. *Journal of Asian Earth Sciences, 127*, 32-46.

Ji, W.H., Chen, S.J., Zhao, Z.M., Li, R.S., He, S.P., Wang, C. (2009). Discovery of the Cambrian volcanic rocks in the Xainza area, Gangdese orogenic belt, Tibet, China and its significance. *Geological Bulletin of China, 9*, 1350-1354.

Ji, W. Q., Wu, F. Y., Chung, S. L., and Liu, C. Z. (2012). Identification of Early Carboniferous granitoids from southern Tibet and implications for terrane assembly related to the Paleo-Tethyan evolution. *The Journal of Geology, 120*, 531-541.

Jochum, K. P., Willbold, M., Raczek, I., Stoll, B. and Herwig, K. (2005). Chemical Characterisation of the USGS Reference Glasses GSA-1G, GSC-1G, GSD-1G, GSE-1G, BCR-2G, BHVO-2G and BIR-1G Using EPMA, ID-TIMS, ID-ICP-MS and LA-ICP-MS. *Geostandards and Geoanalytical Research, 29*, 285-302.

Johnston, S., Gehrels, G., Valencia, V. and Ruiz, J. (2009). Small-volume U–Pb zircon geochronology by laser ablation-multicollector-ICP-MS. *Chemical Geology, 259*, 218-229.

Jones, C.R. (1970). *The Geology and Mineral Resources of the Grik Area, Upper Perak*. Ipoh, Perak: Geological Survey Headquarters.

Jones, C.R. (1973). Lower Paleozoic. In: Gobbett, D. J. and Hutchison, C. S. (Eds.), *Geology of Malay Peninsula* (pp. 25-60). New York: Wiley-Interscience.

Jones, D. S., Barnes, C. G., Premo, W. R., and Snoke, A. W. (2011). The geochemistry and petrogenesis of the Paleoproterozoic Green Mountain arc: A composite (?), bimodal, oceanic, fringing arc. *Precambrian Research, 185*, 231-249.

Jiang, Q. Y., Li, C., Su, L., Hu, P. Y., Xie, C. M., and Wu, H. (2015). Carboniferous arc magmatism in the Qiangtang area, northern Tibet: Zircon U–Pb ages, geochemical and Lu–Hf isotopic characteristics, and tectonic implications. *Journal of Asian Earth Sciences, 100*, 132-144.

Kawakami, T., Nakano, N., Higashino, F., Hokada, T., Osanai, Y., Yuhara, M., Charusiri, P., Kamikubo, H., Yonemura, K. and Hirata, T. (2014). U-Pb zircon and CHIME monazite dating of granitoids and high-grade metamorphic rocks from the Eastern and Peninsular Thailand-A new report of Early Paleozoic granite. *Lithos, 200*, 64-79.

Kemp, A. I. S., Hawkesworth, C. J., Paterson, B. A., and Kinny, P. D. (2006). Episodic growth of the Gondwana supercontinent from hafnium and oxygen isotopes in zircon. *Nature, 439*, 580-583.

Kemp, A. I. S., Hawkesworth, C. J., Foster, G. L., Paterson, B. A., Woodhead, J. D., Hergt, J. M., Gray, C.M. and Whitehouse, M. J. (2007). Magmatic and crustal differentiation history of granitic rocks from Hf-O isotopes in zircon. *Science, 315*, 980-983.

Kinny, P.D. and Maas, R. (2003). Lu–Hf and Sm–Nd isotope systems in zircon. *Reviews in Mineralogy and Geochemistry, 53*, 327-341.

Kröner, A., Alexeiev, D.V., Hegner, E., Rojas-Agramonte, Y., Corsini, M., Chao, Y., Wong, J., Windley, B.F., Liu, D. and Tretyakov, A.A. (2012). Zircon and muscovite ages, geochemistry, and Nd–Hf isotopes for the Aktyuz metamorphic terrane: evidence for an Early Ordovician collisional belt in the northern Tianshan of Kyrgyzstan. *Gondwana Research, 21*, 901-927.

Lan, C.Y., Usuki, T., Wang, K.L., Yui, T.F., Okamoto, K., Lee, Y.H., Hirata, T., Kon, Y., Orihashi, Y., Liou, J.G. and Lee, C.S. (2009). Detrital zircon evidence for the antiquity of Taiwan. *Geosciences Journal, 13*, 233-243.

Lee, J., Hacker, B.R., Dinklage, W.S., Wang, Y., Gans, P., Calvert, A., Wang, J.L., Chen, W.J., Blythe, A.E., McClelland, W. (2000). Evolution of the Kangmar Dome, southern Tibet: structural, petrologic, and thermochronologic constrains. *Tectonics, 19*, 872–895.

Lee, J., Whitehouse, M.J. (2007). Onset of mid-crustal extensional flow in southern Tibet: evidence from U/Pb zircon ages. *Geology, 35*, 45-48.

Lee, H.Y., Chung, S.L., Ji, J., Qian, Q., Gallet, S., Lo, C.H., Lee, T.Y. and Zhang, Q. (2012). Geochemical and Sr–Nd isotopic constraints on the genesis of the Cenozoic Linzizong volcanic successions, southern Tibet. *Journal of Asian Earth Sciences, 53*, 96-114.

Li, X.H., Zhou, H., Chung, S.L., Ding, S., Liu, Y., Lee, C.Y., Ge, W., Zhang, Y. and Zhang, R. (2002). Geochemical and Sm–Nd isotopic characteristics of metabasites from central Hainan Island, South China and their tectonic significance. *Island Arc, 11*, 193-205.

Li, C., Cheng, L.R., Yu, J.J., Zhang, B.F., Zhai, Q.G., Huang, X.P., Chen, S.M., Xu, F. and Zhang, Y.C. (2006). *1: 250, 000 geological report of Mayer Kangri with geological map*. Changchun: Institute of Geological Survey, Jilin University.

Li, C., Xie, Y.W., Sha, S.L., Dong, Y.S. (2008). SHRIMP U–Pb zircon dating of the Pan-African granite in Baxoi County, eastern Tibet, China. *Geological Bulletin of China, 27*, 64–68.

Li, G., Wang, Q., Huang, Y., Chen, F. and Dong, P. (2015). Discovery of Hadean–Mesoarchean crustal materials in the northern Sibumasu block and its significance for Gondwana reconstruction. *Precambrian Research, 271*, 118-137.

Li, C., Arndt, N. T., Tang, Q., and Ripley, E. M. (2015). Trace element indiscrimination diagrams. *Lithos 232,* 76-83.

Li, G., Wang, Q.F., Huang, Y.H., Gao, L. and Yu, L. (2016). Petrogenesis of middle Ordovician peraluminous granites in the Baoshan block: implications for the early Paleozoic tectonic evolution along East Gondwana. *Lithos, 245*, 76-92.

Li, S., Zhao, S., Liu, X., Cao, H., Yu, S., Li, X., Somerville, I., Yu, S. and Suo, Y. (in press). Closure of the Proto-Tethys Ocean and Early Paleozoic amalgamation of microcontinental blocks in East Asia. *Earth-Science Reviews*.

Liew, T.C. (1983). *Petrogenesis of the Peninsular Malaysia granitoid batholiths*. (Unpublished doctoral dissertation). Australia National University, Canberra, Australia.

Liew, T.C. and McCulloch, M.T. (1985). Genesis of granitoid batholiths of Peninsular Malaysia and implications for models of crustal evolution: evidence from a Nd–Sr isotopic zircon study. *Geochimica et Cosmochimica Acta, 49*, 587–600.

Liew, T.C. and Page, R.W. (1985). U-Pb zircon dating of granitoid plutons from the West Coast of Peninsular Malaysia. *Journal of the Geological Society of London, 142*, 515-526.

Lin, Y.L., Yeh, M.W., Lee, T.Y., Chung, S.L., Iizuka, Y. and Charusiri, P. (2013). First evidence of the Cambrian basement in Upper Peninsula of Thailand and its implication for crustal and tectonic evolution of the Sibumasu terrane. *Gondwana Research, 24*, 1031-1037.

Liu, S., Hu, R., Gao, S., Feng, C., Huang, Z., Lai, S., Yuan, H., Liu, X., Coulson, I.M., Feng, G. and Wang, T. (2009). U-Pb zircon, geochemical and Sr-Nd-Hf isotopic constraints on the age and origin of Early Palaeozoic I-type granite from the Tengchong-Baoshan Block, Western Yunnan Province, SW China. *Journal of Asian Earth Sciences, 36*, 168-182.

Liu, Y.S., Ye, P.S., Wu, Z.H. (2012). SHRIMP zircon U–Pb dating and petrogeochemistry of Ordovician granite bodies in the southern segment of Gaoligong Mountain, western Yunnan Province. *Geological Bulletin of China, 31*, 250–257.

Ludwig, K.J. (2003). *User's Manual for Isoplot 3.75: A Geochronological Toolkit for Microsoft Excel*. Berkeley: Berkeley Geochronological Center.

MacKenzie, W. S., Donaldson, C. H., and Guilford, C. (1982). *Atlas of igneous rocks and their textures*. London: Longman.

Meert, J. G. (2003). A synopsis of events related to the assembly of eastern Gondwana. *Tectonophysics, 362*, 1-40.

Meert, J. G., and Van Der Voo, R. (1997). The assembly of Gondwana 800-550 Ma. *Journal of Geodynamics, 23*, 223-235.

Metcalfe, I. (1996). Gondwanaland dispersion, Asian accretion and evolution of eastern Tethys. *Australian Journal of Earth Sciences, 43*, 605-623.

Metcalfe, I. (2000). The Bentong–Raub suture zone. *Journal of Asian Earth Sciences, 18*, 691-712.

Metcalfe, I. (2002). Permian tectonic framework and palaeogeography of SE Asia. *Journal of Asian Earth Sciences, 20*, 551-566.

Metcalfe, I. (2011). Tectonic framework and Phanerozoic evolution of Sundaland. *Gondwana Research, 19*, 3-21.

Metcalfe, I. (2013a). Tectonic evolution of the Malay Peninsula. *Journal of Asian Earth Sciences, 76*, 195-213.

Metcalfe, I. (2013b). Gondwana dispersion and Asian accretion: Tectonic and palaeogeographic evolution of eastern Tethys. *Journal of Asian Earth Sciences, 66*, 1-33.

Middlemost, E. A. (1994). Naming materials in the magma/igneous rock system. *Earth-Science Reviews 37,* 215-224.

Miller, C., Thöni, M., Frank, W., Grasemann, B., Klötzli, U., Guntli, P. and Draganits, E. (2001). The early Palaeozoic magmatic event in the Northwest Himalaya, India: source, tectonic setting and age of emplacement. *Geological Magazine, 138*, 237-251.

Miyashiro, A. (1975). Classification, characteristics, and origin of ophiolites. *The Journal of Geology, 83*, 249-281.

Mondal, R. and Baidya, T.K. (2015). Titaniferous Magnetite Deposits Associated with Archean Greenstone Belt in the East Indian Sheild. *Earth Sciences, 4*, 15-30.

Mu, S.Y., Wang, C.H., Wang, M., Chen, R., Zeng, C.X., Chen, H.G., Xiong, X.G., Lu, D.B., Yue, L., Yi, C.X., He, Y.Z., Zhu, X., Bian, S.W., Xu, A.Q. and Zhao, W.L. (2005). *1: 250, 000 geological report of Dinggu with geological map*. Guiyang: Guizhou Institute of Geological Survey.

Murphy, J.B. and Nance, R.D. (1991). Supercontinent model for the contrasting character of Late Proterozoic orogenic belts. *Geology, 19*, 469-472.

Nebel, O., Nebel-Jacobsen, Y., Mezger, K. and Berndt, J. (2007). Initial Hf isotope compositions in magmatic zircon from early Proterozoic rocks from the Gawler Craton, Australia: a test for zircon model ages. *Chemical Geology, 241*, 23-37.

Ng, S.W.P., Chung, S.L., Robb, L.J., Searle, M.P., Ghani, A.A., Whitehouse, M.J., Oliver, G.J., Sone, M., Gardiner, N.J. and Roselee, M.H. (2015a). Petrogenesis of Malaysian granitoids in the Southeast Asian tin belt: Part 1. Geochemical and Sr-Nd isotopic characteristics. *Geological Society of America Bulletin, 127*, 1209-1237.

Ng, S.W.P., Whitehouse, M.J., Searle, M.P., Robb, L.J., Ghani, A.A., Chung, S.L., Oliver, G.J.H., Sone, M., Gardiner, N.J. and Roselee, M.H. (2015b). Petrogenesis of Malaysian tin granites: Part 2. High precision U–Pb zircon geochronology of the Malaysian tin granites and tectonic model for their emplacement history. *Geological Society of America Bulletin, 127*, 1238-1258.

Oliver, G., Zaw, K., Hotson, M., Meffre, S. and Manka, T. (2014). U–Pb zircon geochronology of Early Permian to Late Triassic rocks from Singapore and Johor: A plate tectonic reinterpretation. *Gondwana Research, 26*, 132-143.

Patchett, P. J. (1983). Importance of the Lu-Hf isotopic system in studies of planetary chronology and chemical evolution. *Geochimica et Cosmochimica Acta, 47*, 81-91.

Pan, G.T., Ding, J., Yao, D.S., Wang, L.Q. (2004). *Guidebook of 1:1,500,000 geologic map of the Qinghai–Xizang (Tibet) plateau and adjacent areas*. Chengdu: Cartographic Publishing House.

Pan, X.P., Li, R.S., Wang, C., Yu, P.S., Gu, P.Y. and Cha, X.F. (2012). Geochemical characteristics of the Cambrian volcanic rocks in Banglecun area on the northern margin of Gangdise, Nyima County, Tibet. *Geological Bulletin of China, 31*, 63–74.

Pang, K.N., Chung, S.L., Zarrinkoub, M.H., Mohammadi, S.S., Yang, H.M., Chu, C.H., Lee, H.Y. and Lo, C.H. (2012). Age, geochemical characteristics and petrogenesis of Late Cenozoic intraplate alkali basalts in the Lut–Sistan region, eastern Iran. *Chemical Geology, 306*, 40-53.

Pearce, J.A. (1982). Trace element characteristics of lavas from destructive plate boundaries. In: Thorpe, R.S. (Ed.), *Andesites: Orogenic Andesites and Related Rocks* (pp 525-548). Chichester: John Wiley & Sons.

Pearce, J. A. (1996). A User's Guide to Basalt Discrimination Diagrams. In: Wyman, D. A. (Ed.), *Trace Element Geochemistry of Volcanic Rocks: Applications for Massive Sulphide Exploration* (pp. 79-113). Manitoba: Geological Association of Canada.

Pullen, A., Kapp, P., Gehrels, G. E., Ding, L., and Zhang, Q. (2011). Metamorphic rocks in central Tibet: Lateral variations and implications for crustal structure. *Geological Society of America Bulletin, 123*, 585-600.

Quigley, M.C., Yu, L.J., Gregory, C., Corvino, A., Sandiford, M., Wilson, C.J.L., Liu, X.H. (2008). U–Pb SHRIMP zircon geochronology and T–t–d history of the Kampa Dome, southern Tibet. *Tectonophysics, 446*, 97–113.

Quek, L.X., Jamil, A., Ghani, A. A., Saidin, M. (2015). Highly Potassic Melagranite of Bintang batholith, Main Range Granite, Peninsular Malaysia. *Current Science, 108*, 2159-2163.

Quek, L.X., Ghani, A.A., Chung, S.L., Li, S., Lai, Y.M., Saidin, M., Hassan, M.H.A., Ali, M.A.M., Badruldin, M.H. and Bakar, A.F.A. (2017). Mafic microgranular enclaves (MMEs) in amphibole-bearing granites of the Bintang batholith, Main Range granite province: Evidence for a meta-igneous basement in Western Peninsular Malaysia. *Journal of Asian Earth Sciences, 143*, 11-29.

Ramezani, J. and Tucker, R.D. (2003). The Saghand region, central Iran: U-Pb geochronology, petrogenesis and implications for Gondwana tectonics. *American Journal of Science, 303*, 622-665.

Roberts, M.P. and Clemens, J.D. (1993). Origin of high-potassium, calc-alkaline, I-type granitoids. *Geology, 21*, 825-828.

Roe, F.W. (1951a). *The geology and mineral resources of the Fraser's Hill area, Selangor, Perak and Pahang, Federation of Malaya, with an account of the mineral resources*. Ipoh: Geological Survey Headquarters.

Roe, F.W. (1951b). *The geology and mineral resources of the neighbourhood of Kuala Selangor and Rasa: Selangor, Federation of Malaya, with an account of the geology of Batu Arang coal-field*. Ipoh: Geological Survey Headquarters.

Rubatto, D. and Gebauer, D. (2000). Use of cathodoluminescence for U-Pb zircon dating by ion microprobe: some examples from the Western Alps. In: Pagel, M., Barbin, V., Blanc, P. and Ohnenstetter, D. (Eds.), *Cathodoluminescence in geosciences* (pp. 373-400). Berlin: Springer Berlin Heidelberg.

Rudnick, R.L. and Fountain, D.M. (1995). Nature and composition of the continental crust: a lower crustal perspective. *Reviews of Geophysics, 33*, 267-309.

Rudnick, R. L., and Gao, S. (2003). Composition of the continental crust. In: Holland, H.D. and Turekian, K.K. (Eds.), *Treatise of Geochemistry* (pp. 1-64). Amsterdam: Elsevier.

Saki, A. (2010). Proto-Tethyan remnants in northwest Iran: geochemistry of the gneisses and metapelitic rocks. *Gondwana Research, 17*, 704–714.

Saunders, A. D., Norry, M. J., and Tarney, J. (1991). Fluid influence on the trace element compositions of subduction zone magmas. *Philosophical Transactions of the Royal Society of London A: Mathematical, Physical and Engineering Sciences, 335*, 377-392.

Schaltegger, U., Fanning, C.M., Günther, D., Maurin, J.C., Schulmann, K. and Gebauer, D. (1999). Growth, annealing and recrystallization of zircon and preservation of monazite in high-grade metamorphism: conventional and in-situ U-Pb isotope, cathodoluminescence and microchemical evidence. *Contributions to Mineralogy and Petrology, 134*, 186-201.

Schandl, E.S. and Gorton, M.P. (2002). Application of high field strength elements to discriminate tectonic settings in VMS environments. *Economic Geology, 97*, 629-642.

Scherer, E., Münker, C., and Mezger, K. (2001). Calibration of the lutetium-hafnium clock. *Science, 293*, 683-687.

Searle, M.P., Whitehouse, M.J., Robb, L.J., Ghani, A.A., Hutchison, C.S., Sone, M., Ng, S.P., Roselee, M.H., Chung, S.L. and Oliver, G.J.H. (2012). Tectonic evolution of the Sibumasu–Indochina terrane collision zone in Thailand and Malaysia: constraints from new U–Pb zircon chronology of SE Asian tin granitoids. *Journal of the Geological Society, 169*, 489-500.

Sevastjanova, I., Clements, B., Hall, R., Belousova, E.A., Griffin, W.L. and Pearson, N., (2011). Granitic magmatism, basement ages, and provenance indicators in the Malay Peninsula: insights from detrital zircon U–Pb and Hf-isotope data. *Gondwana Research, 19*, 1024-1039.

Shellnutt, J. G., and Zhou, M. F. (2007). Permian peralkaline, peraluminous and metaluminous A-type granites in the Panxi district, SW China: their relationship to the Emeishan mantle plume. *Chemical Geology 243*, 286-316.

Shi, C., Li, R.S., He, S.P., Wang, C., Pan, S.J., Liu, Y. and Gu, P.Y. (2010). LA-ICP-MS zircon U–Pb dating for gneissic garnet-bearing biotite granodiorite in the Yadong area, southern Tibet, China and its geological significance. *Geological Bulletin of China, 29*, 1745–1753.

Shu, Y.K. (1989). Geology and Mineral Resources of the Kuala Kelawang area, Jelebu, Negeri Sembilan. Ipoh: Geological Survey Headquarters.

Sone, M. and Metcalfe, I. (2008). Parallel Tethyan sutures in mainland Southeast Asia: new insights for Palaeo-Tethys closure and implications for the Indosinian orogeny. *Comptes Rendus Geoscience, 340*, 166-179.

Song, S., Ji, J., Wei, C., Su, L., Zheng, Y., Song, B. and Zhang, L. (2007). Early Paleozoic granite in Nujiang River of northwest Yunnan in southwestern China and its tectonic implications. *Chinese Science Bulletin, 52*, 2402-2406.

Söderlund, U., Patchett, P.J., Vervoort, J.D. and Isachsen, C.E. (2004). The 176 Lu decay constant determined by Lu–Hf and U–Pb isotope systematics of Precambrian mafic intrusions. *Earth and Planetary Science Letters, 219*, 311-324.

Stampfli, G. M., and Borel, G. D. (2002). A plate tectonic model for the Paleozoic and Mesozoic constrained by dynamic plate boundaries and restored synthetic oceanic isochrons. *Earth and Planetary Science Letters, 196*, 17-33.

Sun, S.S. and McDonough, W.F. (1989). Chemical and isotopic systematics of oceanic basalts: implications for mantle composition and processes. In: Saunders, A.D. and Norry, M.J. (Eds.), *Magmatism in the Ocean Basins* (pp. 313-345). London: Geological Society Special Publication.

Tjia, H.D. (1973). Geomorphology. In: Gobbett, D. J. and Hutchison, C. S. (Eds.), *Geology of Malay Peninsula* (pp. 25-60). New York: Wiley-Interscience.

Torsvik, T.H. and Cocks, R.M. (2009). The Lower Paleozoic paleogeographical evolution of the northeastern and eastern peri-Gondwanan margin from Turkey to New Zealand. *Geological Society, London, Special Publications, 325*, 3-21.

Ustaömer, P.A., Ustaömer, T., Collins, A.S. and Robertson, A.H. (2009). Cadomian (Ediacaran–Cambrian) arc magmatism in the Bitlis Massif, SE Turkey: magmatism along the developing northern margin of Gondwana. *Tectonophysics, 473*, 99-112.

Wang, X.X., Zhang, J.J., Yang, X.Y., Zhang, B. (2011). Zircon SHRIMP U–Pb ages, Hf isotope features and their geological significance of the Greater Himalayan Crystalline Complex augen gneiss in Gyirong Area, south Tibet. *Earth Science Frontiers, 18*, 127–139.

Wang, Y., Xing, X., Cawood, P.A., Lai, S., Xia, X., Fan, W., Liu, H. and Zhang, F. (2013). Petrogenesis of early Paleozoic peraluminous granite in the Sibumasu Block of SW Yunnan and diachronous accretionary orogenesis along the northern margin of Gondwana. *Lithos, 182*, 67-85.

Webber, G. R. (1966). Relative depth of origin of alkali and tholeiitic rocks. *Earth and Planetary Science Letters, 1*, 183-184.

Winchester, J. A., and Floyd, P. A. (1977). Geochemical discrimination of different magma series and their differentiation products using immobile elements. *Chemical Geology, 20*, 325-343.

Woodhead, J.D. and Hergt, J.M. (2005). A preliminary appraisal of seven natural zircon reference materials for in situ Hf isotope determination. *Geostandards and Geoanalytical Research, 29*, 183-195.

Wood, D. A., Joron, J. L., and Treuil, M. (1979). A re-appraisal of the use of trace elements to classify and discriminate between magma series erupted in different tectonic settings. *Earth and Planetary Science Letters, 45*, 326-336.

Wood, D. A. (1980). The application of a Th-Hf-Ta diagram to problems of tectonomagmatic classification and to establishing the nature of crustal contamination of basaltic lavas of the British Tertiary Volcanic Province. *Earth and Planetary Science Letters, 50*, 11-30.

Xing, X., Wang, Y., Cawood, P.A. and Zhang, Y. (2015). Early Paleozoic accretionary orogenesis along northern margin of Gondwana constrained by high-Mg metaigneous rocks, SW Yunnan. *International Journal of Earth Sciences*, 1-18.

Xu, Z.Q., Yang, J.S., Liang, F.H., Qi, X.X., Liu, F.L., Zeng, L.S., Liu, D.Y., Li, H.B., Wu, C.L., Shi, R.D. and Chen, S.Y. (2005). Pan-African and Early Paleozoic orogenic events in the Himalaya terrane: Inference from SHRIMP U–Pb zircon ages. *Acta Petrologica Sinica, 21*, 1-12.

Xu, Y.J., Cawood, P.A., Du, Y.S., Huang, H.W. and Wang, X.Y. (2014). Early Paleozoic orogenesis along Gondwana's northern margin constrained by provenance data from South China. *Tectonophysics, 636*, 40–51.

Yin, A., and Harrison, T. M. (2000). Geologic evolution of the Himalayan-Tibetan orogen. *Annual Review of Earth and Planetary Sciences, 28*, 211-280.

Yew, C.C. (1971). *The geology and mineralization of the eastern Kuala Lumpur area, West Malaysia* (Unpublished master's thesis). University of Malaya, Kuala Lumpur, Malaysia.

Yang, J.-H., Chung, S.-L., Wilde, S.A., Wu, F.-Y., Chu, M.-F., Lo, C.-H. and Fan, H.-R., (2005). Petrogenesis of post-orogenic syenites in the Sulu Orogenic Belt, East China: geochronological, geochemical and Nd–Sr isotopic evidence. *Chemical Geology, 214*, 99–125.

Yang, J., Xu, Z., Li, Z., Xu, X., Li, T., Ren, Y., Li, H., Chen, S. and Robinson, P. T. (2009). Discovery of an eclogite belt in the Lhasa block, Tibet: A new border for Paleo-Tethys?. *Journal of Asian Earth Sciences, 34*, 76-89.

Yang, X.J., Jia, X.C., Xiong, C.L., Bai, X.Z., Huang, B.X., Luo, G. and Yang, C.B. (2012). LA-ICPMS zircon U–Pb age of metamorphic basic volcanic rock in Gongyanghe Group of southern Gaoligong Mountain, western Yunnan Provincem and its geological significance. *Geological Bulletin of China, 31*, 264–276.

Zeng, L., Liu, J., Gao, L.e., Chen, F. and Xie, K. (2009). Early Mesozoic High-pressure Metamorphism Within the Lhasa Block, Tibet and Implications for Regional Tectonics. *Earth Science Frontiers, 16*, 140-151.

Zhai, Q. G., Jahn, B. M., Wang, J., Hu, P. Y., Chung, S. L., Lee, H. Y., Tang, S.H., and Tang, Y. (2015). Oldest paleo-Tethyan ophiolitic mélange in the Tibetan Plateau. *Geological Society of America Bulletin, 128*, 355-373.

Zhang, Z.M., Wang, J.L., Shen, K., Shi, C. (2008). Paleozoic circum-Gondwana orogens: Petrology and geochronology of the Namche Barwa Complex in the eastern Himalayan syntaxis, Tibet. *Acta Petrologica Sinica, 24*, 1627–1637.

Zhang, Z., Dong, X., Santosh, M., Liu, F., Wang, W., Yiu, F., He, Z. and Shen, K. (2012). Petrology and geochronology of the Namche Barwa Complex in the eastern Himalayan syntaxis, Tibet: constraints on the origin and evolution of the north-eastern margin of the Indian Craton. *Gondwana Research, 21*, 123–137.

Zhang, X.Z., Dong, Y.S., Li, C., Deng, M.R., Zhang, L. and Xu, W. (2014). Silurian high-pressure granulites from Central Qiangtang, Tibet: Constraints on early Paleozoic collision along the northeastern margin of Gondwana. *Earth and Planetary Science Letters, 405*, 39-51.

Zhao, S.W., Lai, S.C., Gao, L., Qin, J.F. and Zhu, R.Z. (2017). Evolution of the Proto-Tethys in the Baoshan block along the East Gondwana margin: constraints from early Palaeozoic magmatism. *International Geology Review, 59*, 1-15.

Zhu, D., Pan, G., Mo, X., Liao, Z., Jiang, X., Wang, L., and Zhao, Z. (2007). Petrogenesis of volcanic rocks in the Sangxiu Formation, central segment of Tethyan Himalaya: A probable example of plume–lithosphere interaction. *Journal of Asian Earth Sciences, 29*, 320-335.

Zhu, D.C., Zhao, Z.D., Niu, Y., Dilek, Y., Wang, Q., Ji, W.H., Dong, G.C., Sui, Q.L., Liu, Y.S., Yuan, H.L. and Mo, X.X. (2012). Cambrian bimodal volcanism in the Lhasa Terrane, southern Tibet: record of an early Paleozoic Andean-type magmatic arc in the Australian proto-Tethyan margin. *Chemical Geology, 328*, 290-308.

Zhu, D. C., Zhao, Z. D., Niu, Y., Dilek, Y., Hou, Z. Q., and Mo, X. X. (2013). The origin and pre-Cenozoic evolution of the Tibetan Plateau. *Gondwana Research, 23*, 1429-1454.

LIST OF PUBLICATIONS AND PAPER PRESENTED

Publication(s) in related fields

1. **Quek, L.X.**, Ghani, A.A., Chung, S.L., Li, S., Lai, Y.M., Saidin, M., Hassan, M.H.A., Ali, M.A.M., Badruldin, M.H. and Bakar, A.F.A. (2017). Mafic microgranular enclaves (MMEs) in amphibole-bearing granites of the Bintang batholith, Main Range granite province: Evidence for a meta-igneous basement in Western Peninsular Malaysia. *Journal of Asian Earth Sciences, 143*, 11-29.

Presentation at international or national conference(s)

1. Petrology and Geochemistry of the Low-Grade Meta-Igneous rocks in the Main Range Orogenic belt in Western Peninsular Malaysia (National Geoscience Conference 2016)